1989

Two new instruments for analytical chemistry: A. Constant potential pulse polarography (CPPP) and differential CPPP (DCPPP) for determination of metals in the presence of oxygen in flowing systems; B. Versatile laser-based analytical instrument for detection of jet-cooled molecular species

Bryan J. Isaac
Iowa State University

Order Number 9014910

Two new instruments for analytical chemistry: A. Constant potential pulse polarography (CPPP) and differential CPPP (DCPPP) for determination of metals in the presence of oxygen in flowing systems; B. Versatile laser-based analytical instrument for detection of jet-cooled molecular species

Isaac, Bryan J., Ph.D.

Iowa State University, 1989

U·M·I
300 N. Zeeb Rd.
Ann Arbor, MI 48106

Two new instruments for analytical chemistry: A. Constant potential pulse polarography (CPPP) and differential CPPP (DCPPP) for determination of metals in the presence of oxygen in flowing systems; B. Versatile laser-based analytical instrument for detection of jet-cooled molecular species

by

Bryan J. Isaac

A Dissertation Submitted to the
Graduate Faculty in Partial Fulfillment of the
Requirements for the Degree of
DOCTOR OF PHILOSOPHY

Department: Chemistry
Major: Analytical Chemistry

Approved:

Signature was redacted for privacy.

In Charge of Major Work

Signature was redacted for privacy.

For the Major Department

Signature was redacted for privacy.

For the Graduate College

Iowa State University
Ames, Iowa

1989

TABLE OF CONTENTS

PREFACE

This dissertation is arranged in two sections, each corresponding to work under the direction of one of my two major professors. The research on polarography is presented first, as it was the most recent project. Following Section I the research in the area of jet spectroscopy is presented.

Each of these projects were carried out by the author under the direction of the respective major professors and members of their research staff. Dr. Gerald J. Small directed the work in jet spectroscopy, with additional guidance from Dr. John M. Hayes. Dr. Dennis C. Johnson directed the work on constant potential pulse polarography.

List of Acronyms and Symbols

Acronym	Meaning
A/D	analog-to-digital
AAS	atomic absorption spectroscopy
AC	alternating current
CPPP	constant potential pulse polarography
DC	direct current
DCP	DC polarography
DCPPP	differential constant potential pulse polarography
DME	dropping mercury electrode
DPP	differential pulse polarography
FIA	flow injection analysis
GC	gas chromatography
HPLC	high performance liquid chromatography
IC	ion chromatography
LC	liquid chromatography
LD	laser desorption
LIF	laser-induced fluorescence
LN_2	liquid nitrogen
LOD	limit of detection
MPI	multiple photon ionization
MS	mass spectrometry
MW	molecular weight
NPP	normal pulse polarography
PAR, PARC	Princeton Applied Research (Corporation)

ppb	parts per billion
ppm	parts per million
RPP	reverse pulse polarography
S/N	signal-to-noise ratio
SDCP	sampled DC polarography
TOFMS	time-of-flight mass spectrometry
UV	ultra-violet

Symbol	Meaning
A	area of mercury drop
C	concentration
C_{Ox}^{b}	bulk concentration of oxidized species
D_{Ox}	diffusion rate of oxidized species
E	potential
E^{o}	standard reduction potential
E_d	detection potential
E_i	initial potential
$E_{1/2}$	half-wave potential
E_1	potential during first part of waveform
E_2	potential during second part of waveform
F	Faraday
i	current
i_a	anodic current
i_c	cathodic current

i_d	diffusion current
i_{lim}	limiting (diffusion) current
k	Boltzmann's constant
K	constant
m	mass flow rate of mercury
n	number of electrons exchanged in the reaction
N	number of points
[Ox]	concentration of oxidized species
P	pressure
R	ideal gas constant
[Red]	concentration or reduced species
t	time
t_d	time of detection (delay after pulse initiation)
t_i	initial time
t_m	time at measurement
t_p	time duration of pulse
t_s	time sampling current
t_1	time at the first measurement
t_2	time at the second measurement
T	temperature (in Kelvin)
Δ	change
ω	frequency

GENERAL INTRODUCTION

This thesis details the development of two new instruments which offer advantages useful in meeting some of the complex needs in analytical chemistry.

The first instrument is one which allows the practical use of polarography in flowing samples. It is shown that removal of dissolved oxygen is not necessary, thus saving a previously required time-consuming step. Detection is accomplished by constant potential pulse polarography (CPPP). Further freedom from interference due to reduction of hydrogen ion in acidic solution is offered by CPPP. CPPP is shown to have a detection limit of 10^{-7} M for the metals studied, demonstrating needed sensitivity. A differential method has also been developed, differential CPPP (DCPPP), and was shown to offer increased selectivity, with resolution on the same scale as differential pulse polarography (DPP).

The second instrument is designed to extend the range of sample introduction methods for jet spectroscopy to include gas chromatography and laser desorption. Versatile detection is shown by laser-induced fluorescence (LIF) and multiphoton ionization (MPI). Capabilities of the instrument include a detection limit of 9 ppm aniline in Helium carrier gas using MPI, determined under optimized instrumental conditions.

As one who aspires to be an educator, the research covered here has been a rare opportunity to investigate projects in two separate areas of analytical chemistry. It is my desire that these methods and principles can be used in research as well as in the education of college students.

SECTION I.

CONSTANT POTENTIAL PULSE POLAROGRAPHY (CPPP) AND DIFFERENTIAL CPPP (DCPPP) FOR DETERMINATION OF METALS IN THE PRESENCE OF OXYGEN IN FLOWING SYSTEMS

CHAPTER 1. INTRODUCTION

Modern analytical chemistry makes wide use of measurements made in flowing liquids. Discrete analyses conducted in flowing media give advantages for automation and high sample throughput (1). In view of the continuing growth of such techniques, and of the importance of the analysis of flowing liquids, it is good to consider the application of present analytical methods to flowing solutions of analytes.

Polarography is an analytical technique which has reached a relatively mature stage of development. Many textbooks have been published on classical polarography (2,3) as well as recent books on modern polarographic methods (4,5). As a technique polarography enjoyed popularity in determination and detection of heavy metals from its discovery in 1922 (6) until the mid 1950s, when atomic absorption spectroscopy (AAS) became routinely used for heavy metal determinations. Only in recent years, with the advances derived from pulse potential techniques, has polarography begun to become competitive with AAS for sensitivity (7).

Although polarography has been applied to continuous monitoring in flowing liquids, polarography presents the general drawback that to make reductive measurements oxygen must be removed from the test liquid. Because reductive determinations of metals is a primary application of polarography, this limitation strips polarography of most of its advantages.

Early applications of polarography beyond the batch mode made use of

the cathodic reactivity of oxygen in the development of oxygen sensors (8). Advances beyond the application to oxygen could be made only by devising methods of oxygen removal (9, 10), one of which was to place the entire system in a drybox with an inert gas atmosphere (11). Available polarographic instruments for detection of flowing samples accomplish deoxygenation by purging with another gas such as nitrogen or by passage of sample through a sulfite bed (12). For each of the above methods of oxygen removal, additional steps are required in the analysis procedure.

Constant potential pulse polarography (CPPP) has been found to eliminate the prerequisite step of oxygen removal for polarographic analysis, as was first demonstrated by Neuburger and Johnson (13). Hara and Nomura used a waveform similar in many respects to CPPP, called modified normal pulse polarography (MNPP). They used MNPP to detect barium and alkali metals in acidic solutions, though detection in the presence of dissolved oxygen was not shown (14-16).

While the signals recorded are typically anodic currents, these signals reflect reductive processes. The selectivity among species in solution is also based on the cathodic processes occurring at the electrode. Because CPPP is insensitive to dissolved oxygen for a judicious choice of detection potential, it is a technique which is readily applicable for polarographic analysis of flowing solutions (13, 17).

A differential method of MNPP was also developed, though it has not been shown in either oxygen-containing or flowing solutions (18). In this work, differential CPPP (DCPPP) is introduced and demonstrated for application in air-saturated solutions and in flowing streams. This

method offers an increase in selectivity over CPPP, as differential pulse polarography (DPP) does over normal pulse polarography (NPP) (19). This advantage of selectivity for DCPPP is shown as well as the quantitative nature of the method.

This thesis will show the quantitative application of polarography to flowing media without interference from the presence of dissolved oxygen using the method of CPPP. The detection limits for CPPP are improved by ca. one order of magnitude for batch analysis, and by nearly a factor of 1000 for flowing samples from the previous levels.

This research will also show the further development of the technique by using DCPPP in order to gain increased selectivity among analytes, while still maintaining freedom from interference from dissolved oxygen. Applications will also be presented which show that CPPP and DCPPP can be used to gain a degree of freedom from the limiting effects due to the presence of hydrogen ion in acidic solutions. Detection for DCPPP is shown at approximately the same concentration level as for CPPP, both in the batch mode and in a flowing stream.

CHAPTER 2. INSTRUMENTATION

This dissertation is based largely on instrumentation and therefore it is important to thoroughly explain the equipment used and the modifications made to the equipment. The basic information can be found in this chapter, whereas many of the effects resulting from the choice of specific instrumentation and variations in the instrumental settings will be discussed in the chapters relating specifically to those effects. Although the experimental arrangement varied over time, the majority of the work was done with the setup described here. Many of the changes and the reasons stimulating these changes will also be covered.

Equipment

The instrumentation used in this project is at the same time simple and complex. Polarography has been in use for many decades with instrumentation that has become standard. The instrumental system used for this work is shown schematically in Figure 1. It can be seen that the potentiostat was interfaced to a computer, lending a "high-tech" feel to the arrangement, though in reality the majority of the equipment can be found in any modern polarography laboratory.

At the heart of the instrumental scheme was the potentiostat. The model used for the largest part of this work was the Princeton Applied Research Model 174A Polarographic Analyzer. This instrument was developed in the early 1970s and has long been a standard workhorse in

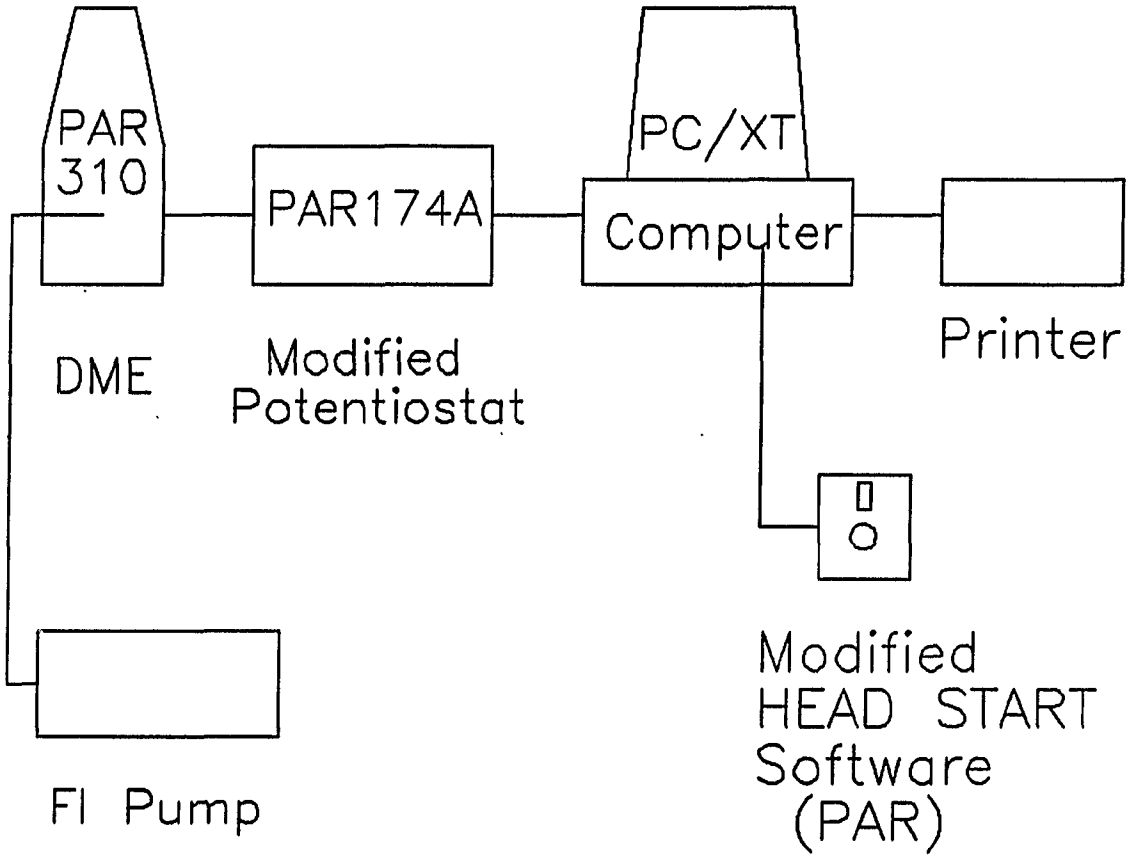

Figure 1. Schematic of instrumental apparatus

the polarography industry. The potentiostat was equipped to do DC polarography (DCP) and sampled DC polarography (SDCP) as well as the standard pulsed techniques; normal, reverse, and differential pulse polarography (NPP, RPP, and DPP, respectively). It was modified in our laboratory to also provide the constant potential pulse polarography (CPPP) waveform.

The polarographic cell was a Model 310 Polarographic Detector, also made by EG&G Princeton Applied Research. It was a solenoid-driven device, designed to dispense a measured quantity of mercury each time the solenoid was activated. This operation was in contrast to earlier models which allowed mercury to flow freely, with the mercury drop size determined by the choice of time delay before measurement. As in the earlier models, a drop knocker was used to dislodge the mercury bead prior to dispensing the next drop. This detector allowed the opportunity to purge the sample while it was in the analysis cell, and was manufactured with adaptations especially for flowing stream analysis.

Whereas the free-flow electrodes were known as dropping mercury electrodes (DME), the Model 310 Polarographic Detector in use for this work was the so-called static mercury drop electrode (SMDE). The difference between the SMDE and the DME was that the electrode size did not change after the solenoid passed a metered amount of mercury in the SMDE, as opposed to a constantly growing mercury drop electrode with the DME. This did affect the noise and current characteristics, as will be discussed in Chapter 8.

The computer was a Zenith Data Systems model Z-159-12, commonly

referred to as a PC-XT "clone." This model was driven by the 8088 CPU chip, one of many industry standards. The computer had a working area of 640K RAM and a clock speed of 8 MHz. It was equipped with a 8087-2 math co-processor chip and a 20-Mb hard drive for data storage. An Epson FX-86e dot matrix printer provided hard copies of all output.

The interface used was the National Instruments Model PC2A GPIB board. This was an IEEE driver, compatible with most equipment which can be interfaced to a computer. Software for the GPIB board was used as supplied by National Instruments and installed as per instructions supplied by EG&G PARC.

The pump used for the flowing stream work was a Rabbit HP from Rainin Instrument Co., Inc. It had a usable flow rate range of ca. 0.1 to 2.0 mL per minute. The arrangement used included a Rheodyne manual injection valve with a large sample loop of 2.0 mL, manufactured from 1.0 mm Teflon tubing. The flow volume between injector and detector was ca. 0.25 mL.

The flow cell used was part of the Model 310 Polarographic Detector from EG&G PARC. It consists of a small tube-like device mounted vertically on the end of the mercury capillary. Sample from the pump entered through the bottom and issued upwards from a nozzle-like opening, bathing the mercury drop. A hole drilled perpendicularly in the tube allowed fluid to flow from the mercury drop into the surrounding cell. The device is illustrated in Figure 2.

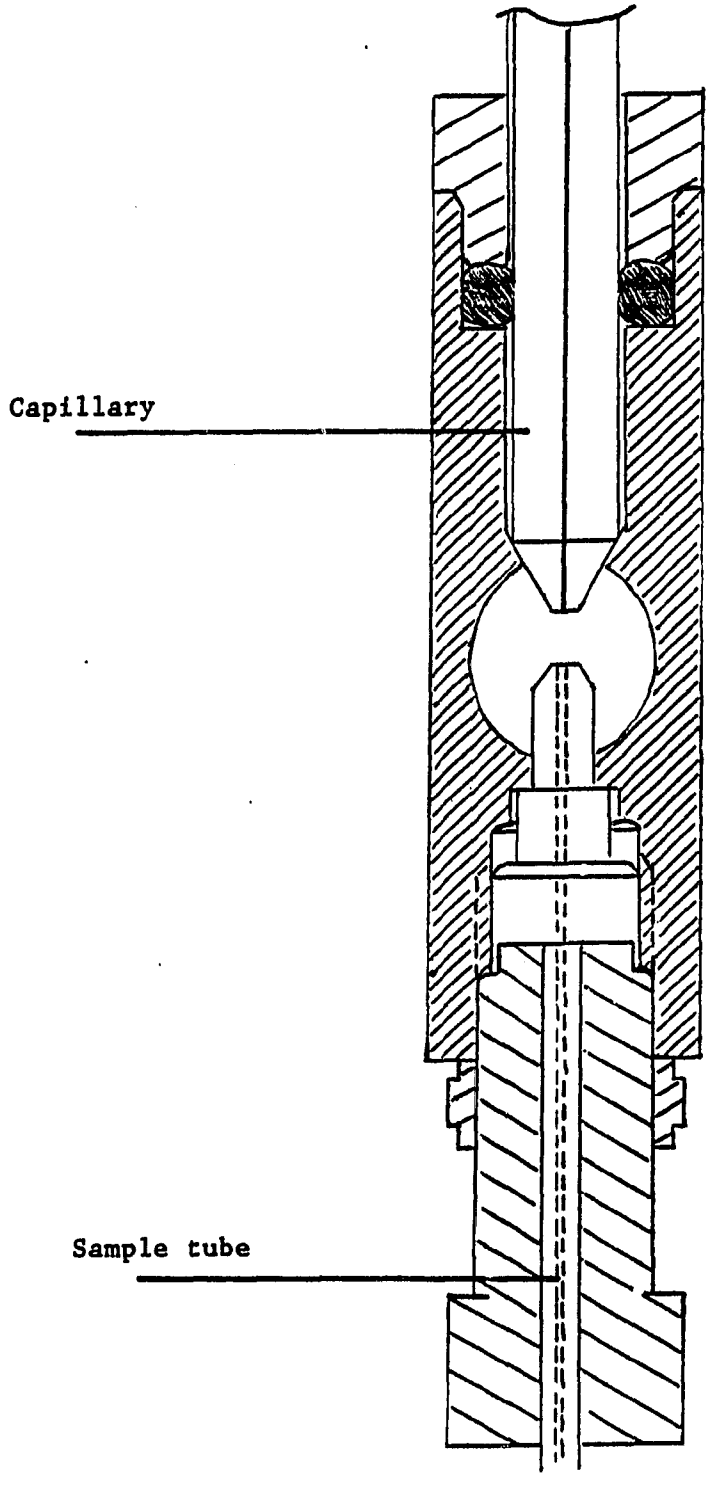

Figure 2. Diagram of flow cell

Modifications to Potentiostat

The potentiostat modified and used in this work was the Princeton Applied Research Model 174A Polarographic Analyzer. Although it was manufactured for DCP, SDCP, NPP, RPP, and DPP, it was not capable of providing a potentiometric waveform adequate for CPPP. However, the modifications were easily performed to allow generation of the CPPP waveform.

The CPPP waveform is shown in Figure 3c. It can be considered as being made up of two components, a ramping potential for most of the drop life and a brief pulse near the end of the drop life to a ramped potential raised by a specified potential increment. Measurement of current is made near the end of the potential pulse. It was found that both the ramp and pulse potential components were provided by the Model 174A. In addition the instrument provided the necessary timing and measurement features for CPPP (which are actually the same as for NPP and RPP).

It was found, upon consideration of the internal circuitry of the Model 174A, that the pulsed and ramped portions of the potential were generated separately within the potentiostat. It was also discovered that the ramped and pulsed components could be combined to form the newly synthesized waveform. Because the CPPP waveform could be reduced to a combination of two other techniques, both of which were provided in the Model 174A, the method of combining the pulsed and ramped components to form the CPPP input signal was attempted. Figure 3 shows the CPPP input signal and those for DCP and RPP. When one considers adding the ramp from DCP to the pulsed portion of the RPP signal, one can see that

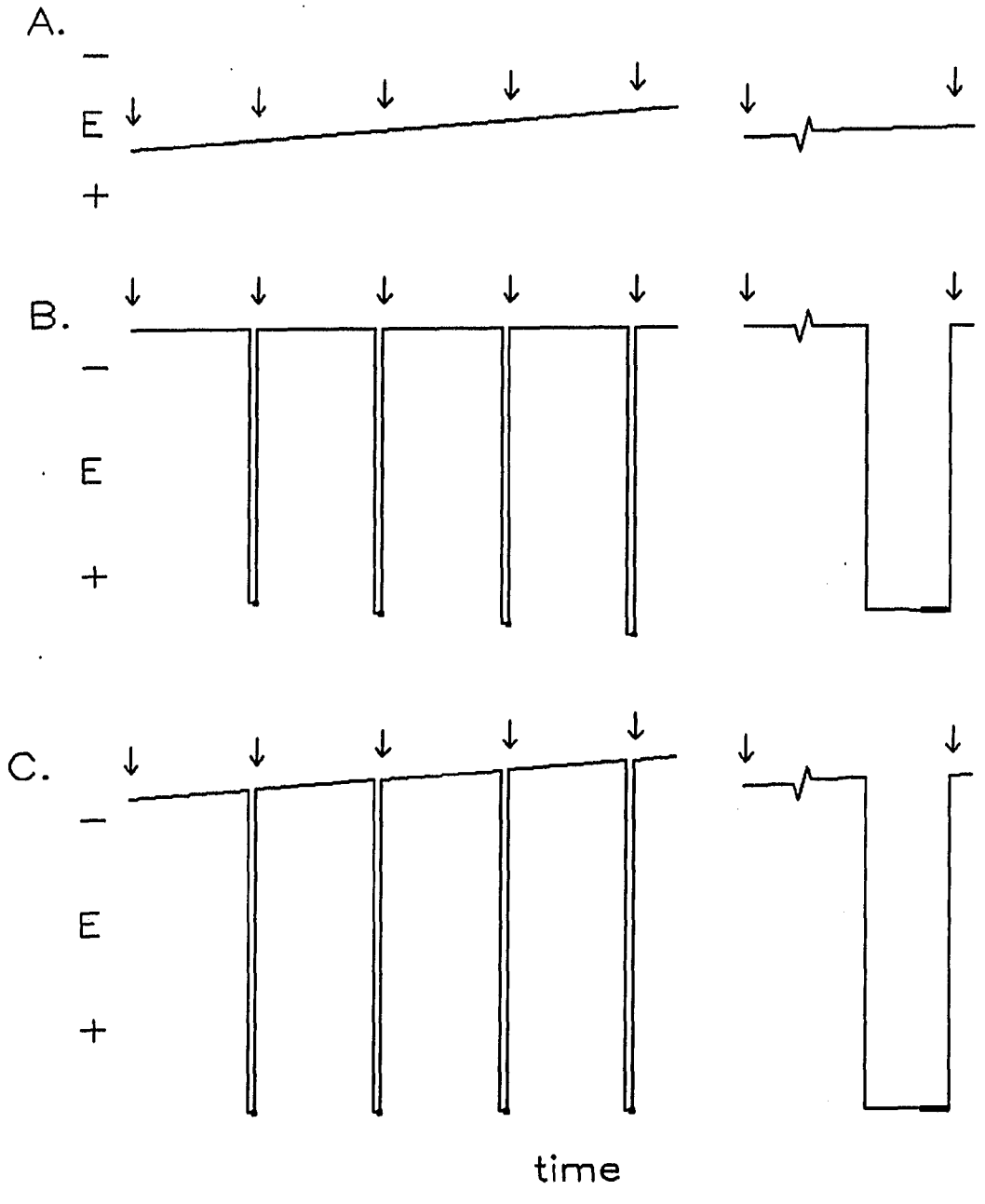

A. DCP B. RPP C. CPPP

Arrows denote drop fall, shaded portions represent periods of current sampling

Waveforms at right depict response during one drop lifetime

Figure 3. Applied potential waveforms for DCP, RPP, and CPPP

the CPPP waveform is produced.

The combination of the ramped and pulsed components of the potential output was accomplished instrumentally by inserting a 20 kΩ resistor (and necessary connecting wire) between test point TP102 and the lead connecting resistor R58 with pin 10 of interface J36 mounted on the rear panel. The addition of a switch to this connection allowed the Model 174A to be used either for CPPP or to be returned to its unaltered state. These modifications are illustrated in Figure 4, which is a partial electronic schematic of the Model 174A. The timing relationships of pulse application and current measurement for CPPP are the same as for NPP or RPP, i.e., the pulse is applied near the end of the drop life with a duration of 57 ms and current measurement is made during the last 16.7 ms of the pulse period.

The current response of the Model 174A potentiostat was originally intended for output to a chart recorder. Because we required that the data be transferred to the computer, an analog-to-digital (A/D) converter was used. For the data presented, the A/D converter used was that in the Model 273 potentiostat which had been interfaced to the computer in the early stages of this effort.

The initial design of the apparatus was built around the EG&G PARC Model 273 Potentiostat/Galvanostat. This instrument was easily interfaced both to the computer and to the polarographic detector. The software provided for the computer-interface potentiostat was the Head Start Electrochemistry Software by EG&G PARC. All of this equipment can be purchased as an integrated system and is sold by EG&G PARC.

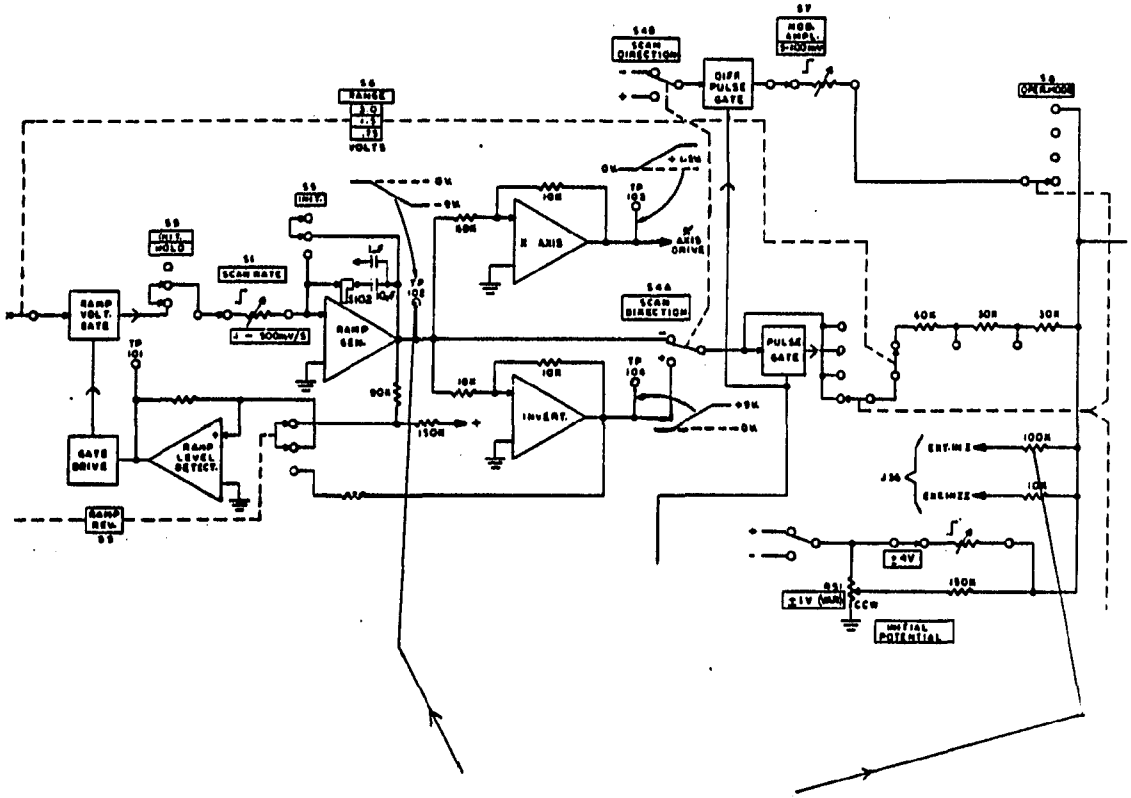

Figure 4. Partial schematic of Model 174A Potentiostat showing modifications necessary to allow CPPP operation

It was determined early in the research effort that the commercial Head Start software required major modification to accommodate the pulse polarographic techniques, and that the Model 273 potentiostat was incapable of performing these procedures without computer direction. The software was subsequently altered, vide infra, to allow each of the polarographic methods, including CPPP, to be performed.

It was apparent that the noise levels in these programmed methods were substantially higher than for methods which were "built in" to the potentiostat itself, e.g., cyclic voltammetry. After unsuccessful attempts at elimination of the noise source or sources, a change was made to the Model 174A potentiostat. The noise considerations are described in Chapter 8.

Software and Modifications to Software

The software used to direct the experiment from the computer was the "Head Start" Electrochemistry Software, version 1.2, from EG&G PARC. This package was intended for a wide variety of electrochemical techniques but unfortunately did not include pulse polarographic methods. The program was written in BASIC and was modified in this research to provide the necessary methods. Modifications made for work with the Model 174A potentiostat are given in Appendix I.

The changes to the software were made in two versions, each for a different purpose. The first set of modifications were those needed to direct operation with the Model 273 potentiostat, and the second version

was written to allow work to commence with the Model 174A. For the Model 273, commands to create the pulsed polarography waveforms were added. When the Model 174A was used, these potential waveforms were already part of the potentiostat function, so those commands were not necessary. The computer did need to be prompted to read the output of the Model 174A potentiostat through the A/D converter of the Model 273, however, so it was required that those instructions be added to the program. For both methods, modifications were made to customize the output for graphing as well as for computerized mathematical differentiation and smoothing of data. The quantity of the changes made (ca. 2 pages), when contrasted with the dimensions of the main program (ca. 60 pages of single-spaced type), indicates that the core of original program remained substantially intact.

The adaptations made for operation with the Model 273 consisted of commands to apply the appropriate potential bias and instructions to control the timing of the mercury drops, potential pulses, and current measurements. Many of the commands used were taken from a set of instruction codes for the Model 273, such as "BIAS" and "DISP," the control commands for applying a specified potential and dispensing a new mercury drop, respectively. The list of command codes was extensive, although some functional aspects were limited. In this case the program was altered to allow the computer to take over control of portions of the sequence for which it was better adapted than the potentiostat.

The most notable problem in the case of operation with the Model 273 was in recording a scan using timing sequences which did not repeat.

That is, if one desired to wait approximately one second after formation of the drop before applying a potential pulse, then execute a precise delay of ca. 40 ms before current measurement, this was not feasible with the Model 273. The only option by which to achieve the desired precision in timing was to take data points at regular intervals throughout the drop lifetime, i.e., one 16.7-ms measurement every 57 ms, applying a potential pulse only during the last 57 ms. This would have resulted in ca. 140 data points (of which only one would be of value) per drop, easily exceeding the storage limit of the Model 273 in a polarographic scan requiring more than 50 drops to cover the desired voltage range.

Because of the timing limitations of the Model 273 potentiostat described above, the computer was given control over the timing of the pulse application and current measurement. Although timing reproducibility could only be obtained on the order of 10 ms, due in large part to the IEEE interface, polarographic scans then became feasible, though characterized by a large amount of noise in the data. The increase in noise related to this irreproducibility in timing is described in Chapter 8 and was the chief reason for the substitution of the Model 174A potentiostat in place of the Model 273.

Changes made in the Head Start software to allow operation with the Model 174A included commands for the Model 273 to read the current output of the Model 174A, digitize the value, and report it to the computer. The current measured by the Model 174A is converted within the potentiostat to a potential in the range of -10 V to +10 V. This potential is the value recovered and digitized by the Model 273. A sample-and-hold

circuit in the Model 174A potentiostat retained the measured value which was read by the A/D converter. Because the timing of the potential pulse profiles and measurement step was established at the Model 174A potentiostat, irreproducibility of timing at the computer or Model 273 potentiostat was not a factor in the measurement.

Additional modifications were made to the program relating to data manipulation and storage. These were not affected when the substitution of potentiostats took place as they were unrelated to the measurement process. These instructions altered the format of the stored values such that they could be read into data manipulation and smoothing files and also into Grapher, a commercial graphics software package used to view the resulting scans. Further modifications allowed the user to inform the computer of changes in potential scan rate and current range settings at the Model 174A. The program then manipulated the measured values appropriately such that the data output reflected actual values and consistent units.

CHAPTER 3. POTENTIAL WAVEFORMS AND CURRENT RESPONSE IN POLAROGRAPHY

Polarography has developed remarkably since its first application in 1922 (6). The most significant modifications to the technique in this author's opinion are the variations introduced in the applied potential waveform. Through these advances, gains have been realized in sensitivity, in selectivity, and in discrimination against unwanted signals, to name only a few aspects. The more common variations are discussed in this chapter.

I have already stated that constant potential pulse polarography (CPPP) offers discrimination against interference from oxygen reduction, yet affords analysis of metals reduced in the same potential range as oxygen. To understand why CPPP is different from other existing polarographic methods in this regard, it is instructive to look first at the various potential waveforms applied in each of these polarographic methods.

DC Polarography

The oldest method, DC polarography (DCP), was the original method used by Heyrovsky (6). It utilizes a ramped potential which changes linearly from positive to negative polarity for a cathodic process, shown in Figure 5. As the applied potential is increased in reducing power, species in solution are detected when their reduction potentials are exceeded. The current resulting from the electrochemical reduction of

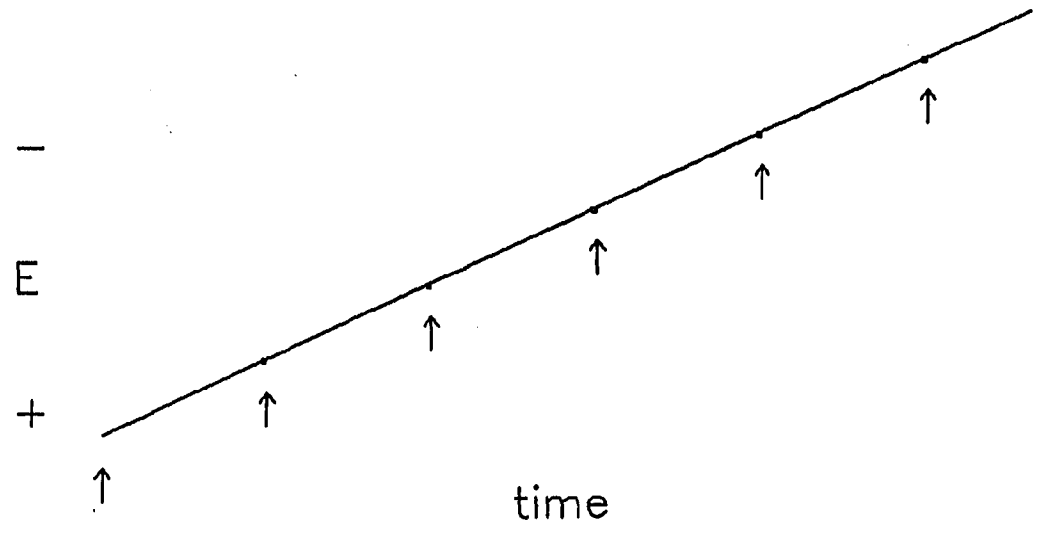

Shaded dots indicate SDCP sampling time

Figure 5. Applied potential waveforms for DCP and SDCP

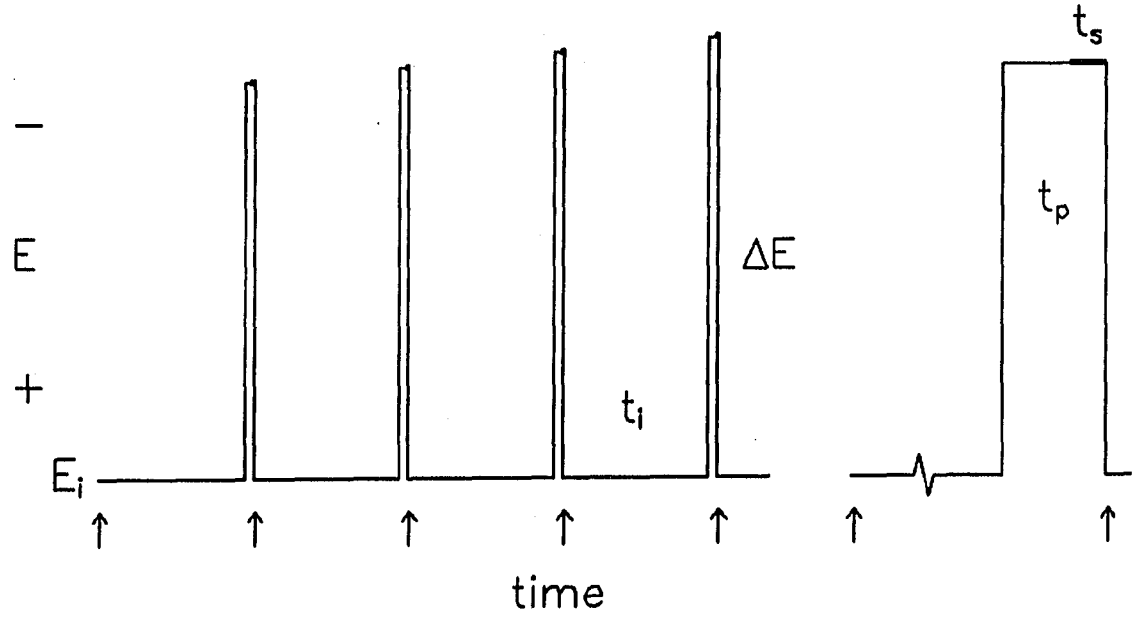

Shaded portions indicate time of current sampling

Detail at right shows response during one drop lifetime

Figure 6. Applied potential waveform for NPP

each species is monitored continuously throughout the life of the mercury drop.

The response from DCP is a current which rises and falls with the formation and loss of each mercury drop. As the drop forms, the current increases, finally reaching its maximum value at the end of each drop lifetime. This repetitious modulation in current is characteristic of DCP.

The current response over a scan of potential is described in the following section, and can be distinguished from sampled DC polarography by the repetitive current pattern for each mercury drop in DCP.

Sampled DC Polarography

The development of the sampled DC polarographic technique (SDCP), also known as Strobe or Tast polarography (20) was an improvement to DCP. A report on the first instrument capable of performing this method appeared in 1957 (21). The potential waveform for SDCP is shown with that for DCP in Figure 5. The waveform is identical for both techniques, but differences exist in the method of signal measurement. The current is sampled in SDCP for only a short time interval, e.g., 16.7 ms, very close to the end of the drop life, instead of monitored continuously as in DCP. The interval of 16.7 ms corresponds to 1/60 second, a value chosen to match a full cycle of the 60-Hz AC power supply, so that noise arising from this source is minimized.

The choice to measure current at the end of the drop lifetime

ensures that the maximum current is taken for each drop, since the current increases with increasing electrode area. This effect is described by the Ilkovic equation for the dropping mercury electrode (DME) and is discussed in the section below on normal pulse polarography. The act of sampling the current once per drop eliminates the repetitious modulation of current which occurs in DCP, presenting a major advantage in appearance for the sampled method.

Normal Pulse Polarography

An advance over the two DC techniques is normal pulse polarography (NPP), which grew out of the work on square wave voltammetry done by Barker and Gardner (22). The applied potential waveform is illustrated in Figure 6 and is characterized by pulses to potential values which progress from positive to negative polarity, the same direction as in DCP and SDCP. These pulses are superimposed on an unchanging background potential and are applied so that a pulse occurs near the end of each drop lifetime. The duration of the pulse, t_p, is commonly about 60 ms, of which the last 16.7 ms, t_s, is used to sample current. The delay of ca. 40 ms allows for non-faradaic current to dissipate (23). The initial potential, E_i, is usually chosen so that no faradaic processes are occurring. This value is usually slightly positive of the first wave for oxygen reduction, ca. +0.2 V vs. Ag/AgCl.

Let us look now at the response throughout the potential range for these polarographic techniques. This is discussed in the polarography

literature, and readers are encouraged to consult several texts for a more detailed discussion of the response (2-5, 24). The polarographic response for a solution with dissolved oxygen present is shown in Figure 7; this figure will be useful for reference throughout the following discussion.

Beginning with an applied potential > 0 volts (V) vs. Ag/AgCl, one scans over the potential range in the negative direction. Positive of 0 V there is usually little or no faradaic current. The reduction of oxygen occurs at approximately 0.0 V as described by the following chemical equations:

Acidic solution: $O_2 + 2H^+ + 2e^- \rightleftharpoons H_2O_2$

Basic solution: $O_2 + 2H_2O + 2e^- \rightleftharpoons H_2O_2 + 2OH^-$

The oxygen reduction pathway is dependent on pH and will follow one or both of the above equations.

When the potential reaches approximately -0.8 to -1.0 V vs. Ag/AgCl, a second reaction occurs which is also dependent on pH. This reaction is the reduction of hydrogen peroxide, a product of oxygen reduction.

Acidic solution: $H_2O_2 + 2H^+ + 2e^- \rightleftharpoons 2H_2O$

Basic solution: $H_2O_2 + 2e^- \rightleftharpoons 2OH^-$

The major source of hydrogen peroxide in solution is usually the reduction of oxygen, so the reduction of the peroxide also reflects dissolved oxygen in solution. Reduction of oxygen and its peroxide product continue as the applied potential is increased to larger negative values.

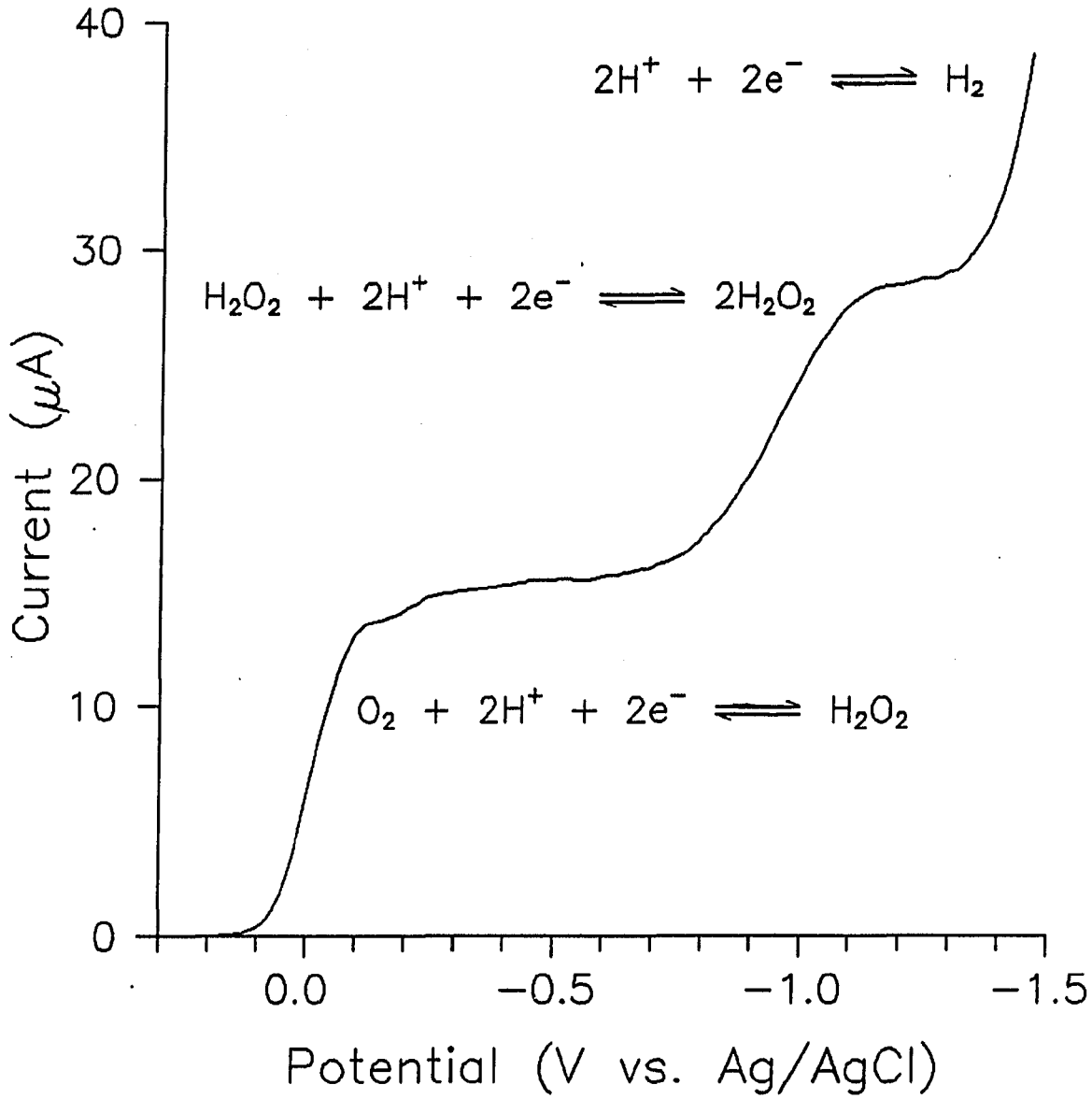

Unpurged solution (no metals) with 0.1 M KNO_3 and 0.001 M HNO_3

Figure 7. Polarogram of solution with dissolved oxygen present (NPP)

A large amount of current is generated from the two reductions due to oxygen in solution. Because of this and the fact that the two reduction waves cover ca. 75% of the polarographic working range, the oxygen in a sample is virtually always removed prior to analysis. Although this step is time-consuming, it is necessary for detection of metals in nearly every circumstance (25-28).

If one scans the potential to larger negative values, one comes to the limit of the polarographic analysis window. The limit is determined in acidic solution by reduction of hydrogen ion. The potential for this reduction is pH-dependent and can occur at potential values as positive as ca. -1.1 V vs. Ag/AgCl. In basic or neutral solutions it is reduction of the solvent or electrolyte cation which determines the negative limit of the analysis range. For example, potassium is a commonly used electrolyte cation which is reduced at -1.9 V vs. Ag/AgCl.

If one were to scan in the opposite direction for anodic processes, it is the oxidation of the mercury itself which limits the potential window at ca. +0.5 V vs. Ag/AgCl. The presence of hydroxide in basic solutions brings the potential of Hg oxidation to a more negative value, +0.3 to 0.0 V vs. Ag/AgCl, depending on pH, thus narrowing the analysis window.

It was stated that NPP offers an increase in sensitivity over DCP. The reasons for this advantage are treated in detail in modern polarography texts (4, 5) and will be discussed only briefly here. In order to describe the basis of a sensitivity increase, it is necessary to set down the equations which describe the relationships between current, time, and

rates of mass transport, and to also discuss sources of current which yield analytically useful signals.

The current used for analysis with the DME is the potential-independent current measured well negative of the reduction potential of a metal, and is described by the Ilkovic equation.

$$i_d = k\ n\ F\ D_{ox}^{1/2}\ m^{2/3}\ t_m^{1/6}\ C_{ox}^b$$

i_d -- diffusion current for DME, Amps

K -- constant

n -- number of electrons transferred

F -- Faraday, 96485 C/eq

D_{ox} -- Diffusion rate for oxidized species, cm^2s^{-1}

m -- mass flow rate of mercury, g/s

t_m -- time of measurement, sec after drop formation

C_{ox}^b -- bulk solution concentration of oxidized species, M cm^{-3}

The current is monitored continuously in the case of DCP, with the instantaneous value at any time given by substitution of t_m into the equation. Measurement in SDCP is made at a single t_m at the end of drop life, yielding a current which is always equal to or greater than the value obtained in DCP by virtue of the choice of measurement at the latest possible time in drop life for SDCP.

The relationship used for NPP to describe the current response as a function of time is the Cottrell equation.

$$i_{lim} = n\ F\ A\ D_{ox}^{1/2}\ \pi^{-1/2}\ t_d^{-1/2}\ C_{ox}^{b}$$

i_{lim} -- limiting current, Amps

n, F, D_{ox}, C_{ox}^{b} -- as used above

A -- area of the electrode, cm^2

t_d -- time delay after initiation of potential pulse prior to measurement, sec

This equation gives the limiting current for the case when the initial potential is positive of the reduction potential of a metal and the pulse potential is a value more negative than the reduction potential. The time delay, t_d, before current measurement is usually about 40 ms after application of the potential pulse.

The ratio of current measured for NPP to SDCP is obtained by dividing the Cottrell equation by the appropriate form of the Ilkovic equation (19).

$$\frac{i_{NPP}}{i_{SDCP}} = \frac{t_m^{1/2}}{(7/3)^{1/2}\ t_d^{1/2}}$$

The constant is derived from other constant terms in the Cottrell and Ilkovic equations. When the values of time typically used in this research are substituted into the equation, i.e., t_m of 1 s for SDCP and t_d of 40 ms for NPP, the current sensitivity enhancement obtained for NPP over SDCP is a factor of 3.3. Applications for which terms in this equation are optimized yield ratios in favor of NPP by a factor of 6 to 7 (19). This demonstrates the sensitivity increase which can be obtained

with NPP in comparison with SDCP. It should be noted that comparison with DCP would yield a ratio even more in favor of NPP, since currents measured in DCP are never greater than those measured for SDCP.

There are more factors to consider than the increase in current measured. Not only is the signal increased when going from DC methods to NPP, but there is also a decrease in the level of noise. The total signal measured in polarography is usually regarded as having two major components; faradaic and non-faradaic current. It is the faradaic signal which is of chief analytical interest, since it is the current coming from redox processes at the electrode. It is this faradaic current which was expressed in the Ilkovic and Cottrell equations.

The non-faradaic signal which must be considered consists largely of charging current, or capacitive current. This is current which is independent of the trace concentration of any analyte, but which results from the fact that the electrode/solution interface acts like a capacitor. A change in the potential of one side of the interface, e.g., the electrode, results in a change in the charge at the other side, creating a net current flow. A change in the size of the electrode creates an increase in the surface area of the electrode/solution interface, requiring more charge to keep the charge density at the interface constant.

The major causes of charging current at the DME are changes in the applied potential of the electrode and changes in electrode size. Comparing NPP and DC methods, the rate of change in applied potential is identical for DCP, SDCP, and NPP during the time of current measurement, implying no difference in charging current due to changes in applied

potential. This overlooks the application of a potential spike for NPP, which increases the charging current level. The time delay employed before measurement, i.e. 40 ms, allows this current to dissipate before sampling occurs (23). If the potential pulse for NPP was to a constant potential, the magnitude of which would be incremented slightly from one drop to the next, then the charging current portion of the signal would be reduced relative to DC methods.

The effect of drop growth on current in SDCP and NPP is minimized by sampling the current at the end of the drop lifetime, when the rate of change in area is small compared to earlier in the drop life. Current in DCP shows a larger capacitive current due to sampling during the early part of the drop lifetime. The current for NPP is sampled under the same conditions as for SDCP, so no benefit is realized in discrimination against charging current. Even so, NPP is usually regarded as having limits of detection at the DME which are one to two orders of magnitude better than for DC methods (29).

It should be noted that all of the equations used in this chapter have been derived for the DME. The static mercury drop electrode (SMDE) was used in the research undertaken here. The equations describing current in the case of the SMDE are not the same as for the DME, due to differences in drop growth rate. For the SMDE, the drop is no longer growing continuously, like the DME. Instead, the only period of drop growth is at the beginning of the drop lifetime. Thus, the terms in the Ilkovic equation based on drop growth rate are no longer precisely applicable. They are used in this chapter for comparison purposes,

however, because they do describe the basic phenomena which must be taken into account. The major advantage of the SMDE is that the drop does not change in area during the measurement interval near the end of drop life. This eliminates any charging current due to growth of the drop.

Reverse Pulse Polarography

A variation of the pulsed technique is reverse pulse polarography (RPP), for which the potential waveform is shown in Figure 8. This technique was introduced by Oldham and Parry (30), and was named scan-reversal polarography at the time. In a comparison of applied potential waveforms for RPP and NPP, one notices that the potential pulses are now incremented in the positive direction and that the potential value employed during drop formation for RPP is in a region where faradaic processes are likely to occur.

The reversal of the direction of the potential scan and the fact that redox processes are often occurring during formation of the drop indicates that measurements in RPP will often consist of both reductive and oxidative processes. Oxidative processes are normally not seen in NPP or DC methods, with the exception of measurements at large positive potentials. The reason for this is that most metal ions in solution are already in their highest oxidation states. For RPP, however, reduction of these metal cations takes place during the largest part of the drop lifetime, before the application of the potential pulse used for measurement. When the detection pulse is applied, the potential can be positive

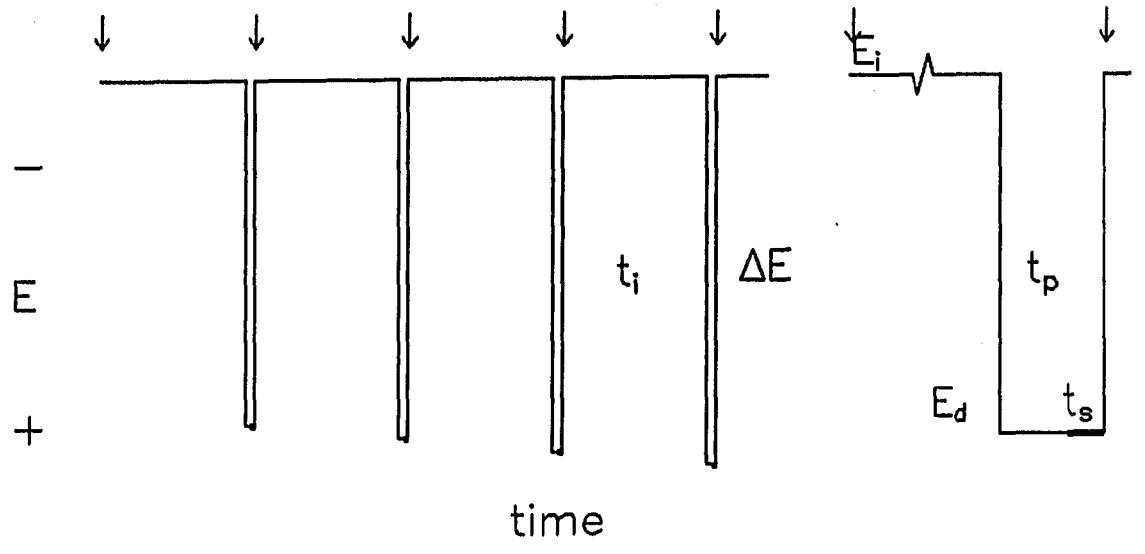

Figure 8. Applied potential waveform for RPP (shading shows time of sampling and detail at right illustrates waveform for one drop lifetime)

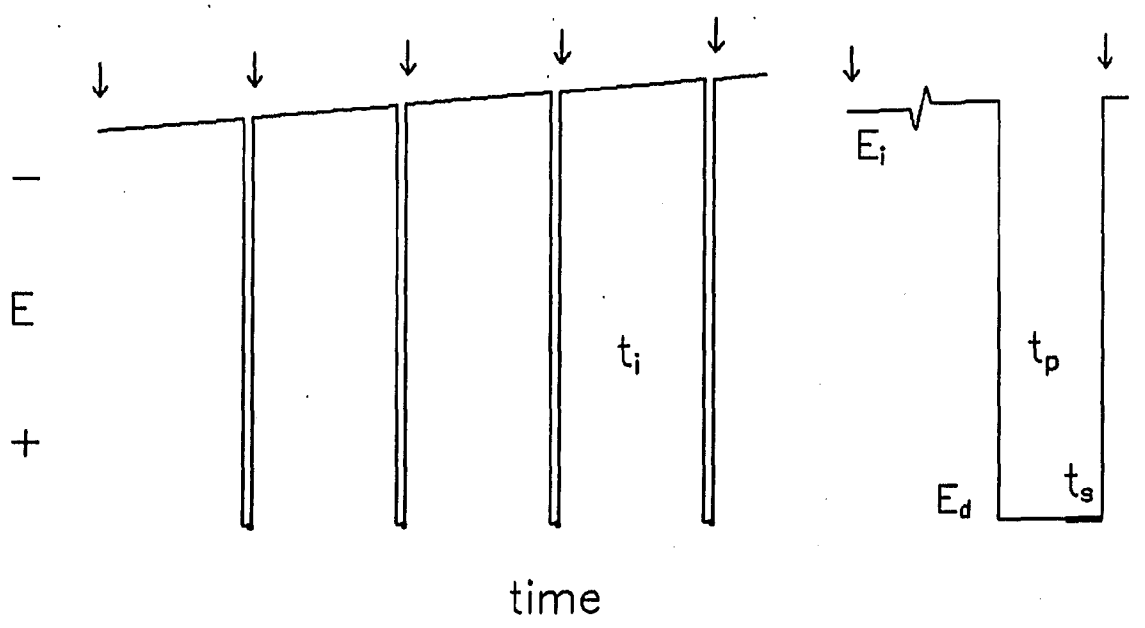

Figure 9. Applied potential waveform for CPPP (shading shows time of current sampling and detail at right shows response for one drop lifetime)

of the oxidation potential for the metal, causing oxidation of the metal which was earlier reduced.

It must be noted that under certain conditions, e.g., when the detection potential is > 0.0 V vs. Ag/AgCl, RPP is insensitive to the presence of oxygen, due to the irreversibility of oxygen at mercury. Because the potential, E_i, is constant during the majority of the drop life, the only selectivity offered by RPP is in that same potential window, i.e., > 0.0 V vs. Ag/AgCl. Although the selectivity is limited, the use of an amperometric form of RPP, reverse pulse amperometry, has been demonstrated for detection of reducible metals without interference from oxygen in flow-injection and liquid chromatographic analyses (31), and in cation-exchange chromatography (32).

Sensitivity in RPP for metals which are reduced and then measured during the oxidative pulse is less than for NPP. When the potential pulse is less than 5% of the drop lifetime, the current ratio versus SDCP at the DME is approximated by the following equation.

$$\frac{-i_{RPP}}{i_{SDCP}} = \frac{n_{Red}}{n_{Ox}} \left(\left(\frac{3\ t_1}{7\ t_2} \right)^{1/2} - 1 \right)$$

n_{Red} -- number of electrons involved in reduction reaction

n_{Ox} -- number of electrons involved in oxidation reaction

t_1 -- time before application of potential pulse

t_2 -- delay time between pulse application and signal measurement

Derivation of this equation is given in a paper by J. Osteryoung and

Kirowa-Eisner, who reviewed the theory of the method and assigned it the preferred name, reverse pulse polarography (33). Substitution of the same time parameters that were used for the NPP comparison earlier yields a sensitivity ratio of 2.3, indicating an anodic current for RPP 2.3 times greeter than the cathodic current for SDCP. This corresponds to 70% of the sensitivity of NPP for the same conditions.

Constant Potential Pulse Polarography

The potential waveform used in this research was constant potential pulse polarography (CPPP). The initial published work with this method indicated reduced capacitive current (34), but did not recognize the freedom of interference from oxygen reduction.

Figure 9 illustrates the applied potential sequence, which does have similarities to the other polarographic techniques. The potential ramp in the negative direction is similar to DCP, and the pulse of positive polarity is seen in RPP. During most of the drop lifetime, the applied potential is increasing in the negative direction. Toward the end of drop life, a positive pulse is applied which brings the potential to a constant value. Current measurement is made during the last portion of the pulse, allowing time for charging current to decrease.

One can more easily visualize these processes in CPPP by referring to the NPP wave for an oxygen-containing solution, as was shown in Figure 6. Notice first that the potential at which the measurement is made, E_d, is chosen such that there is no current from any faradaic process. This

potential value will normally be > 0 V vs. Ag/AgCl.

When the scan in the negative direction begins, the first reduction encountered is that of oxygen to hydrogen peroxide. Since the current measurement is made on the following potential pulse, E_d, and not at the potential where the oxygen reduction is taking place, E_i, one does not record any cathodic current for the reaction. However, one must be aware of any reaction products that would produce current at the detection potential. From the equations for oxygen reduction given above, one sees that hydrogen peroxide is formed by oxygen reduction in acidic conditions. The formal oxidation potential for H_2O_2 is ca. +1.4 V vs. Ag/AgCl, so no oxidation of hydrogen peroxide will take place at the measurement potential.

In basic solution an additional product is formed, the hydroxide anion. The oxidation described occurs at ca. +0.1 V vs. Ag/AgCl when hydroxide is present.

$$2OH^- + Hg \rightleftharpoons Hg(OH)_2 + 2e^-$$

Because the oxidation potential of this reaction is dependent on solution pH, anodic current may result, depending on the pH and on the choice of detection potential. If the detection potential is carefully chosen and if the solution to be analyzed is not highly basic, no current will follow from either oxygen or its reaction products in the potential region where a large oxygen reduction current normally interferes.

The second polarographic wave, the reduction of hydrogen peroxide, results in formation of water or hydroxide, dependent on pH conditions.

Water is not oxidized at the detection potential of the CPPP waveform, so if conditions are chosen to avoid high alkalinity, no interference is noted.

It can be seen from this that the presence of dissolved oxygen is not a problem to the technique of CPPP. It remains to be seen, however, how materials of interest are determined. In this regard, the method is comparable to RPP, where a metal is reduced early in the drop lifetime to an amalgam within the mercury drop and is then oxidized from the electrode at the measurement step. The currents recorded are usually anodic as they represent oxidative processes.

The technique of constant potential pulse polarography (CPPP) has been used to gain freedom from interference due to reduction of dissolved oxygen, as demonstrated by Neuburger and Johnson (13). The technique was further extended to air-saturated flowing samples (13, 17).

The magnitude of current resulting for CPPP is the same value as for RPP, since both processes measure an anodic signal resulting from a previous cathodic process at the drop.

$$\frac{-i_{CPPP}}{i_{SDCP}} = \frac{n_{Red}}{n_{Ox}} \left(\left(\frac{3\ t_1}{7\ t_2} \right)^{1/2} - 1 \right)$$

The sensitivity is therefore expected to be ca. 70% of that for NPP, though signals for CPPP are anodic, instead of cathodic as in NPP.

Visual presentation of data for CPPP is done in a slightly different manner than for the other polarographic methods. The current measured is usually plotted against the detection potential, but for CPPP this

potential is unchanging. The potential which is scanned is the applied potential prior to the detection pulse. It is actually the value of the scanned potential which determines which species are measured in the later detection sequence, so I have chosen in this thesis to plot current vs. the scanned potential. Secondly, because the anodic currents measured represent reductions occurring at the previous potential, I have also chosen to plot this current in the positive direction in order to mimic a reductive response. Data from CPPP will be presented as shown in Figure 10.

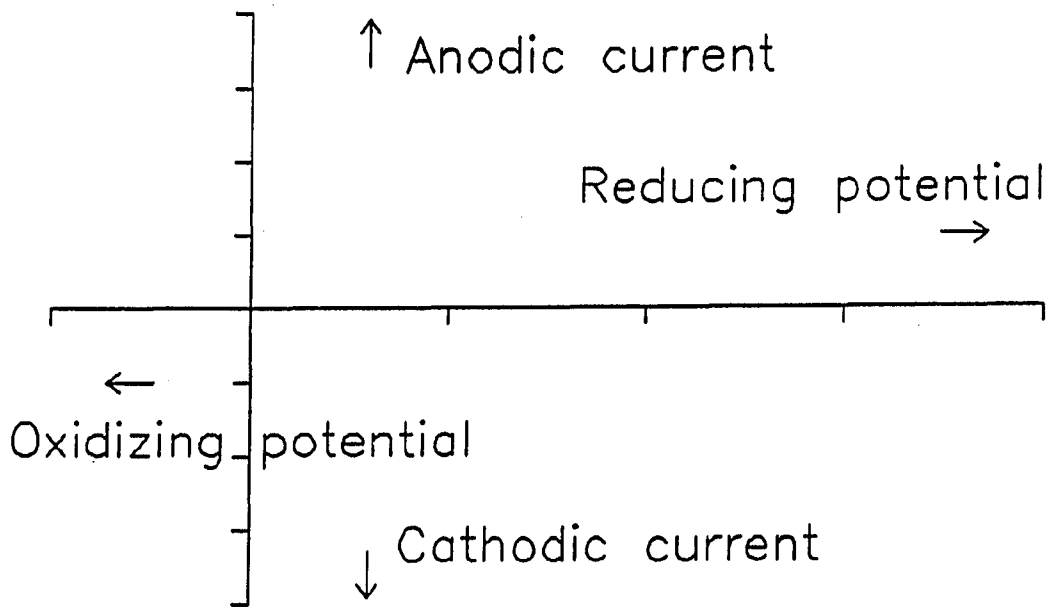

Figure 10. Axes used for presentation of CPPP data

CHAPTER 4. EXPERIMENTAL PARAMETERS

The use of constant potential pulse polarography makes polarographic analysis much less time-consuming. The chief benefit of the technique compared to the more traditional methods is the elimination of the oxygen-removal step. According to manuals accompanying commercial instruments, this is only a four-minute process under normal conditions (35). In this laboratory it was found that even an eight-minute purge step left a small oxygen wave which would interfere with certain trace metals. Others report using still longer purging times (14-16, 18).

The other requirement is the same for all electrochemical techniques, the necessity of having an acceptable ionic strength, which usually means adding some supporting electrolyte. These electrolytes are chosen to avoid any interference, i.e., they cannot be electroactive in the potential region under investigation. Potassium nitrate was used here, since potassium cation is reduced at -1.9 V vs. Ag/AgCl at mercury and nitrate anion is not electroactive in the working range.

Any acid, base, or buffer used should also be inactive at the mercury electrode. For these studies nitric acid was used, because the nitrate ion is not active. A phosphate buffer was also used at several pH values. The phosphate ions, PO_4^{3-}, HPO_4^{2-}, and $H_2PO_4^-$, are also electroinactive (2). The cation used in the salts was potassium. The other electrolytes used were tetraalkylammonium salts, chiefly tetraethylammonium hydroxide. The tetraethylammonium cation is not reduced prior to -2.2 V vs. Ag/AgCl. All chemicals were used as received

from Aldrich, Baker, Fisher, Fluka, and Mallinckrodt.

The reference electrode was the saturated silver/silver chloride electrode and all potentials given in this work are relative to the Ag/AgCl reference (0.222 V vs. NHE). Capillaries used for the SMDE were cleaned and siliconized following the procedure given in the instrument manual (35). The polarographic detector was used on the small drop size.

One must also consider the parameters in the applied potential waveform, in order to optimize response and guarantee freedom from interference. The factors governing effect of changes in the waveform are discussed in the following section.

Effect of Detection Potential on Current Response

The choice of detection potential, E_d, is critical to the successful application of CPPP. A single detection potential is used in the waveform, so the processes occurring at that potential are reflected in every measurement. To avoid any unwanted signals, detection must be in a potential region having no interference from faradaic processes. The basis for choosing a detection potential is the avoidance of interference, primarily from oxygen, hydroxide, or chloride.

Oxygen

The most obvious region to be avoided when choosing a detection potential for analysis of a solution saturated with oxygen is the range where oxygen reduction takes place, negative of ca. +0.0 V vs. Ag/AgCl.

This is in itself a strict limitation, because the working range of the mercury electrode is from ca. +0.5 V to -2.0 V.

The effect of using a detection potential where oxygen is reduced is recognizable. The use of such a potential does not render the method impotent since for a large part of the analysis range the baseline will remain constant, though non-zero. Interferences from oxygen do result at certain potentials, however, and it is important to identify those processes and their effects.

The wave for oxygen reduction occurs at about 0.0 V vs. Ag/AgCl, as was shown in Figure 7. The reduction is detectable at potentials as positive as +0.25 V, causing the current measured to be slightly cathodic (in the negative direction for these CPPP scans). At the beginning of the potential scan, the cathodic current decreases slightly, even though more oxygen is reduced at these potentials. The reason for this decrease can be found in the diffusion characteristics and in the fact that the current measurement does not take place at the more strongly reducing potential, but back at the more positive initial potential, e.g., +0.25 V for this discussion. One can see that more oxygen is reduced as the potential becomes more negative by looking at the Nernst equation.

$$E = E^{o} - \frac{0.0591}{n} \log \left(\frac{[Red]}{[Ox]} \right)$$

One can see that the equilibrium expression in the log term is shifted in favor of the reduced form, hydrogen peroxide, when the potential becomes more negative.

The increased reduction of oxygen as the potential is scanned depletes the diffusion layer more rapidly than does operation at the initial value of +0.25 V. Because the diffusion layer surrounding the electrode is depleted to a greater and greater extent as the potential becomes more reducing, the apparent concentration of reactant at the drop is slightly less when the potential is pulsed back to the measurement value than it would be if the potential were held at the same measurement potential during the whole of drop life.

This effect on the diffusion layer is illustrated in Figure 11. At point B in the scan, some reduction takes place, but the equilibrium does not favor complete reaction. As the potential is scanned in the negative direction to points C, D, or E, the reaction takes place to a greater extent. Note that the concentration at the drop is now less than for point B. The reduction current would therefore be expected to be less than it was previously due to the decreased surface concentration when the potential is pulsed back to the value at point B, and current measurement made after a short delay.

Although it is possible that oxygen could react to form hydroxide, which allows the oxidization of mercury at the positive detection potential, this result can be avoided by the use of a buffer at low pH. In a highly buffered solution, sufficient hydrogen ion will be present to react with hydroxide so that little or no hydroxide will be produced. Any hydroxide that is produced will combine with the local excess of hydrogen ion and not interfere.

The only source of current expected from the choice of a detection

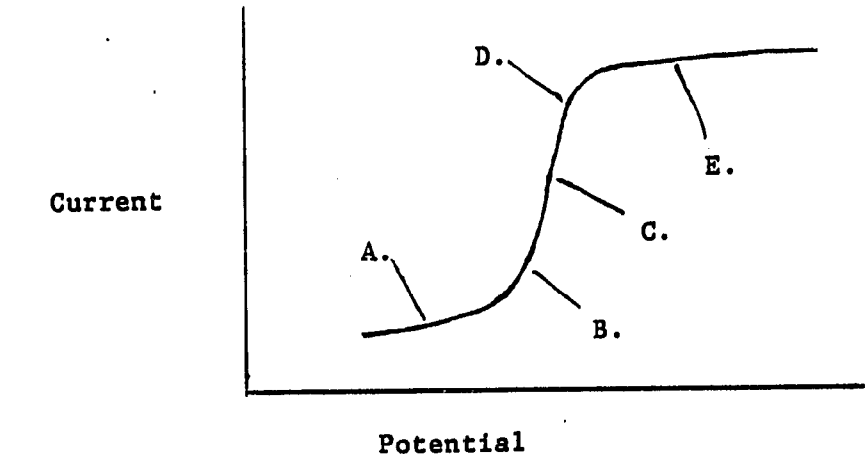

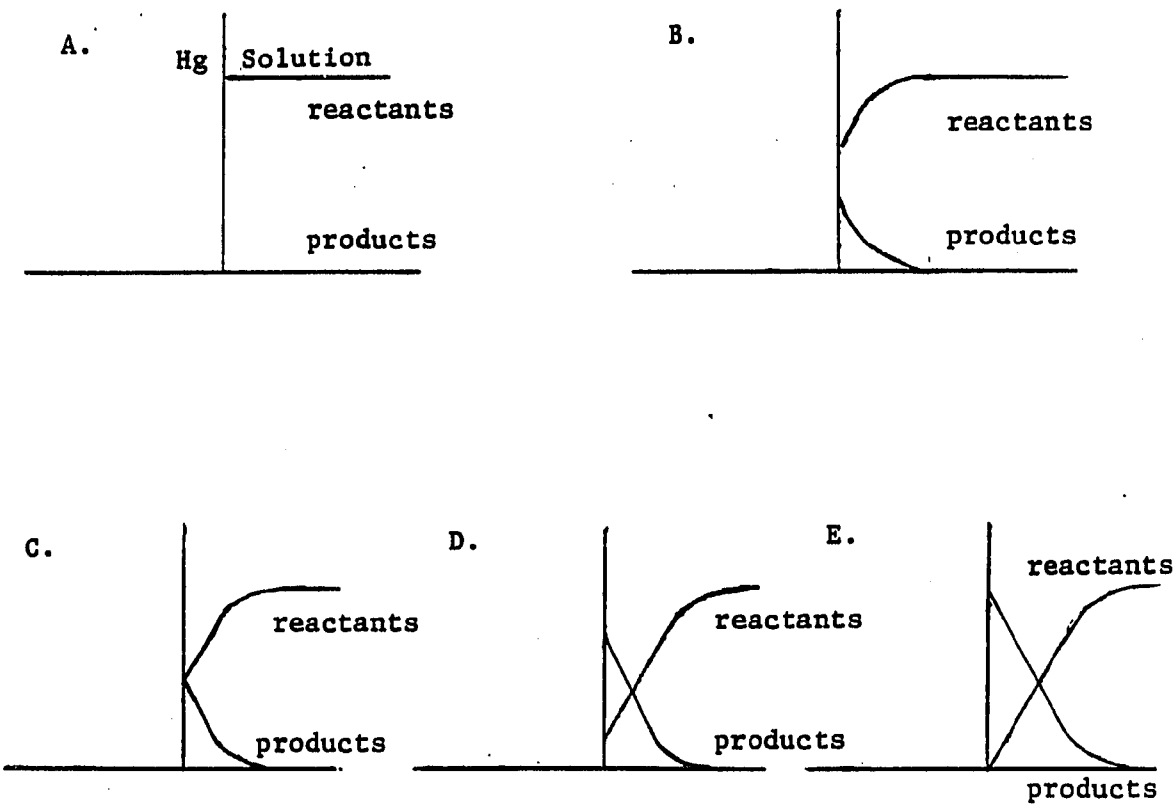

Figure 11. Concentration profiles at the diffusion layer for various potentials near the half-wave potential

potential on the positive edge of oxygen reduction is due to the slight reduction of oxygen. When the potential is scanned further into the reduction wave, the current should decrease due to depletion of oxygen at the electrode surface. The current becomes constant as the region of mass-transport limited oxygen reduction is reached. These effects are shown in Figure 12.

It is interesting to note that as the potential reaches the reducing power necessary to further reduce oxygen, i.e., reduction of hydrogen peroxide at -1.0 V vs. Ag/AgCl, no effect is seen in the measured signal. I believe that this is evidence that oxygen is the species measured at the detection potential.

Reaction of hydrogen peroxide at the electrode does not directly consume any more oxygen, so the reduction of peroxide does not affect the local concentration of oxygen. On the other hand, if hydroxide was produced, an increase in anodic current would result, as discussed in the section below. This hydroxide, however, is consumed when sufficient quantities of hydrogen ion are present.

Further confirmation of the dependence of the current on oxygen alone is shown by the polarogram of a solution from which oxygen has been purged, in the same figure, Figure 12.

Hydroxide

Hydroxide gives an oxidative signal beginning at ca. +0.1 V vs. Ag/AgCl. The interference caused by hydroxide can usually be avoided by the choice of low pH. Because the potential of the mercury oxidation is

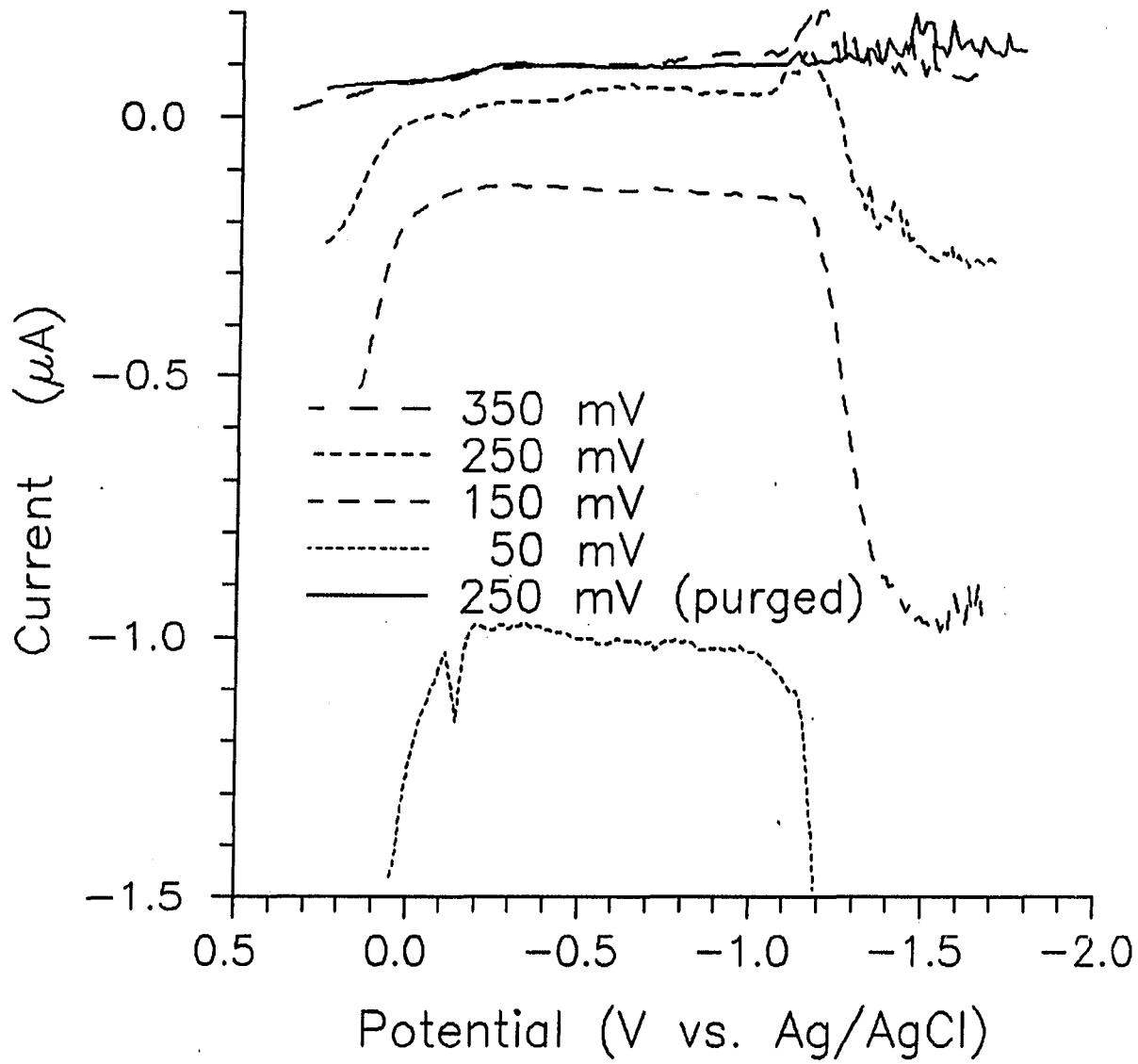

Solutions contain 0.1 M KNO_3 and were buffered at pH 1.84 with KH_2PO_4 and H_3PO_4 at concentrations of ca. 0.09 and 0.002 M

Figure 12. Effect of CPPP detection potential on the contribution of oxygen reduction to signal

shifted negative by the presence of hydroxide, and the amount of hydroxide present can be controlled by working in acidic conditions, the choice of detection potential value is not usually altered to reflect concern over hydroxide. In any case it is wise to be aware of the signs indicating the presence of hydroxide.

To avoid interference from hydroxide, one must be concerned with any reaction that affects hydroxide concentration. Reduction of oxygen and hydrogen peroxide are two major sources of hydroxide. Unless an adequate concentration of hydrogen ion exists, the hydroxide produced will not be immediately consumed by reaction with hydrogen ion. However, at conditions more acidic than pH 3, no interference from hydroxide is noted prior to ca. -1.4 V.

Hydroxide interference begins to be noticeable at a pH of about 3, or at higher pH values for strongly buffered solutions. The effect is due to the increase in hydroxide concentration resulting from reductions of oxygen and then hydrogen peroxide.

The appearance of anodic current from mercury oxidation is not expected to occur at the detection potential until the hydrogen ions at the drop are consumed by reduction of oxygen or hydrogen peroxide and the hydrogen ion mass-transport is insufficient to neutralize resulting hydroxide. The increase in oxidation current will begin either with the oxygen reduction wave, reduction of hydrogen peroxide, or may even delay until hydrogen ion reduction begins at ca. -1.4 V, as discussed in Chapter 5. Whatever the case, the result will be a strong anodic wave easily surpassing any signals from trace metals in solution. Figure 13

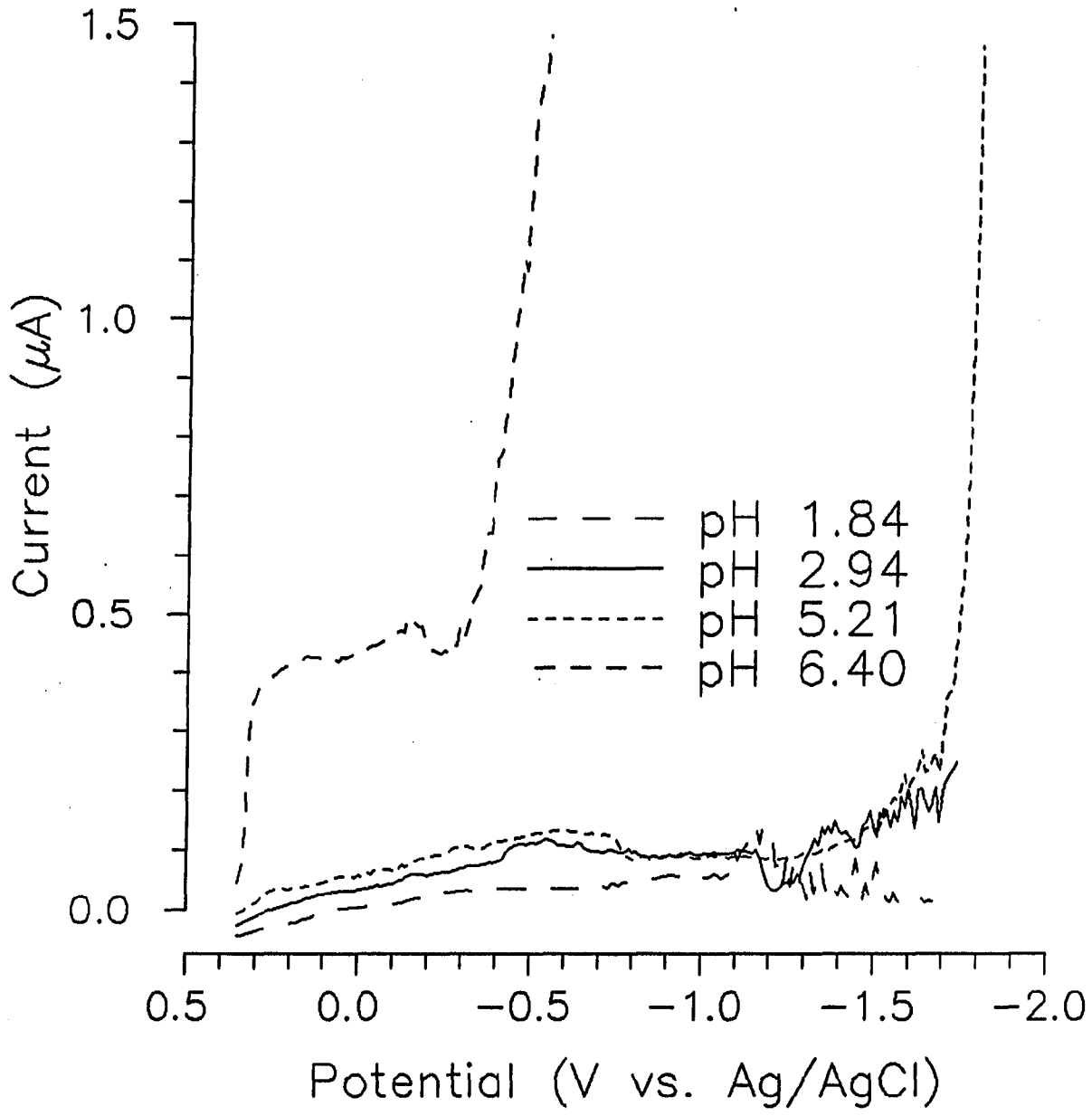

Solutions contain 0.1 M KNO_3 and were buffered at the stated pH values with KH_2PO_4 and H_3PO_4.

Figure 13. Effect of pH on detection of hydroxide

shows this effect for strongly buffered samples in a flowing stream. All samples are detected at the same potential, +0.35 V vs. Ag/AgCl, and the pH is adjusted from one sample to the next. Note that at pH 6.4 an anodic (positive) hydroxide wave appears almost immediately and increases when the edge of the hydrogen peroxide reduction begins.

The effect of hydroxide will be noticeable and complex in weakly buffered samples more basic than pH 4. Reduction of oxygen will produce substantial quantities of hydroxide in these samples. This can be deduced from the concentration of dissolved oxygen in aqueous solution, usually about 0.25 mM (36). The requirement for hydrogen is four ions per oxygen molecule, or 1 mM hydrogen ion, when reduction of oxygen and hydrogen peroxide are both occurring. This is ten times the quantity of hydrogen present in an unbuffered pH 4 solution. For this reason, unbuffered solutions more basic than ca. pH 3 are not used in this work.

The effect of hydroxide production resulting from oxygen reduction would be expected to be an anodic wave beginning at about the potential for oxygen reduction. The potential for this anodic wave may be slightly offset from the oxygen reduction potential, since the available hydrogen ions will first react with oxygen, delaying formation of hydroxide. The wave for oxidation of hydroxide should reach its mass-transport limited value as oxygen reduction becomes mass-transport limited.

When the potential for reduction of hydrogen peroxide is reached, additional anodic current from oxidation of hydroxide would be observed. This current will be proportional to the concentration of oxygen, since all hydrogen peroxide in solution is usually due to oxygen reduction.

Thus the anodic wave at reduction potential for H_2O_2 will be observed with a current response equal to or greater than the response at oxygen reduction, since the first wave can be diminished slightly by the small amount of hydrogen ion present.

Chloride

The choice of certain detection potentials may also result in interferences due to the presence of chloride. Although chloride ion is not usually added to the solution, it is present in the filling solution of the Ag/AgCl reference electrode and can enter the analysis solution by diffusion. If the level of solution in the reference cell is higher than the solution level in the analysis cup, as is the case in this work, hydrostatic forces serve to increase the rate of chloride diffusion into the cell. The rate of chloride concentration increase in the analysis cell is not noticeable during the time of a potential scan.

Chloride ion is detected at E > ca. +0.3 V vs. Ag/AgCl by the following oxidation.

$$2Cl^- + 2Hg \rightleftharpoons Hg_2Cl_2 + 2e^-$$

Unlike hydroxide, no other reactions produce chloride, so our attention can be focused to this one potential region.

At the beginning of the scan, the potential throughout the lifetime of the drop is constant, remaining at a value where formation of mercurous chloride occurs. The current recorded is either limited by the Nernst equation or by mass transport, as discussed earlier for oxygen

interference. The technique thus gives a response resembling SDCP.

As the scan progresses, the potential moves through the half-wave region, i.e., the potential region of sloping current response governed by the Nernst equation. The response takes on characteristics similar to NPP or RPP as the potential is scanned away from the chloride reaction potential, since one pulses into the region of activity only for the detection step. The current reaches a constant value in the potential region where chloride is not oxidized at all, reflecting the full sensitivity of the pulse technique at mass transport-limited conditions.

This is just the opposite of the behavior of oxygen as discussed earlier. The reason for the difference is that the measurement potential for oxygen was positive of its reduction potential, with the scan leading to increased reduction. In the chloride case the scanned potential moves out of the chloride oxidation wave, so that no reaction takes place except at the detection potential.

Considering the interferences posed by oxygen, hydroxide, and chloride, the choice of measurement potential is usually chosen to be slightly positive of the first current due to oxygen reduction, or about +0.2 to +0.3 V vs. Ag/AgCl. This choice often will show the effects of hydroxide and chloride in solution, but because currents resulting from these sources are generally much smaller than the effects caused by oxygen reduction, the foregoing choice is made.

Metals

A large number of metals can be detected by CPPP, though fewer than for the more traditional polarographic methods. Oxygen is one species which is not detectable, though it can be indirectly detected under certain conditions. Thus what appears to be a drawback is actually applied to the benefit of CPPP.

The reduction product of a species must be electroactive in order for the species to be determined by CPPP. For most metals this requirement is easily met, as is seen in the common use of RPP, where most materials are determined by their oxidations instead of their reduction potential.

It is an additional requirement for CPPP that the reduction products be oxidized at the detection potential, which is a constant. Generally this means that the electrode reaction must be either reversible or quasi-reversible.

Another factor which influences the detectability of a metal is its solubility in mercury. During the negative potential part of the drop life, analytes are reduced. The reduction products are formed at the drop surface and either dissolve into the mercury drop or diffuse into solution. When the positive potential pulse is applied, oxidizable material at the electrode/solution interface reacts. Though some diffusion may take place, the time frame of the pulse and current measurement is short enough that most of the material involved is already near the electrode surface. This favors detection of material in the mercury drop, since this material is often closer to the interface. This is

shown by Hsi and Johnson for reverse pulse amperometry, similar to RPP, who found that Fe^{2+} was detected poorly, presumably because it was not accumulated in the mercury drop (32).

Still another restriction is that CPPP is not sensitive to any material which forms a skin on the mercury drop. This limitation is shared with all of the pulse techniques because each employs a short time delay in order to avoid high charging currents. This short delay is the period when materials at the drop surface are reacted, thus they are not measured at all in any of the pulsed techniques. These species include cobalt, which is known to form a skin on the drop surface during reduction (32). When the oxidizing potential is applied, the delay in measurement precludes observation of any cobalt signal.

Figure 14 shows a polarogram by CPPP of Pb^{2+}, Cd^{2+}, and Zn^{2+} in a solution with dissolved oxygen present. The detection potential, E_d, was +0.25 V vs. Ag/AgCl. The waves corresponding to the reductions of these three metals occur from left to right in the same order as listed above. Note the lack of interference from dissolved oxygen in solution.

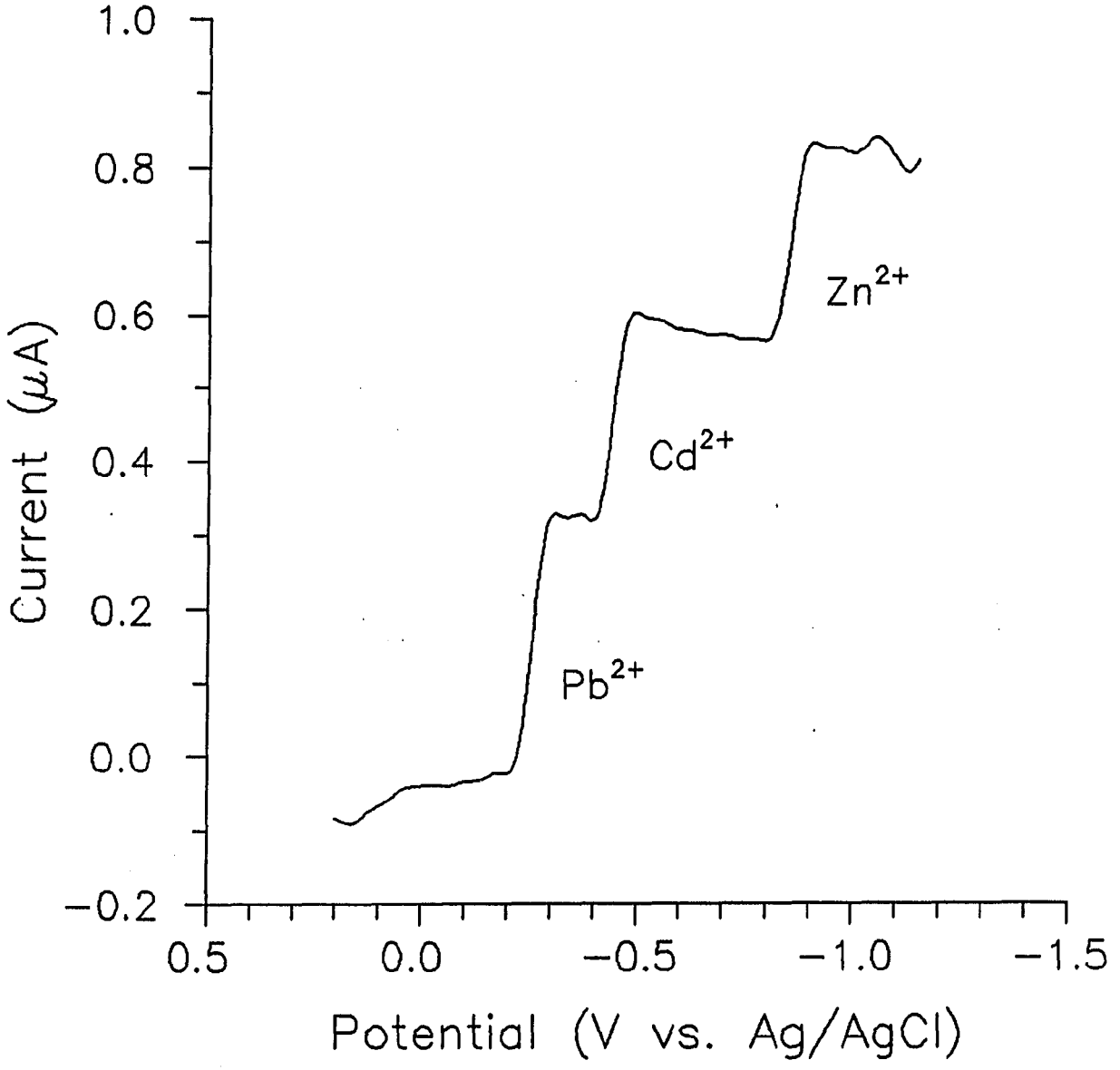

1×10^{-5} M $Pb(NO_3)_2$, $Cd(NO_3)_2$, and $Zn(NO_3)_2$
in 0.1 M KNO_3 with 0.001 M HNO_3

Figure 14. Detection of Pb^{2+}, Cd^{2+}, and Zn^{2+} in the presence of dissolved oxygen by CPPP

CHAPTER 5. FREEDOM FROM INTERFERENCE IN CONSTANT POTENTIAL PULSE POLAROGRAPHY: HYDROGEN

It has been shown that CPPP allows the analysis of metals without interference from dissolved oxygen in the range of oxygen and hydrogen peroxide reduction (13). There is another advantage offered by CPPP. It can be used to gain a degree of freedom from one of the deleterious effects of acidic solutions. The presence of high concentrations of acidic hydrogen can substantially narrow the analysis window for polarographic methods by limiting the negative potential range. Figure 15 shows the encroachment of the negative potential limit in NPP with increasing acidity.

Response at Hydrogen Reduction

Hydrogen reduction has a very high overpotential at the mercury electrode, making polarography an excellent tool for determination of metals normally reduced concurrently with hydrogen at other electrodes. High concentrations of hydrogen ion shift the potential of this reaction substantially to more positive values, however, causing increasing interference in highly acidic conditions.

The reduction of hydrogen ion produces molecular hydrogen, which is electrochemically inactive in the polarographic working range.

$$2H^+ + 2e^- \rightleftharpoons H_2\ (gas)$$

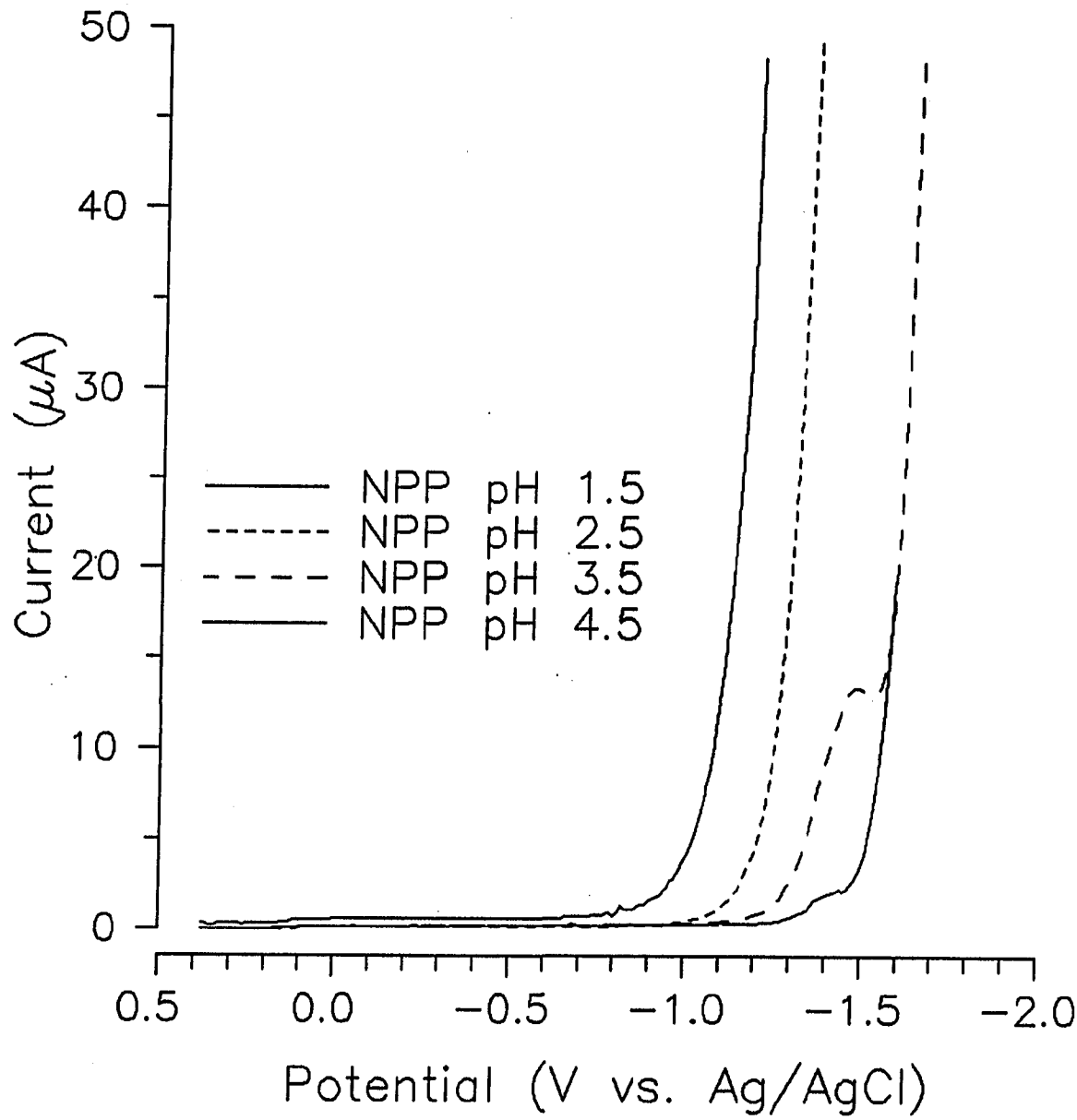

Solutions made with 0.1 M KNO_3; pH adjusted with HNO_3

Figure 15. Narrowing of potential window with increasing acidity for NPP

CPPP can be used to look "under" the wave for reduction of hydrogen ion, as neither reactant nor product are electroactive at the detection potential.

The formation of hydrogen gas at the electrode surface presents some interesting questions. It is assumed in polarography texts that H_2 is electroinactive, as it is mentioned in all the major textbooks as a possible purging gas. Indeed, hydrogen has been used commonly as purging gas, and may well serve this purpose, though it appears that possible oxidation had not been investigated. Since the vast majority of polarographic applications are in negative potential regions, where oxidation of hydrogen would be unlikely, oxidation at more positive potentials would not have interfered. Might hydrogen be oxidized at a mercury electrode at more positive potentials? If so, this would wreak havoc in CPPP, in which the highly soluble molecular hydrogen is produced and then measurement is made at a potential which may be positive enough for its oxidation.

This question is answered easily by looking at a CPPP scan of a highly buffered solution. In this case sufficient quantities of hydrogen ion are available to react with oxygen and hydrogen peroxide as well as to be reduced at the electrode. If the molecular hydrogen product was electroactive one would expect a large oxidation current to be present. This is clearly not the case, as is shown in Figure 16. Note, instead, the lack of interference from the acidic hydrogen. Solutions for both scans were of pH 2.5, and the one used for NPP was purged of dissolved oxygen.

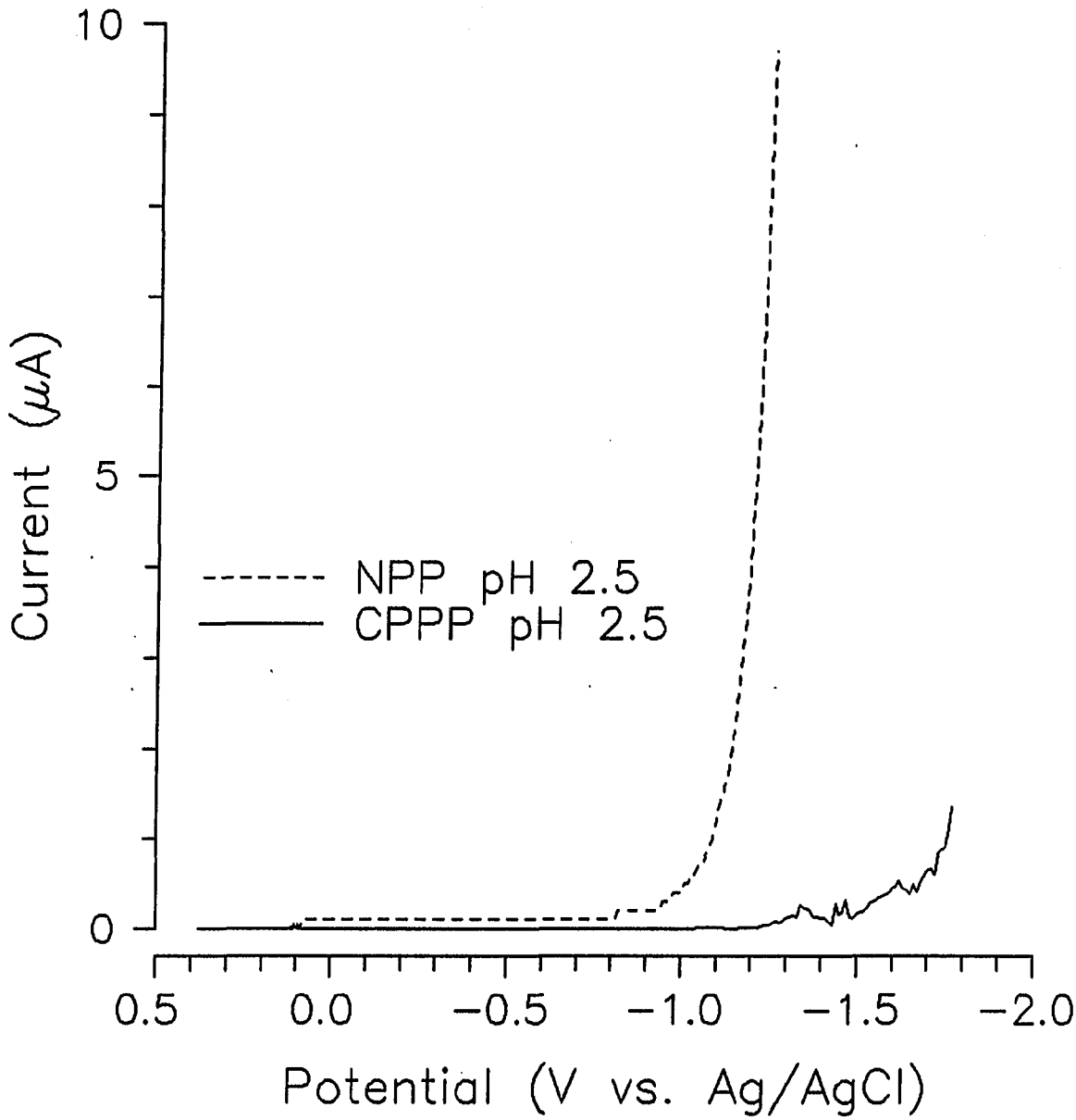

0.1 M KNO_3 and 0.003 M HNO_3

Figure 16. Comparison of detection by NPP and CPPP in acidic solution

Another way by which the reduction of hydrogen ion might cause current to flow could be a result of depleting the hydrogen ion concentration at the drop. This would lead to formation and anodic detection of hydroxide by oxygen and peroxide reduction. This possibility has already been raised in the discussion in Chapter 4 on avoidance of hydroxide interference in CPPP. Now there is yet a third reaction competing for the acid hydrogen.

$$O_2 + 2H^+ + 2e^- \rightleftharpoons H_2O_2$$

$$H_2O_2 + 2H^+ + 2e^- \rightleftharpoons 2H_2O$$

$$2H^+ + 2e^- \rightleftharpoons H_2$$

The potential region of interest here is one where all three reactions occur for the majority of the drop life, so it is quite possible that H^+ may not be present at quantities sufficient to allow each of these reactions to occur at the rate limited by mass transport of the other reactants. Reactions of O_2 and of H_2O_2 would then proceed by consuming water and forming hydroxide, again resulting in an anodic current at the detection potential.

To calculate the expected concentration requirement for hydrogen ion, we must look first at the hydrogen ion consumed by reaction with oxygen. In Chapter 4 it was determined that the requirement for hydrogen ion is four times the solution concentration of oxygen, or 1.0 mM, for complete reaction with both oxygen and hydrogen peroxide. Thus for solutions of pH 3 or greater, hydrogen ion would be depleted at the elec-

trode. When the potential for hydrogen reduction is reached, the depletion will be even more severe, and one must rely on consumption of hydroxide produced at the electrode by hydrogen ion still in solution.

There is another difference between the case of hydrogen ion and the freedom of CPPP from oxygen interference. The difference is that the product formed is a gas, molecular hydrogen. This gas dissolves into solution while production at the electrode is small, but with increasing production, small bubbles are formed. Formation of hydrogen bubbles occurs even before the limiting current for hydrogen ion reduction is reached, indicating that the solution layer surrounding the drop is saturated with the gas.

The bubbles can create considerable disturbances for the drop, often completely dislodging it. Before bubbles are formed in quantities of this magnitude, they disturb the diffusion characteristics of the cell by adding another source of convection. It has also been observed here and reported by others that the hydrogen bubbles adhere to the surface of the drop (15). This would cause additional disturbance of current measurement.

The formation of these bubbles at the drop surface may also cause a local purging of oxygen from solution near the electrode. The usual method of purging is to bubble a gas, usually N_2, H_2, or argon, through the solution. Assuming equal activities for oxygen on the inside and outside of the bubble, oxygen would be drawn out of solution into the gas bubble. It would then be carried away as the bubble rises out of the solution. Hydrogen bubbles formed at the electrode could purge the local

area by the same mechanism.

The effect such purging would have on measured current must be considered. Reaction of O_2 at the electrode does not give rise to any considerable current in CPPP. However, if previous reduction of oxygen resulted in production of hydroxide during the initial part of the waveform, such purging would cause a decrease in hydroxide production and thus a decrease in anodic signal. This decrease would be expected to be related to the effectiveness of the local purging phenomenon. It should be realized that the hydrogen ion which is consumed to form the hydrogen purge gas would have reacted with the hydroxide previously formed, so the magnitude of the change in signal is a not easily found.

It is apparent that the phenomena occurring at the potential for hydrogen ion reduction are complex. Our experiments suggest that detection in acidic solution by CPPP is possible until visible bubble formation occurs. Usually the signal becomes noisy in the region of hydrogen ion reduction, then the signal dips in the cathodic direction followed by strong anodic current, as shown by the CPPP scan in Figure 17. While this could be due to some initial purging of the local solution followed by increased current from hydroxide production due to the increased convection, it is not clear from thought or experiment what the actual phenomena are. Some may argue that the effect shown in Figure 17 is actually due to the low solubility of nickel in mercury. This low solubility would still yield a traditional wave-like response, though with less sensitivity than for more soluble metals.

One way to counter the apparent requirement of highly acidic solu-

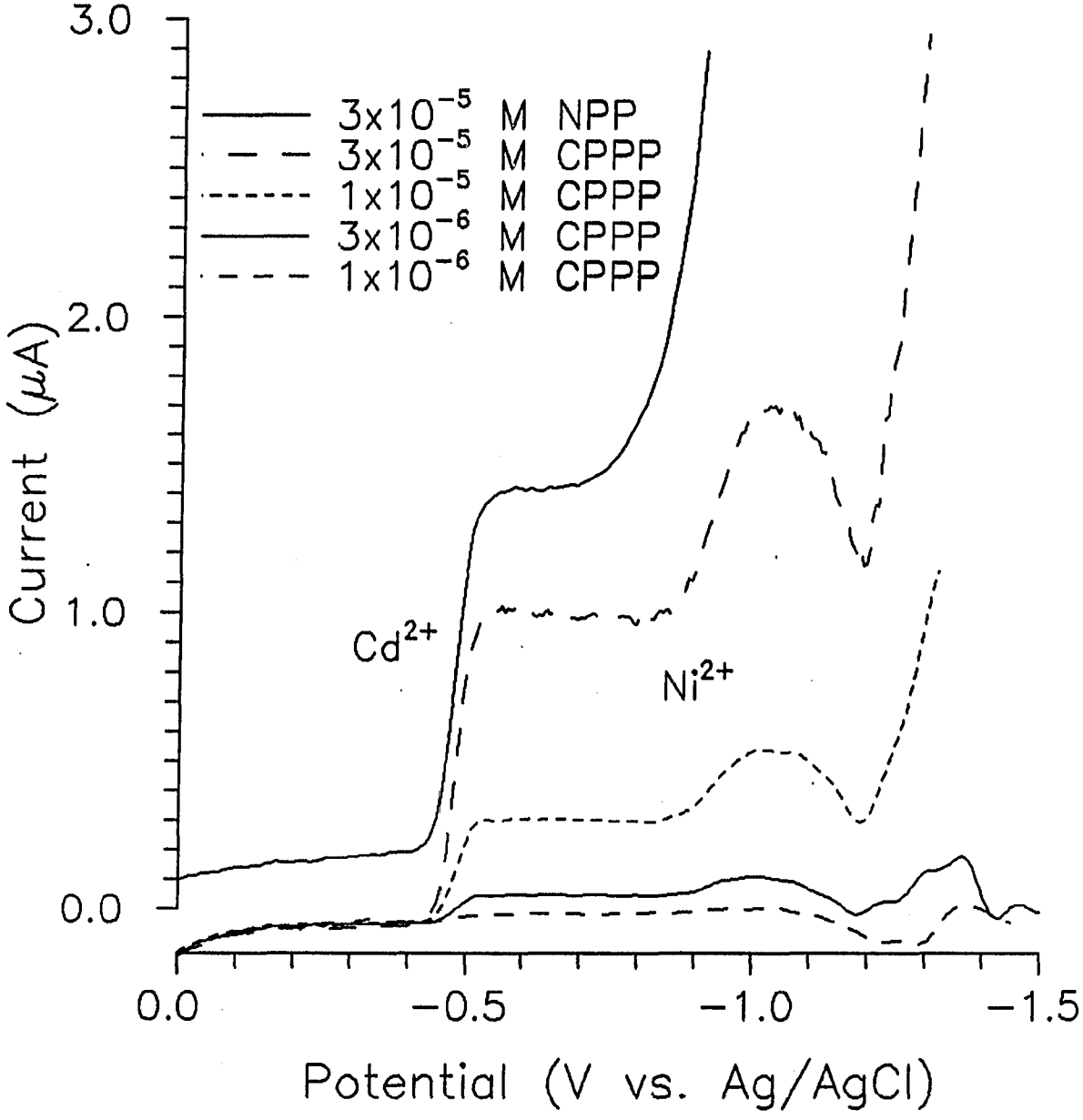

Both samples contain 0.1 M KNO_3 and 0.1 M HNO_3 (pH 1)

NPP sample: purged
CPPP samples: not purged

Figure 17. Detection of Cd^{2+} and Ni^{2+} in acidic solution by NPP and CPPP

tions is to use buffers with relatively high buffer capacities, such as phosphate buffers at concentrations greater than 1 x 10^{-3} M. These provide the hydrogen ion needed at the electrode while not requiring that the pH be adjusted to extremely acidic values.

Aside from the irregularities caused by formation of large quantities of hydrogen gas, which occur well beyond the analysis window for the other polarographic methods, a range of several hundred millivolts is added to the negative end of the polarographic potential window for acidic solutions by the CPPP techniques as was illustrated in Figure 16.

Detection of Metals at Large Negative Potentials

It was shown that CPPP can be used to extend the potential range suitable for analysis by allowing one to detect metals normally hidden under hydrogen reduction. Many metal species are reduced just beyond the normal working limits of polarography. In acidic solutions this can include zinc, which is reduced at -1.0 V, and nickel, reduced at -1.1 V. CPPP now extends the analysis range closer to the alkali and alkaline earth metals, which have reduction potentials of -1.9 to -2.1 V.

Figure 17 shows detection of cadmium and nickel in an acidic solution of pH 1 by NPP and CPPP. The hydrogen ion reduction wave is not sufficiently resolved from the nickel wave in NPP to quantitatively determine the nickel present, while for CPPP the nickel reduction is removed from the hydrogen ion wave. It is clear from this that CPPP can be used to look a few hundred mV into the hydrogen ion reduction wave.

CHAPTER 6. DIFFERENTIAL CONSTANT POTENTIAL PULSE POLAROGRAPHY

The standard polarographic techniques discussed so far suffer from the disadvantage of poor selectivity. In the full extent of the polarographic window, ca. 2 V, only a maximum of 15 analytes can be resolved in a single sample, given proper spacing of their reduction potentials. The development of differential pulse polarography (DPP) was one step toward improving the selectivity on the basis of reduction potential. In this research the application of differentiation is made to constant potential pulse polarography, and the resulting enhancement in selectivity is shown. The new method is called differential constant potential pulse polarography (DCPPP).

Potential Waveform and Current Response

The application of a derivative method to CPPP can best be explained in view of the analogous advance that DPP presented in comparison with NPP. In this section the applied potential waveforms and current responses for DPP and DCPPP are presented, and the similarities and dissimilarities of both techniques are noted.

Differential pulse polarography

Differential pulse polarography (DPP) was an advance in polarography which afforded improved selectivity over DCP, SDCP, NPP, and RPP. The applied potential waveform for DPP is most closely related to that of

NPP, and was developed, with NPP, from the work on square wave polarography by Barker and Gardner (22). The waveform for DPP is shown in Figure 18. It can be seen that DPP differs from the other polarographic methods in that two measurements of current are taken on each drop; at times t_1 and t_2, before and after the application of a potential pulse.

The applied potential for most of the drop lifetime is a linearly increasing ramp in the negative direction. Near the end of drop life a 10 to 100 mV potential pulse with negative polarity is applied to the ramp, commonly with a duration, t_p, of about 60 ms. The two measurements of current for 16.7 ms are then taken, and the signal retained is the difference between the two currents, $i(t_1) - i(t_2)$. DPP is very sensitive, having detection limits in the range of 10^{-8} M (37).

The equation for current was derived by Parry and Osteryoung (19).

$$i_{max} = \frac{n^2 F^2}{4 R T} A C \Delta E \sqrt{\frac{D}{\pi t}}$$

It is assumed that the potential scan during the lifetime of the drop is small relative to ΔE. The DPP current sensitivity would be expected to be similar to that of NPP, which utilizes a similar applied potential waveform. The response for reduction of a metal species is in fact greater for DPP than for NPP by about one order of magnitude (37).

Differential constant potential pulse polarography

The similarities between DPP and differential constant potential pulse polarography (DCPPP) are more clear in intent than they are from

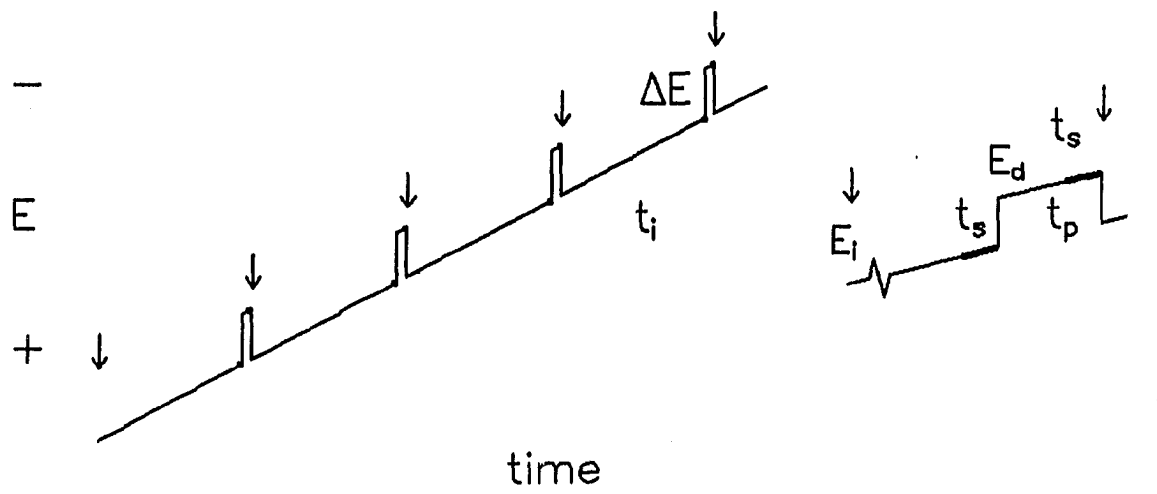

Figure 18. Applied potential waveform for DPP (detail at right shows waveform during one drop lifetime)

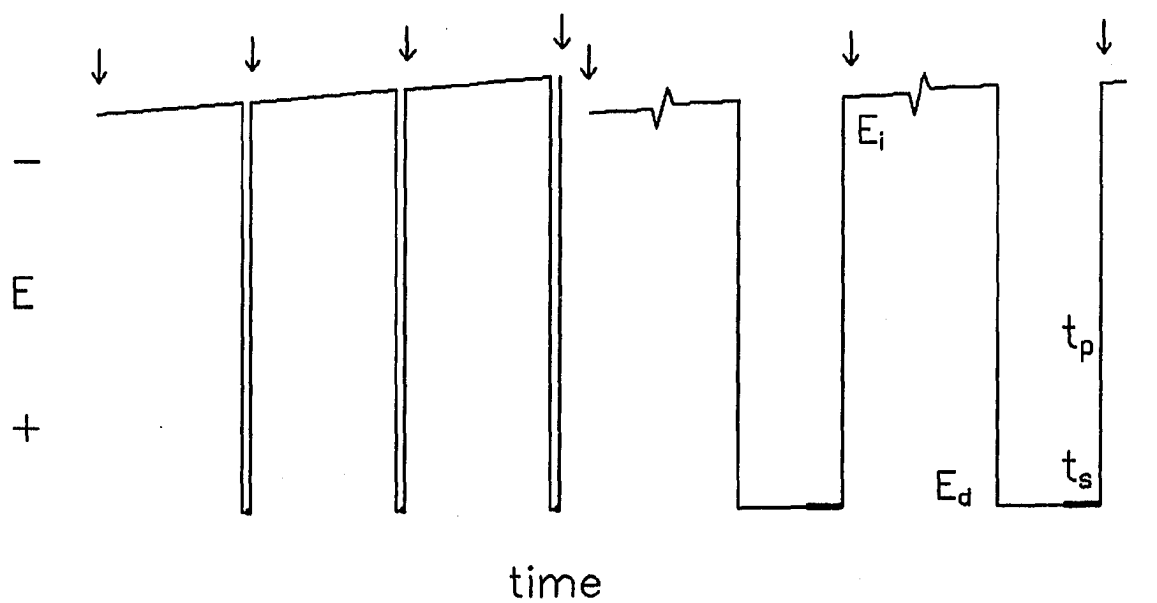

Figure 19. Applied potential waveform for DCPPP (detail at right shows waveform during one measurement cycle, or two drop lifetimes)

visual comparison of the applied potential waveforms. It is the goal of increased resolution and increased sensitivity, i.e., benefits of the differential method (38), the major tie between the two techniques.

The applied waveform for DCPPP is shown in Figure 19 and is taken from two cycles of the CPPP waveform. The potential is scanned linearly in the negative direction until near the end of drop life, when a pulse to the constant measurement potential, E_d, is applied. Signal measurement takes place during the last 16.7 ms of each pulse application, allowing a delay of ca. 40 ms for charging current to dissipate.

The derivative is approximated by subtracting the current values for consecutive drops and dividing by the potential increment between drops. Thus a single DCPPP data point is obtained from two drops. The fact that two drops are required for a single measurement does not make DCPPP two times more slow than DPP, however, since three drops yield two points, and a scan of 250 drops yields 249 usable DCPPP data points. The use of more than one measurement per drop for DCPPP, however, is not feasible. The act of measurement for DCPPP is in itself a process which interferes with the subsequent measurement. Measurement for DPP does not interfere -- it is merely observation of current which is already flowing.

The reason for the interference caused by the measurement step in a subsequent reading during the life of the same electrode is given below. It is clear from the equation for current in CPPP that both the time prior to the pulse and the time delay following application of the detection pulse affect the magnitude of the signal.

$$\frac{-i_{CPPP}}{i_{SDCP}} = \frac{n_{Red}}{n_{Ox}} \left(\left(\frac{3\ t_1}{7\ t_2} \right)^{1/2} - 1 \right)$$

The time, t_1, at the potential value, E_i, can be considered as a preconcentration period, while the time, t_2, at the detection potential, E_d, is the measurement period. Thus any change in potential to E_d depletes the oxidizable material at the electrode, requiring more time at E_i to build up the concentration for the second measurement to the same value as for the first measurement.

DCPPP is based on CPPP and therefore shares many of the same advantages, namely the freedom from interference from dissolved oxygen and a degree of freedom from the interference due to hydrogen ion reduction. These characteristics are illustrated in Figure 20, which is analogous to Figure 17. Figure 20 shows DPP and DCPPP scans of solutions of 3×10^{-5} M Cd^{2+} and Ni^{2+} at pH 1. The DPP solution was purged before analysis. It is clear that Ni^{2+} is observable by DCPPP, but not by DPP due to the overwhelming hydrogen ion reduction wave in DPP.

Enhancement of Resolution

The poor resolution of polarography has already been noted in passing. DCP analysis of a solution affords resolution of compounds for which $E_{1/2}$'s are separated by ca. 180/n mV or more, according to Muller (39). Fisher et al. rigorously calculated the separation required for two successive waves of equal n and equal height (40). For a 1% overlap

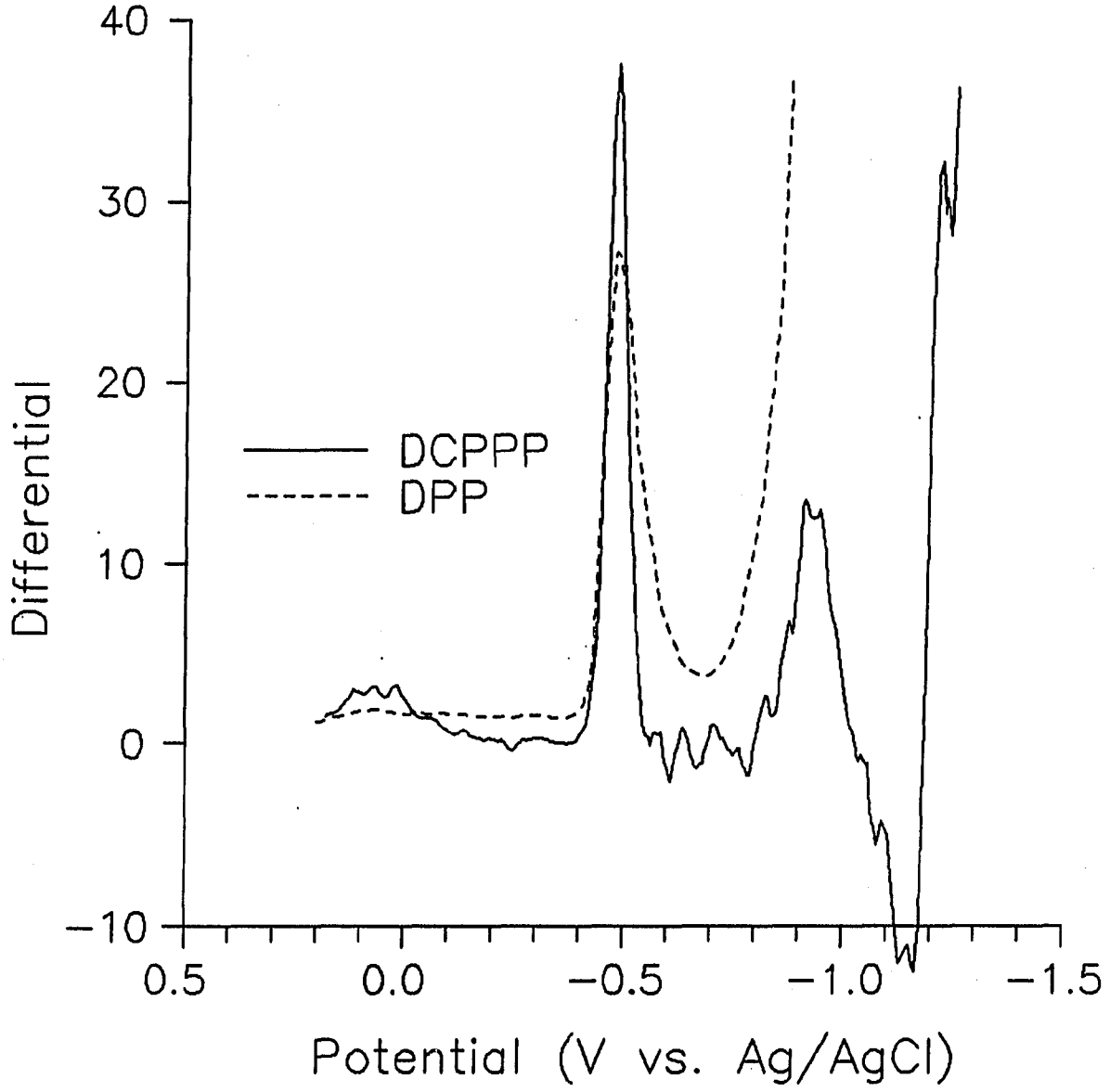

3×10^{-5} M Cd^{2+}, Ni^{2+} in 0.1 M KNO_3 with 0.1 M HNO_3
DPP sample: purged
DCPPP sample: not purged

Figure 20. Detection of Cd^{2+} and Ni^{2+} in acidic solution by DPP and DCPPP

they calculated a required separation, $\Delta E_{1/2}$, of 236/n mV for reversible processes. In a scan of 2 V, this allows resolution of no more than 17 species with well-placed 2-electron reductions.

One advantage of differential polarographic methods is improved selectivity on the potential axis. The first application of a derivative method was to DCP, for which the theory is reviewed by Fisher et al. (40). Calculation of required separation for a 1% overlap for the same conditions given above yields 154/n mV for the first derivative method, compared with 236/n mV for the underivatized scan. A slightly better value of 143/n mV is reported for the use of the second derivative. It is clear that the use of the first derivative results in much better resolution than does the underivatized technique.

The technique of DPP gives an approximation of the derivative for each drop, as opposed to the two-drop derivative DCP method cited above. Barker and Gardner report the full width at half the peak height, or half-width, of a reversible wave as 90.4/n mV for DPP (22). This is not a value for separation of $E_{1/2}$'s yielding only 1% overlap as above. For a true comparison with the numbers given above, Fisher et al. gave the half-width for a first derivative DCP wave as 90.5/n mV (40), essentially the same as the value for DPP. It can be concluded that the required separation is also the same, 154/n mV for a 1% overlap. Thus DPP also shows the advantage of improved resolution. It is also a more common method over derivative DCP and shows the additional advantage of higher sensitivity, or a greater response to the same phenomenon (4).

The application of a derivative technique to CPPP, i.e., DCPPP,

shows the same resolution effect as does the derivative of DCP. This can be shown from the potential dependence of the method. This potential dependence of the current for CPPP is the same as for DCP, SDCP, and NPP, and is shown in the Heyrovsky-Ilkovic equation (41).

$$E = E_{1/2} + \frac{R\,T}{n\,F} \ln\left(\frac{i_d - i}{i}\right)$$

This equation shows the exponential nature of the polarographic wave at the $E_{1/2}$ potential, this nature being identical for each of the above methods. From this equation Fisher et al. found the separation needed to achieve a specified resolution (40). Therefore, the derivative method, DCPPP, offers substantially improved resolution compared with CPPP by the same factor that derivative DCP and DPP show improvement over DCP.

The enhancement in resolution is illustrated in Figures 21 and 22. Both figures were obtained from the same solution, in which four analytes were present. Two of the analytes, lead and cadmium, have $E_{1/2}$ values which are separated by ca. 190 mV. $E_{1/2}$ values for the other two metals, vanadium and zinc, are separated by only ca. 90 mV under the solution conditions present. The solution was made such that approximately equal wave heights would be observed for each analyte.

Figure 21 gives the response for SDCP, NPP, and CPPP. Solutions analyzed by SDCP and NPP were purged prior to analysis, while the dissolved oxygen was not removed for analysis by CPPP. It is clear the the resolution is nearly the same for each of these techniques. Lead and cadmium waves are easily resolved, as Fisher et al. predicted, since

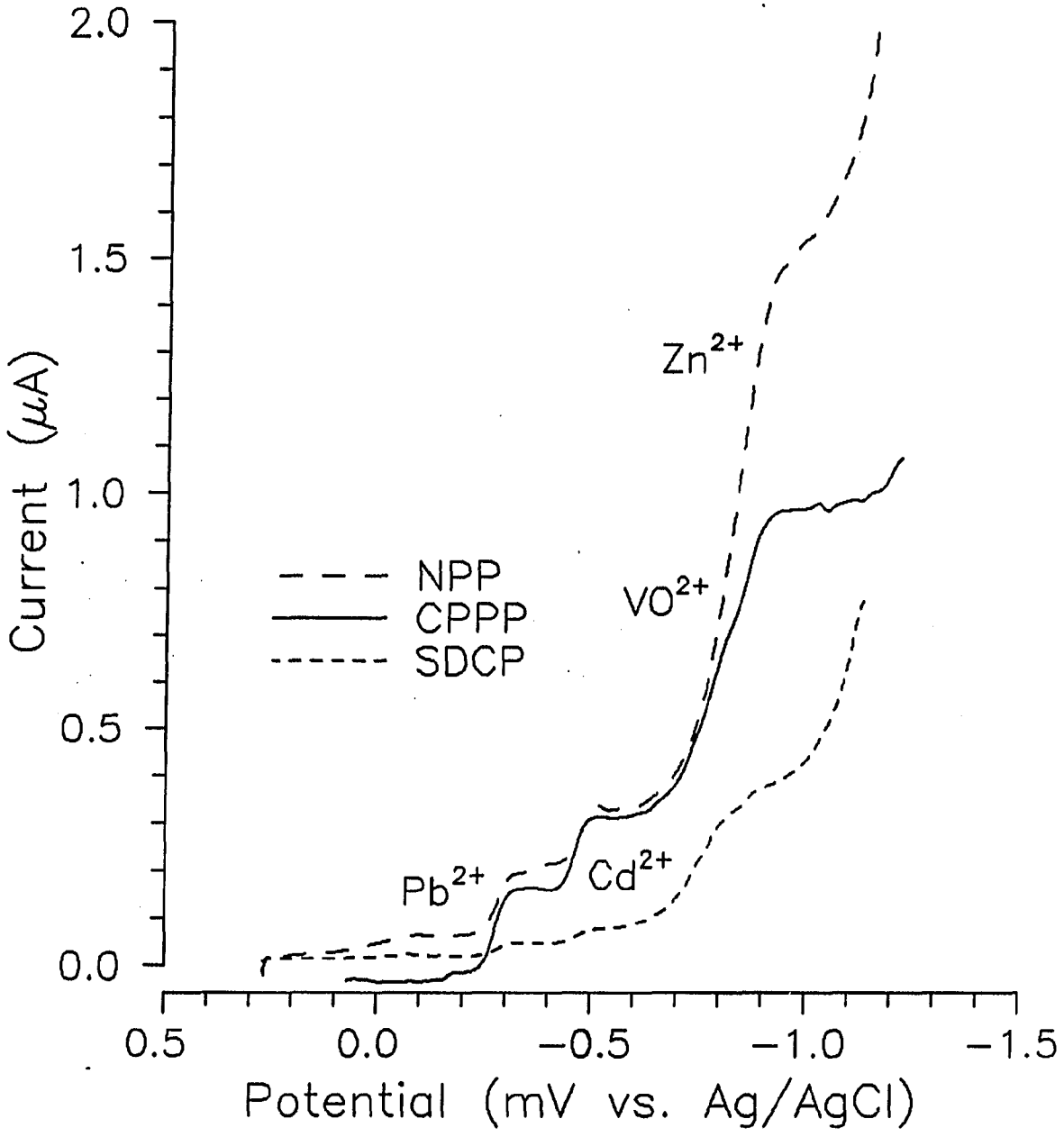

5×10^{-6} M Pb^{2+}, Cd^{2+}, and Zn^{2+} and 5×10^{-5} M VO^{2+}
in 0.1 M KNO_3 and 0.001 M HNO_3 at E_d = 0.25 V vs Ag/AgCl

Figure 21. Resolution of lead, cadmium, vanadium, and zinc by NPP, SDCP, and CPPP

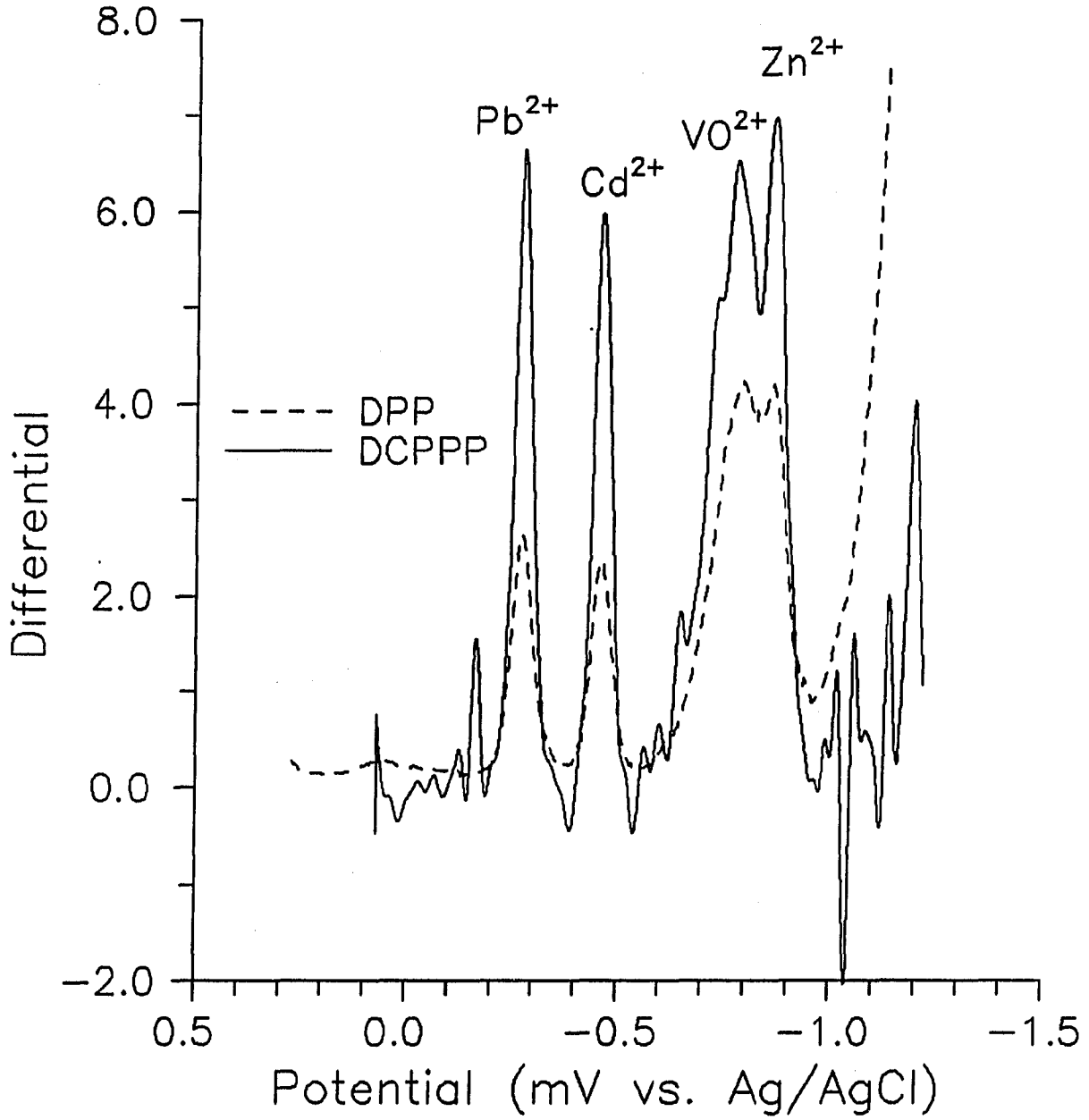

5 x 10^{-6} M Pb^{2+}, Cd^{2+}, and Zn^{2+} and 5 x 10^{-5} M VO^{2+}
in 0.1 M KNO_3 and 0.001 M HNO_3 at E_d = 0.25 V vs Ag/AgCl

Figure 22. Resolution of lead, cadmium, vanadium, and zinc by DPP and DCPPP

their reduction potential separation, i.e., 190 mV, is greater than the value of 236/2, or 119 mV, given in their work (40). Separation is not seen for vanadium and zinc, however.

The results for analysis by the differential methods are shown in Figure 22. The solution analyzed by DPP was purged of oxygen prior to analysis, while the solution used for DCPPP was not. The increased resolution of DPP and DCPPP over the techniques used in Figure 21 is immediately apparent. Peaks for lead and cadmium show FWHM values of ca. 50 mV, compared with 90.5/2, or 45 mV, predicted by Fisher et al. (40).

Although baseline resolution is not obtained for vanadium and zinc, the individual peaks are recognizable and it is evident that more than one species is present. It is not clear if the overlap between peaks in the figure is more or less than 1% at the peak position, but according to the calculations given by Fisher et al., for species with n equal to 2, this degree of separation should be seen for peaks separated by 77 mV, approximately the amount seen here. It can be seen, however, that the wave for vanadium is substantially wider than for zinc, due either to a 1-electron reduction or some irreversibility in the electrochemical reaction. It should be noted that the resolution for these two derivative techniques is about equal, just as each of the non-derivative methods resulted in similar, though poorer, resolution.

Sensitivity

Differential techniques can also be used to gain an additional degree of sensitivity. This was shown for DPP by Christie and Osteryoung (42) and is illustrated here for DCPPP.

A look at the applied potential waveforms for DPP and NPP suggests that their level of sensitivity to concentration should be similar. The advantage rests with DPP, however, due to reduced contribution of charging current relative to faradaic current. Subtraction of the two measurements made on each drop for DPP results in virtual elimination of charging current, since the charging current contribution to each measurement is nearly identical.

First, the rate of growth of the electrode is very nearly the same for the measurements made ca. 50 ms apart, at one second into the drop life. Second, the effect of the slowly changing applied potential is approximately the same for each measurement, provided the charging current spike due to the initial application of the potential pulse is allowed to decay. Reduction in charging current by this differential method results in a signal which is more closely related to the faradaic part of the current at the electrode. The faradaic contribution does change due to the change in reduction potential, so the difference in faradaic current is measured, thus yielding the increased sensitivity of the method (19, 38).

The sensitivity for DCPPP is related to that of its mathematical partner, CPPP. Once again, the differential nature of the DCPPP technique is expected to result in better sensitivity characteristics due to

a reduction in the charging current contribution in the signal relative to CPPP. Charging current for CPPP at the SMDE consists of one major factor; the capacitive response to the application of the detection potential pulse. The other factors normally contributing to charging current are already minimized by the choice of instrumental apparatus and by the potential characteristics of the applied waveform. The drop does not continue to grow in size after the solenoids pass the metered amount of mercury, and the potential during measurement does not change in the CPPP method. Precise reproduction of the timing characteristics of the measurement, specifically the delay time, t_d, after the detection pulse application, implies equal charging currents for each drop. DCPPP eliminates this contribution, since the difference between the current measured for each of the two drops is taken and the charging current portion is thus subtracted out.

One variable that is found for DCPPP that affects DPP only very slightly is the noise caused by variation in drop size. Irreproducibility in this factor has an increased adverse affect on sensitivity for DCPPP relative to a single-drop measurement. The effect of the drop size irreproducibility is chiefly a change in faradaic current, which is directly related to the area, A, of the electrode by the Cottrell equation.

$$i_{lim} = n F A D_{ox}^{1/2} \pi^{-1/2} t_d^{-1/2} C_{ox}$$

It should be clear that changes in size from one drop to the next will also adversely affect the sensitivity of CPPP.

This effect is magnified for DCPPP, where each data point reflects measurements from two drops. Depending on the magnitude of variation in drop size compared with the benefits of the reduction in charging current contribution to the signal, the sensitivity of DCPPP may be either worse or better than for CPPP. The net effect of the two factors are found to be about equal and DCPPP is slightly less sensitive than CPPP. This is shown in the section on detection limits in Chapter 8. The effect of the irreproducibility in drop size as a contributor to noise in the signal will be treated in the section of Chapter 8 on noise considerations.

CHAPTER 7. FLOW INJECTION ANALYSIS

Polarographic analyses are traditionally performed in the batch mode in a small cell with a sample capacity of ca. 10 mL. Typically the analysis would consist of a potential scan taking from 2 to 5 minutes, depending on scan speed, plus an additional 10-15 minutes for each solution, since the usual polarographic detection methods required removal of dissolved oxygen. In addition to the extra time required, the necessity of oxygen removal virtually eliminated the advance from determinations in the quiescent cell to detection in flowing streams.

This limited polarography as a feasible option for detecting analytes separated by LC, HPLC, or IC. Although attempts to purge the flowing sample by several workers have been made, including purging of the entire system (9), placement of the analysis system into a purged glove box (11), and passage of analyte through a sulfite reactor bed to remove oxygen (12), none of these methods has been deemed universally satisfactory (43). It has also been noted that the tubing used in many flowing systems is itself permeable to oxygen (31).

CPPP has been shown capable of application in solutions with dissolved oxygen present, and is therefore not limited to analysis in batch solutions from which oxygen is readily removed. CPPP has been applied to determinations in flowing systems with satisfactory results by Neuburger and Johnson (13). They demonstrated the feasibility of the method by looking at flow injection polarographic analysis of copper from a plating bath. Although CPPP analysis of quiescent samples was shown at concen-

tration down to 5 x 10^{-6} M, analyses in the flowing stream were restricted to metal concentrations greater than 10^{-4} M. Other workers achieving detection in flowing streams without removal of dissolved oxygen include Hara and Nomura, who used a similar potential waveform (17).

Another novel approach was demonstrated by Trojanek et al., who used a mercury wall separating the flowing stream from a detection cell (44). Metals were reduced and deposited into the mercury on the flowing stream side, and detected by anodic stripping on the other side of the mercury wall. The limit of detection given was 4 x 10^{-7} M for Cd^{2+}, although the response was not linear below 2 x 10^{-6} M. These workers noted the dependence of detection on diffusion parameters of the metals within the mercury. They also stated that preparation of a stable working electrode was a considerable problem, the mercury electrode being deposited into a 0.2 mm hole in a piece of Nickel foil.

In this thesis, the method of Neuburger and Johnson is refined, decreasing the detection limit by three orders of magnitude to the range of 10^{-7} M for flowing samples without removal of dissolved oxygen. Analysis of flowing samples is further extended with the use of DCPPP, adding the additional selectivity of the differential technique.

Effect of Flow at the Electrode on Signal

The use of flowing media in polarographic analysis requires a different cell design than would be used for a quiet solution. The changes in cell design imply the possibility of changes in response for

applications with flowing samples. The changes expected are related to the altered solutions dynamics at the mercury drop, e.g., changes in diffusion and mass-transport limited flow. Examination of these characteristics is critical for CPPP, especially when one considers that the species measured in CPPP are not the original species present in solution, but are reaction products which might be carried away from the electrode under adverse flow conditions. While it is clear from this and previous work that not all reaction products are removed from the electrode, the effects caused by fluid flow at the drop require examination.

Illustrated in Figure 23 is the response of current to changes in the flow rate of solution at the drop. The solid curves are polynomial fits of the data, using polynomials of the second degree. The increasing nature of the response is enough to say that the measured species is apparently being concentrated at the electrode. This is probably due to reduction of species into the mercury drop, and measurement of the preconcentrated species.

Limit of Detection

Detection limits were investigated for CPPP and DCPPP in the flowing stream using lead and cadmium as representative analytes. In comparison with detection limits found for the case where a static cell is used, one would clearly expect that LOD figures for analysis in the flowing stream would be worse. That is, effects such as the additional noise arising from disturbances of the mercury drop caused directly by the flow charac-

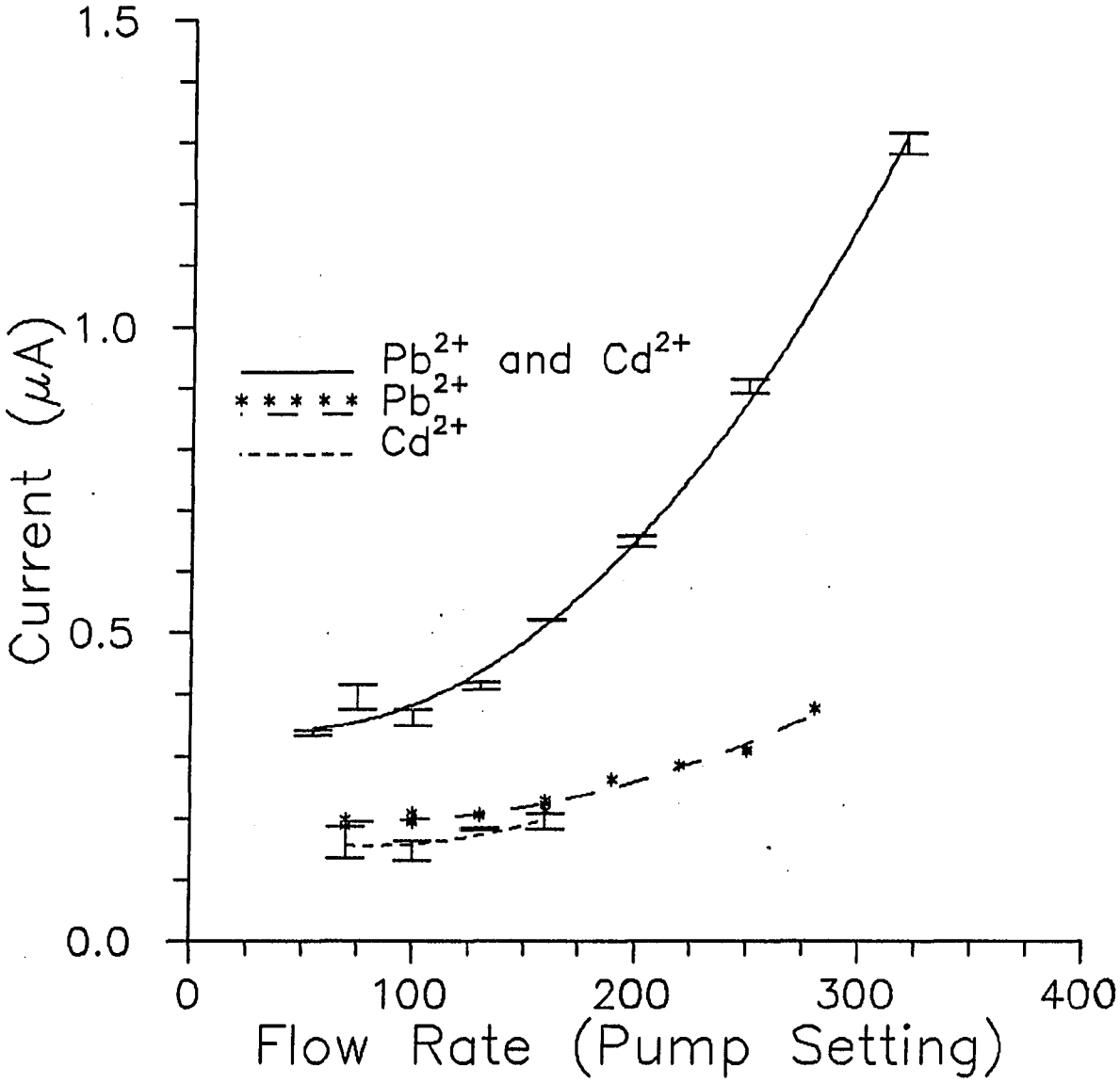

A pump setting of 100 corresponds to 0.19 mL/min and each increment of 100 corresponds to an increase of 0.19 mL/min

Figure 23. Variation of CPPP signal with sample flow rate

teristics of the stream suggest that detection limits would not be as low as in the undisturbed situation.

Traditional measurement of a species by polarography involves a voltammetric scan, with current monitored as potential is scanned over the range of interest. The current is measured in the flat response region before and after the $E_{1/2}$ for the metal being analyzed, the difference giving the current resulting from reduction (or oxidation) of that analyte.

This same mode of analysis can be carried out in a flowing stream by using the CPPP technique. A voltammetric scan is made as the sample flows by the detector, resulting in the same information as for a quiet solution. Analysis in this manner requires that the flowing sample be large enough to bathe the detector throughout a complete scan of the potential range. At a flow rate of 1 mL/min. and a potential scan rate of 10 mV/s, one requires a sample size of ca. 3 mL to scan the complete potential range. In this study of detection limits, a sample size of 2.0 mL was used, with a flow rate of 0.25 mL/min. and a scan rate of 10 mV/s. Though faster flow rates give greater current response, this flow rate allows measurement on a 2 mL sample and avoids the sharp fluctuations in flow apparent at higher pump speeds.

The samples used to find the detection limit in the flowing stream were prepared at pH 2.0, buffered with KH_2PO_4 and H_3PO_4 at concentrations of ca. 0.09 M and 0.002 M, respectively. Though the samples were analyzed by NPP as well as CPPP, oxygen was not removed. This was because additional handling was required after purging and because the tubing

used in the flowing stream work was permeable to gases and would allow the oxygen concentration to build up in the flowing stream anyway. The metals used for the this study were prepared from their nitrate salts, with serial dilutions made to obtain the indicated concentrations.

Figures 24 to 26 show the resulting calibration curves for NPP, CPPP, and DCPPP. All values for this study were taken from duplicate trials. A dotted line near the bottom of each plot represents a value of two times the approximate noise level for each technique. Note that the detection limit is worse for NPP than for CPPP and DCPPP. This arises from the interference caused by oxygen reduction.

The correlation coefficients for the lines shown are 0.9993 for lead as determined by NPP. Although the correlation appears to be high, the line for NPP is based on three points (two for cadmium), so the high correlation may be fortuitous. Correlation coefficients of 0.9983 and 0.9934 for lead and cadmium, respectively, were obtained for CPPP, with 0.9978 and 0.9990 for lead and cadmium, respectively, calculated for DCPPP. The calibration lines for CPPP were drawn based on five concentration points, and for DCPPP, four and five points for cadmium and lead, respectively.

A second detection approach can also be used for determinations in flowing samples. In this scheme a single reduction potential, E_i, is chosen. The CPPP waveform reflects this as a sharp decrease in the slope of the ramped portion, down to 0.01 mV/s or less. The stream is then monitored while a sample is injected. Measurement of current is made before and during the passage of the injected sample, and the difference

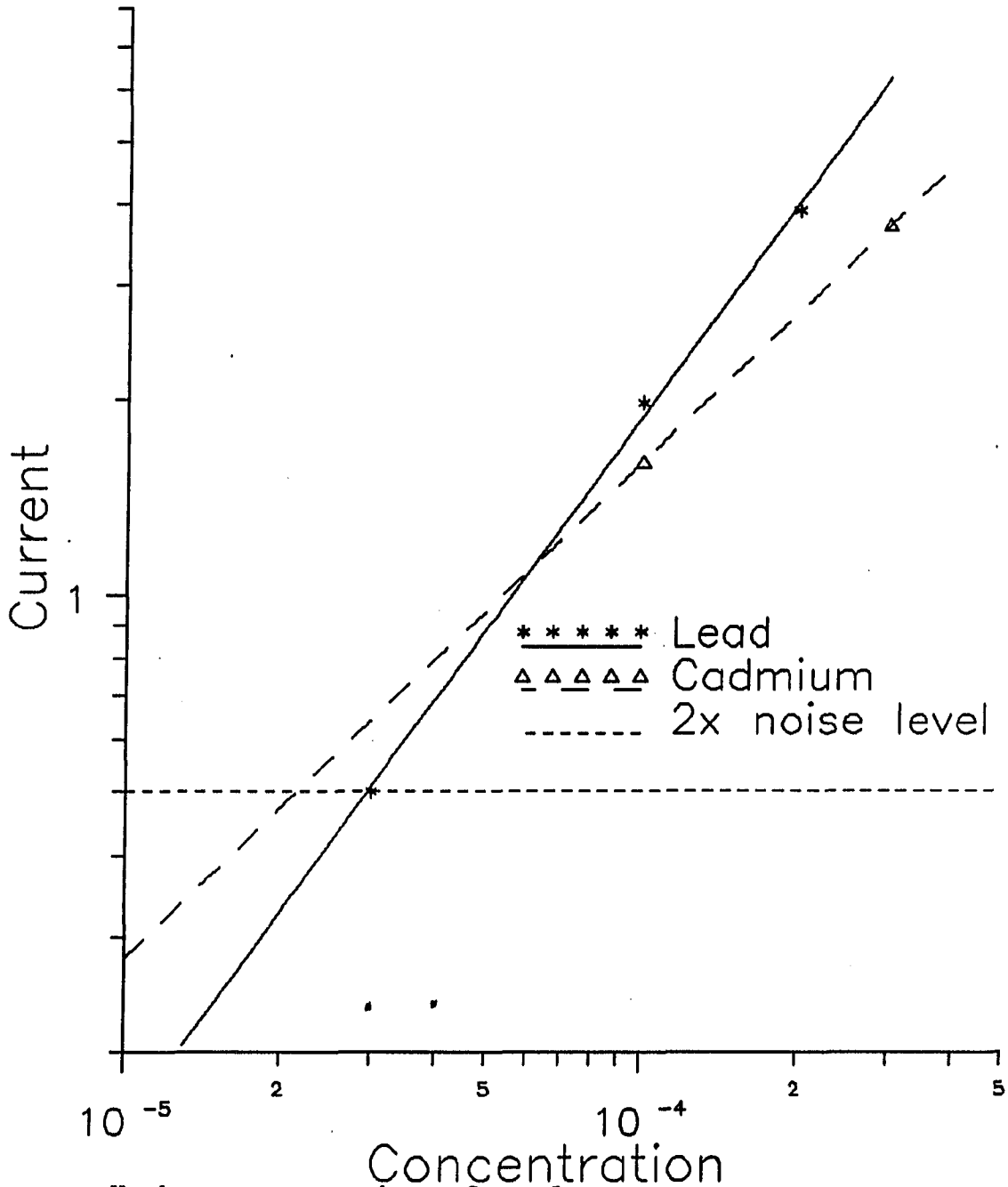

Various concentrations of metals were prepared by dilution of their nitrate salts, buffered at pH 2.0 with KH_2PO_4 and H_3PO_4 at concentrations of ca. 0.09 M and 0.002 M, respectively.

Figure 24. Limit of detection for NPP with flowing samples

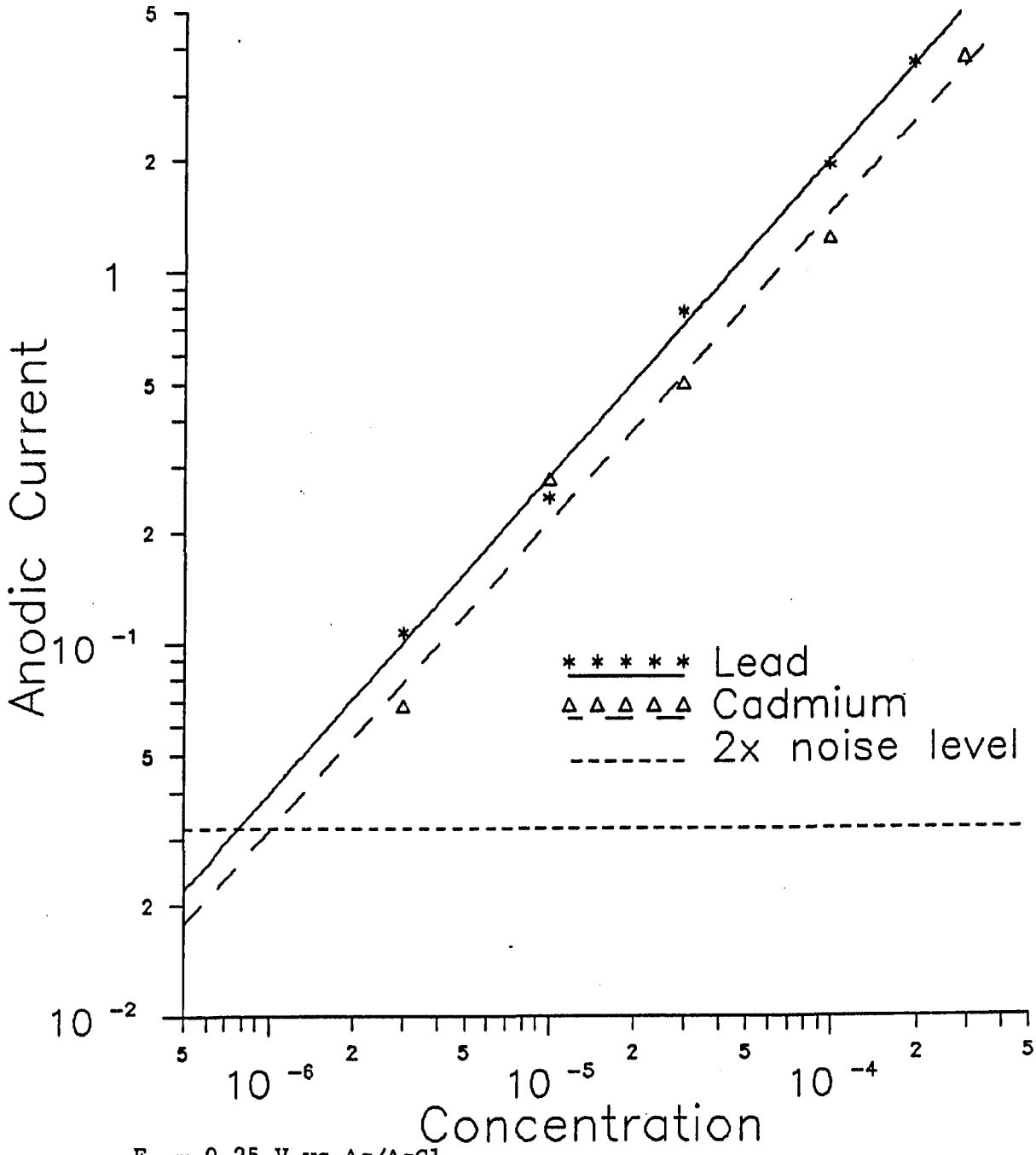

E_d = 0.25 V vs Ag/AgCl

Various concentrations of metals were prepared by dilution of their nitrate salts, buffered at pH 2.0 with KH_2PO_4 and H_3PO_4 at concentrations of ca. 0.09 M and 0.002 M, respectively.

Figure 25. Limit of detection for CPPP with flowing samples

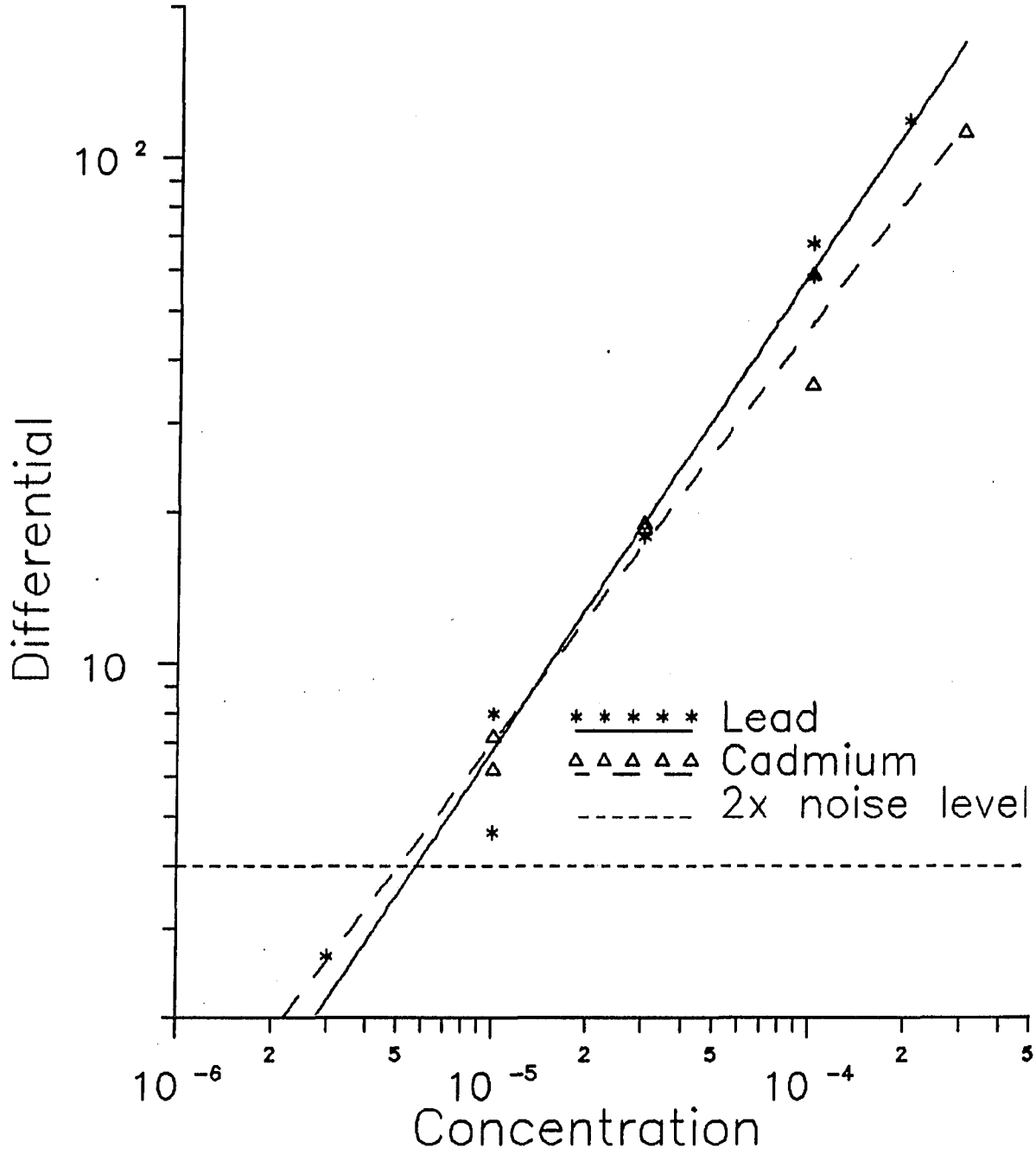

E_d = 0.25 V vs Ag/AgCl

Various concentrations of metals were prepared by dilution of their nitrate salts, buffered at pH 2.0 with KH_2PO_4 and H_3PO_4 at concentrations of ca. 0.09 M and 0.002 M, respectively.

Figure 26. Limit of detection for DCPPP with flowing samples

between the current recorded for the sample and the background is taken. This method indicates whether a sample is present or not, but does not offer the selectivity of a potential scan of the previous technique.

For this second detection scheme, the reduction potentials chosen were -0.400 and -0.610 V vs. Ag/AgCl. A potential of -0.400 V is chosen to reduce lead in solution, and -0.610 V to reduce both lead and cadmium. Current due to lead in solution is calculated as described above, by difference with the background obtained before passage of sample. Measurement of cadmium is slightly more complicated. The current for combined lead and cadmium is found by difference as above at -0.610 V. To obtain cadmium, one must now subtract the current for lead as obtained in the foregoing measurement.

It can be seen that in a mixture of reducible species analysis can become rather complex. If only one species is of interest and if that species can be resolved on the potential scale from others in the mixture, the analysis can be performed by taking data at two potentials, one positive (by ca. 100mV) of the $E_{1/2}$ value and the other negative (by ca. 100 mV). At the value positive of reduction of the species to be determined, all species more easily reduced are measured. At the more negative potential, these species are measured with the addition of the analyte to be determined. The difference between currents obtained at these two potential corresponds to current from the analyte in question.

Figure 27 gives the calibration curve for CPPP using this second mode of detection. As in the study above, all values were taken from duplicate trials, and a dotted line representing a value of two times the

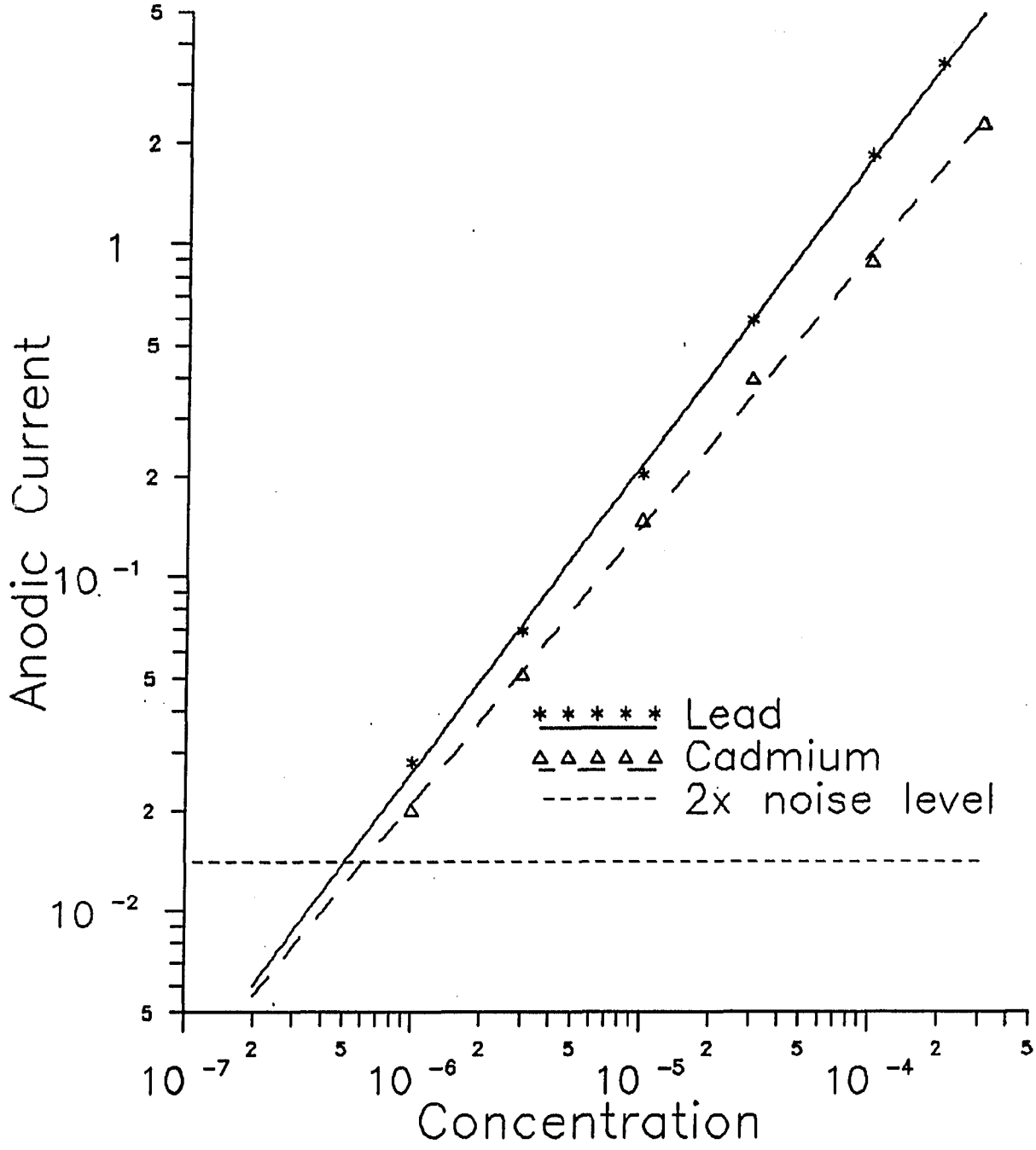

Various concentrations of metals were prepared by dilution of their nitrate salts, buffered at pH 2.0 with KH_2PO_4 and H_3PO_4 at concentrations of ca. 0.09 M and 0.002 M, respectively.

Figure 27. Limit of detection for CPPP with flowing samples using a fixed reduction potential step as described in text

approximate noise level is given. Correlation coefficients of 0.9997 and 0.9992 were obtained for lead and cadmium, respectively. These values represent a slight improvement over the scanned potential methods.

The detection limits for each technique, i.e., NPP, CPPP, and DCPPP using a scanned potential, and CPPP with a constant reducing potential, are indicated in the above figures and are summarized in Table 1.

Table 1. Detection limits for analysis of flowing samples

Method	LOD (2X S/N) Lead	Cadmium
NPP, Potential Scan	3×10^{-5} M	2×10^{-5} M
CPPP, Potential Scan	8×10^{-7} M	1×10^{-6} M
DCPPP, Potential Scan	5×10^{-6} M	5×10^{-6} M
CPPP, Single Potential	5×10^{-7} M	6×10^{-7} M

The lowest detection limits are found using the mode usually associated with flow injection analysis (FIA), i.e., by merely detecting a difference in signal when the sample is either present and not present at the detector. The detection limit of 6×10^{-7} M with the single-potential CPPP method corresponds to ca. 70 ppb for cadmium. It should be noted that the current response is linear through out the ranges shown for each of these methods.

The difference in the LOD for CPPP using the potential scan mode vs. the FIA mode must be in the level of noise, since the same phenomena are measured on a point-to-point scale in the same manner. It is interesting to note that indeed the noise levels differ for each of the CPPP schemes. The value of two times the noise level for the FIA mode is 0.014 μA, while for the scanned potential mode it is 0.032 μA. This difference derives chiefly from the level of signal averaging that can be employed for each method. Detection by CPPP using the FIA approach implies that there are three data regions; before the sample is present at the detector, after it is present, and a transition phase. Ignoring the transition phase, one can average all points in each of the other regions, with the result of two values. While this may be an extreme approach, it clearly contrasts with a potential scan where there are only be a few points on the plateau regions of the curve, for which any noise is not as easily treated in a statistically sound manner.

The benefit of the scanned potential approach is clearly in the realm of selectivity. In one scan of one passing sample, selectivity of several metals on the basis of reduction potential is possible, whereas using CPPP in the FIA mode requires two sets of measurements to selectively isolate only one species. Because the detection limit differs by much less than an order of magnitude, the advantages of the usual potential scan CPPP may still outweigh the slight advantages of LOD for the FIA mode. In either case, the LOD comes very close to that of CPPP in a quiescent solution, as will be shown in the following chapter.

CHAPTER 8. EFFECTS OF NOISE ON SIGNAL

Noise is an integral part of every analytical measurement. Sets of data which are free from noise are often results from analyses of solutions much more concentrated than the detection limit -- concentrations which are not usually in the range of interest. The fundamental limit in any detection method is determined by the level of noise. Therefore, to improve a method or instrumental analysis scheme, one must consider the noise component of the signal and the sources of noise.

Noise with Model 273 Potentiostat Operation

It was stated in the chapter on instrumentation that the EG&G PARC Model 273 Potentiostat/Galvanostat was the instrument initially intended to be at the core of the instrumental apparatus. The reason that the Model 174A Polarographic Analyzer was used in place of the Model 273 was because signals in CPPP operation using the Model 273 exhibited a substantial amount of noise related to the operation of the Model 273.

The noise symptoms from polarograms using the Model 273 were characterized by random data points having absolute values much less than neighboring points. The spacing between these "noise points" appeared to be random, with no discernible frequency dependence, though at least one point in ten was far different than its neighbors. Figure 28 shows a sample polarogram which has a high level of noise in the signal.

It was the author's belief that the timing delay of the measurement

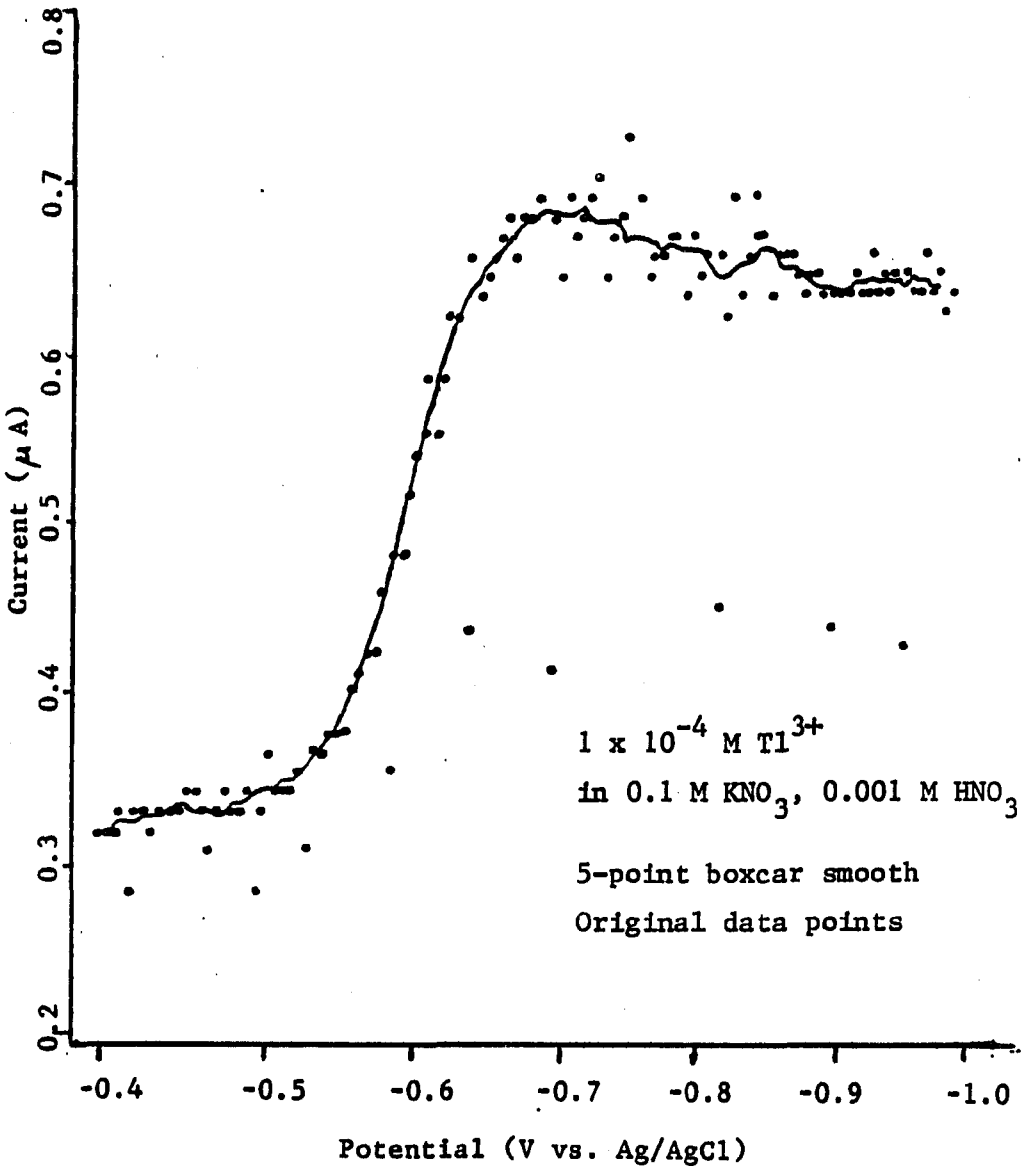

E_d = 0.20 V vs. Ag/AgCl

Figure 28. CPPP data obtained using Model 273 potentiostat

in relation to the potential pulse was irreproducible. This was confirmed by testing with an oscilloscope. An occasional measurement would be displaced by ca. 50 ms from the timing of the other measurements relative to application of the potential pulse. No frequency pattern of this delay could be established, and it was similar to the random occurrence of the "noise points" in the data.

The effect of this can be seen from Figure 29. Part A shows the CPPP waveform, specifically the region of the detection pulse. The period labeled t_d is the delay region where the irreproducibility occurred. Part B of this figure is the expected current response for a metal reduced at E_1 and oxidized at E_2. Sampling of current takes place at time, t_s, and the anodic current sampled is shaded in the figure. Displacement of the sampling period by a 50 ms increase in t_d will clearly result in a smaller measured value of current.

Closer inspection of the oscilloscope trace revealed that not only were occasional delays longer than the others by ca. 50 ms, but that the precision of the other t_d values was only about 10 ms. This 10 ms variation in the timing of the sampling period relative to the potential pulse application also created a substantial fluctuation in current sampled. Because of the high noise levels encountered in operation with the Model 273 potentiostat, the Model 174A was used instead.

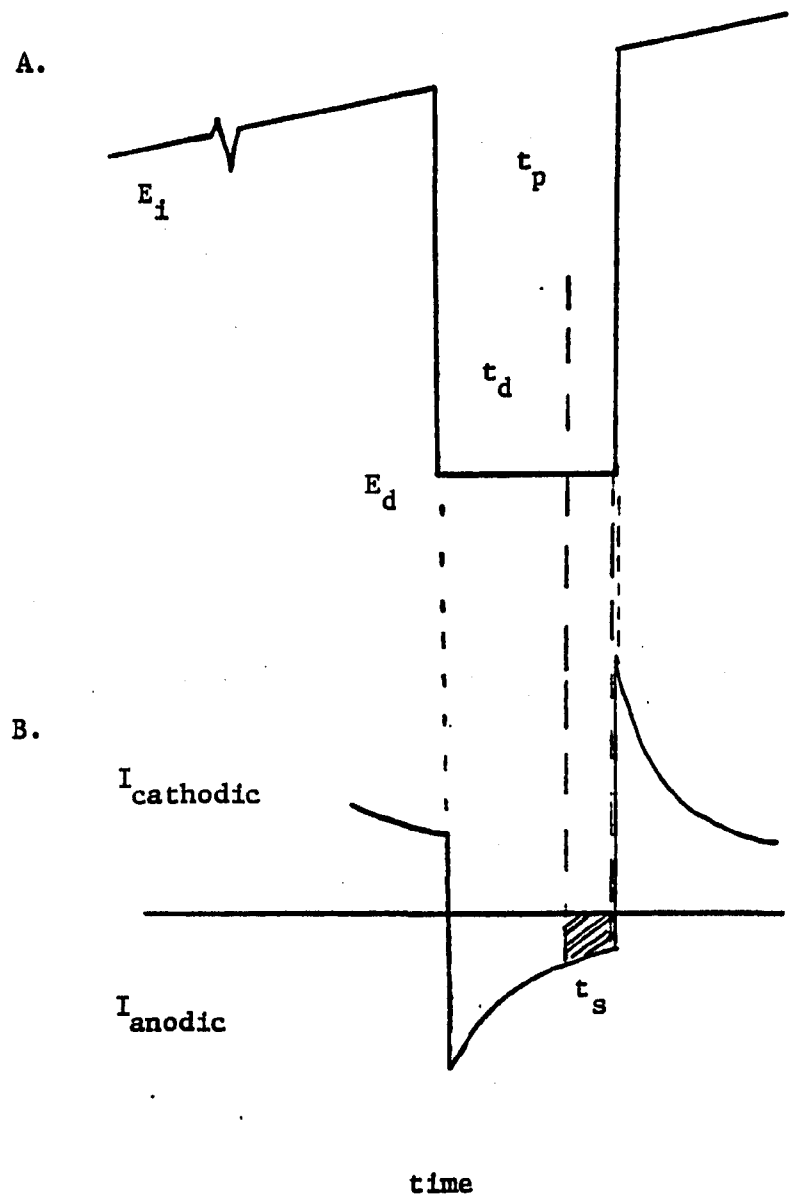

A. Applied potential waveform
B. Current response

Figure 29. Current response in CPPP

Noise Inherent to the Polarographic Technique

Many sources of noise are inherent to polarographic analysis. One of the most obvious sources is the dropping mercury electrode itself, the trademark of polarography. Other sources of noise include fluctuations in the AC power supplying the instrumentation, variability in the measurement potential, or irreproducibility in the timing delay prior to measurement.

The mercury electrode is a source of noise chiefly due to variations in the size of the electrode. The noise arises because the mercury electrode is renewed each time a new drop is formed. The size of each drop is undoubtedly slightly different than the drop before it, since its size is dependent on flow rate of mercury, pressure on the mercury reservoir, and the length of time the mercury is allowed to flow through the solenoid in the case of the SMDE. Each of these factors introduces the possibility of slight variation from drop to drop and must be controlled in order to minimize differences in drop size.

The relationship between drop size and faradaic current can be seen from the Cottrell equation.

$$i_{lim} = n\,F\,A\,D_{ox}^{1/2}\pi^{-1/2}\,t_d^{-1/2}\,C_{ox}^{b}$$

This equation shows that for any set of conditions the current, i_{lim}, is directly proportional to the area of the electrode, A. Thus variation in the size of the mercury drop for each measurement will directly cause variation in the resulting signal measurement.

Another source of noise in pulse techniques is the difficulty of

reproducing a precise detection potential for the pulse application. Variation of a few millivolts can be especially important when the desired observation potential lies on a sloping part of a reduction or oxidation wave, as can be seen from the Heyrovsky-Ilkovic equation solved for current (41).

$$i = \frac{i_d}{1 + \exp\left[-\frac{nF}{RT}(E_{1/2} - E)\right]}$$

i -- current measured

i_d -- diffusion limited current, given by Ilkovic equation

From this equation, it is clear that small changes in potential reflect large changes in current in the region of the $E_{1/2}$ value. This effect can be minimized by choosing a detection potential away from electrochemical waves, either in a plateau region or a range where no faradaic processes occur.

Substantial noise in the signal can result from irreproducible timing in a measurement. When a potential pulse is applied, a large amount of charging current passes, associated with formation of the diffusion layer, as described in Chapter 3. A delay of approximately 40 ms is allowed before measurement of the current begins, which should be sufficient for nearly all of the charging current to dissipate (23).

The faradaic current also decays slowly as a function of time. This relationship is found for pulse techniques in the Cottrell equation above as proportional to $t^{-1/2}$. While the decay of faradaic current is rela-

tively slow, an irreproducible delay time will cause errors due to the variation with time of the faradaic current. This delay must be quite precise in order to minimize noise characteristics. Large variation in this delay time was the probable source of the high level of noise resulting from operation with the Model 273 potentiostat, and it was the reason for our change to the Model 174A.

Analysis in flowing streams is plagued by yet another source of noise. In flowing stream analysis there is a physical disturbance caused to the drop by the moving solution. This disturbance is most easily observed in relation to the pump cycle, i.e., there are regular times in the cycle of the pump when the flow is not constant. The pump was adjusted to optimum conditions, i.e., most constant flow rates, in order to minimize this effect.

Many of the above noise sources are controlled by a particular choice of instrument, be it potentiostat, computer interface, dropping mercury electrode, or flow pump. Choices of apparatus for this research were made with this in mind. For example, the SMDE is claimed to give higher reproducibility in drop size than the DME, in addition to the added benefit of reduced charging current (35).

Smoothing of Data

The fundamental limit in all detection methods is the level of noise in a spectrum or scan. The limit of detection (LOD) is in fact defined to be at a certain factor above the noise, usually three times the signal

to noise ratio (S/N). There are, of course, the sources which are the actual cause of the noise problem, and one would hope to improve the experimental apparatus and method to minimize the level of noise generated by those sources. Since the noise level is in itself the limit of the method, elimination or minimization of all possible contributors of noise demands attention.

It is possible to go beyond the identification and optimization of the sources of noise. One can also treat the noisy data itself. Although this shift in attention from the cause of the problem to the resulting symptoms may seem absurd, it may serve some benefit. The goal of manipulating the resulting signal is to improve the detection characteristics by minimizing noise in the signal, thereby achieving a smoother response function.

One analogy which may be of value in explanation is that of a titration analysis, e.g., titration of an acid with a base. First, the noise sources are identified and optimized, for example, the buret is cleaned and then rinsed with base, and then readings are carefully made. Care is taken to minimize any source of error by such steps. One goes beyond this in typical analyses, however. The sample is usually analyzed in triplicate so that better results may be obtained by averaging trials. This final step -- the averaging of three or more trials for a final result -- is a further statistical treatment aimed at minimizing the random error, or noise, of the method. Note that it is not treatment of the cause of the noise, but of the effect. Methods such as this have been shown to be statistically useful in minimizing random errors, or

optimizing the signal-to-noise aspects of an analysis.

Many approaches to data-smoothing have been discussed in literature reviews (45-47). Several methods have been built into existing analytical instrumentation, such as the time-based filtering capabilities of many analog instruments, which are commonly based on R-C circuits. Other data-smoothing approaches are mathematical in nature, such as simple averaging used in box-car smoothing. Finally, there are more sophisticated mathematical methods, including least-squares filtering (Savitzky-Golay smoothing) and Fourier transform smoothing.

With all noise-reduction methods, one must address the concern of whether the noise is actually reduced relative to the signal or whether the result is only more aesthetically pleasing. A study of several smoothing schemes is presented, with emphasis on box-car filtering, Savitzky-Golay least squares filtering, and Fourier transform smoothing. Each technique will be discussed and then comparisons will be shown.

Moving boxcar filter

Boxcar filtering is essentially a moving average with equal weighting of all points in the range. In a large set of data points, a group of points is averaged together yielding a value which is substituted for the first data point in the set. A second group is then averaged, including all the members of the first set except for the first point, and adding the next point in sequence after the initial set. The averaged value is then inserted in place of the second point and averaging proceeds until all data have been included in the process. The final

number of data points is decreased by one less than the number of points included in each average.

Boxcar smooths using larger groups of points for the smooth result in better signal-to-noise ratios, but they also tend to distort the response. The result of boxcar averaging is that peaks are made broader and shorter and that curved portions are flattened. This is discussed more fully in an analysis by Dessy (45).

Savitzky-Golay moving average

Savitzky-Golay filtering derives its name from the two originators of the method (48). The method is intended to give a series of points which would tend to form a line best fitting the data. The originators of the method defined this "best fit" by the method of least squares, i.e., the square of the differences between computed and original values was minimized for the points considered. Convoluting functions which are the numerical approach to the least squares method were given. This numerical approach exactly reproduces the least squares method, as was shown in derivations by Savitzky and Golay (48). These convolution functions were in the form of weights assigned to each point used in the moving average.

Smoothing by the least squares method of Savitzky and Golay is similar in practice to the boxcar moving average, except that in the Savitzky-Golay scheme the points are not weighted equally. The assigned weights are a function of the number of points to be considered in the convolution range and can be found in reference tables in the original

reference. In general, the points at the center of the averaged range are heavily weighted and points closer to the edge of the range are given lesser weights.

The least squares method of curve fitting is better at maintaining the integrity of features in a scan than is the boxcar filter. The Savitzky-Golay fit results in a reduction in peak height of less than 1% when the number of points within the FWHM is at least a factor of 1.4 times the number of points in the convolution range. A moving boxcar filter distorts peak shapes by reducing peak heights and increasing peak widths, two parameters which commonly relate directly to physical or chemical properties (45).

The enhancement in S/N is the same for Savitzky-Golay filtering as for the boxcar method, i.e., proportional to $N^{1/2}$, where N is the number of points in the convolution range (45). Note, however, that in Savitzky-Golay filtering this enhancement results without the distortions in peak shape that are observed for the boxcar method.

A computer program in QuickBASIC was written by the author to perform boxcar and Savitzky-Golay filtering, in addition to other data manipulation routines. The program can be found in Appendix II. It is programmed with the weighting functions for five- and seven-point Savitzky-Golay least squares fits. Savitzky-Golay filtering can be performed in a few seconds or less over data sets containing several hundred points, so the application of this filter is not highly time-consuming.

Fourier transform smoothing

The Fourier transform is a tool that can be used to gain improvement in the noise characteristics of a set of data points. Smoothing of data by Fourier transform methods is based on manipulation of the various frequencies in the spectrum. In this research, many sources of noise are found at very different frequencies than the useful portion of the data.

One example of the variation in frequency of the data can be observed from changes in the size of the electrode drop. Variations in drop size are a problem in polarographic methods. Small differences in size of successive mercury drops represents noise of a very high frequency, i.e., point-to-point fluctuations. For perspective, a polarographic wave develops over a range of 100 - 200 mV, or over 10 to 20 data points (taken at 10 mV intervals), which corresponds to a low-frequency event when compared with variation on a drop-by-drop scale. Any smoothing method which produces a curve with reduced high-frequency information and which does not disturb the low-frequency information content can be used to improve the signal-to-noise characteristics of an analysis.

The procedure in Fourier smoothing is to take the Fourier transform of the spectrum with respect to time, yielding a spectrum in the frequency domain. This frequency-domain information is then treated with some weighting function, usually to eliminate certain frequency ranges from the spectrum, and is then transformed back to the original form, a spectrum in the time domain (45, 49, 50). In our research the low frequencies are left intact and the high frequency range is eliminated. The resulting curve represents a smoothed version of the original data, with

all of the low-frequency information remaining, but with much of the higher-frequency content gone.

The weighting function used in this work contains a cutoff frequency above which all information is discarded. Below that threshold, all information is kept. A weighting function of the form $(1 - (x/N)^2)$, where x is the frequency point considered and N is the point number of the cutoff frequency, was suggested by Aubanel et al. (50). It appears to this author that their method diminishes the importance of the higher remaining frequencies in the smoothed spectrum, reducing the slope in the range of the $E_{1/2}$ and reducing peak heights for the differential technique. A method of determining the optimum cutoff frequency has been suggested by Lam and Isenhour (51) and was followed for this work.

Fourier transform smoothing is an aid toward improvement of noise statistics when it is known that the noise is of a high frequency. For the random-frequency noise, the transform may also be of help. The effect will not be as advantageous, for the noise that is higher in frequency than the cutoff value can be reduced, but the noise relating to other frequencies remains in the spectrum at unchanged levels. That is the case in this research, although it is known that substantial noise is of a higher frequency than the electrochemical information in the original data.

A computer program in BASIC language has been written to perform the Fourier transforms and smoothing function based on equations taken from the paper by Aubanel et al. (50). A computer-ready algorithm was presented in their paper, but programs written from it were not functional.

The routine used for the present work was found to require less than a minute of computer operation for a typical set of transforms. For larger scans containing ca. 1000 points and smoothed with very high frequency thresholds, about 5 minutes of computer time was required. For a personal computer having a clock speed of 8 MHz this was considered adequate. The program written for this application is presented in Appendix III.

Comparison of Smoothing Methods

It is important to note in all of the data-fitting by either of these methods that no points are arbitrarily discarded. All data are considered in each of these methods and the integrity of the complete data set is maintained. One can achieve, by judicious choice of smoothing methods and parameters, an accurate representation of the original information without "whiting-out" or changing data points. One can have the increased aesthetic appeal of a "clean" data set as well as maintaining the integrity of the data. As was noted in the discussion of Fourier fitting, one can also realize improvement in the signal-to-noise ratio, yielding increased detectability at extremely low levels.

The following set of figures provides a comparison of the smoothing methods described. The first set of curves (Figures 30 and 31) are based on a single data set having a low level of noise. Only a small portion of the curve is given, the region of the cadmium wave. This allows a close-up picture of the response for a plateau and a highly sloping region.

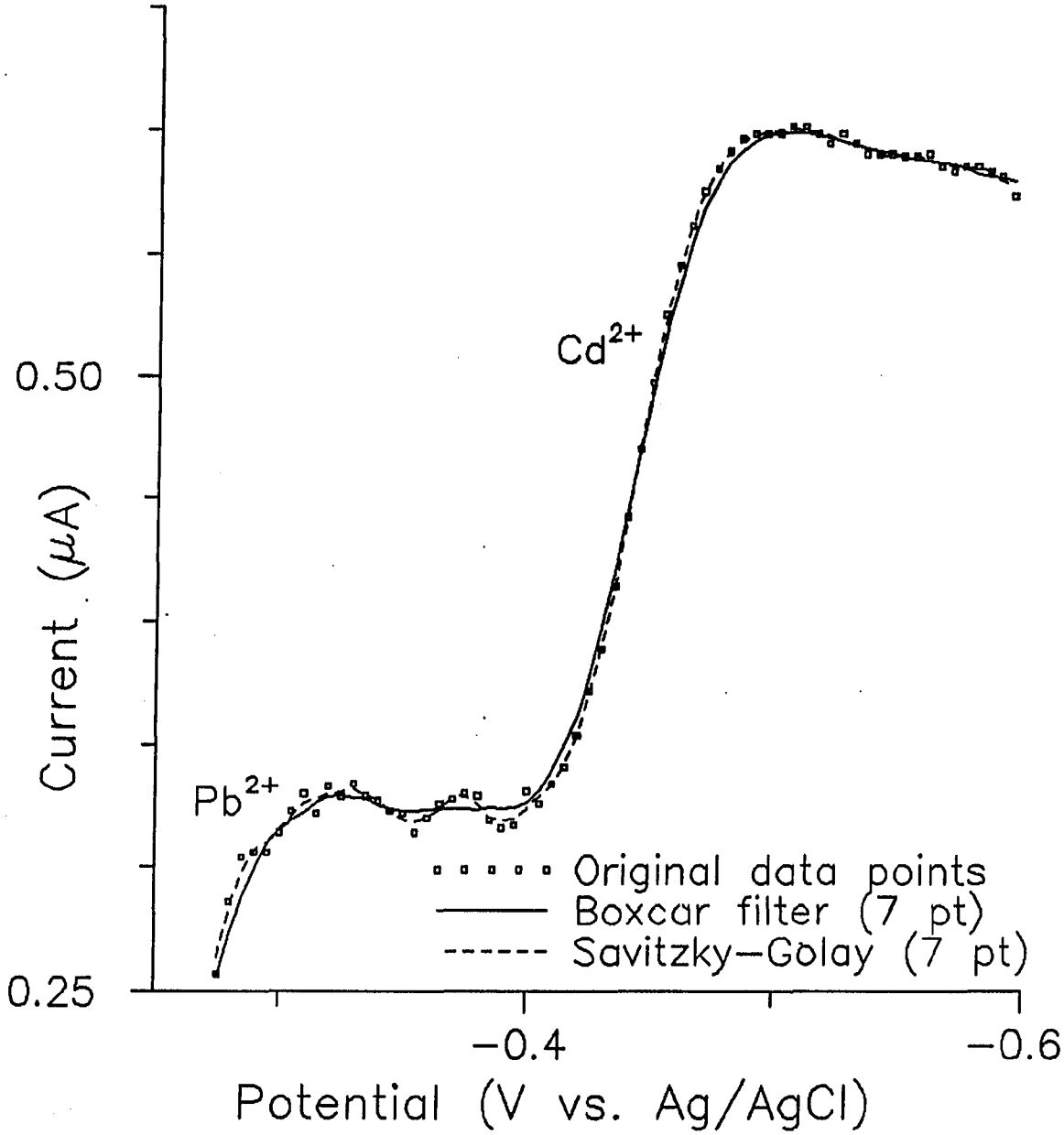

Solution contains 1 x 10^{-5} M Pb^{2+}, Cd^{2+}, 0.1 M KNO_3, and 0.001 M HNO_3

Figure 30. Comparison of data smoothing on a CPPP scan with low noise

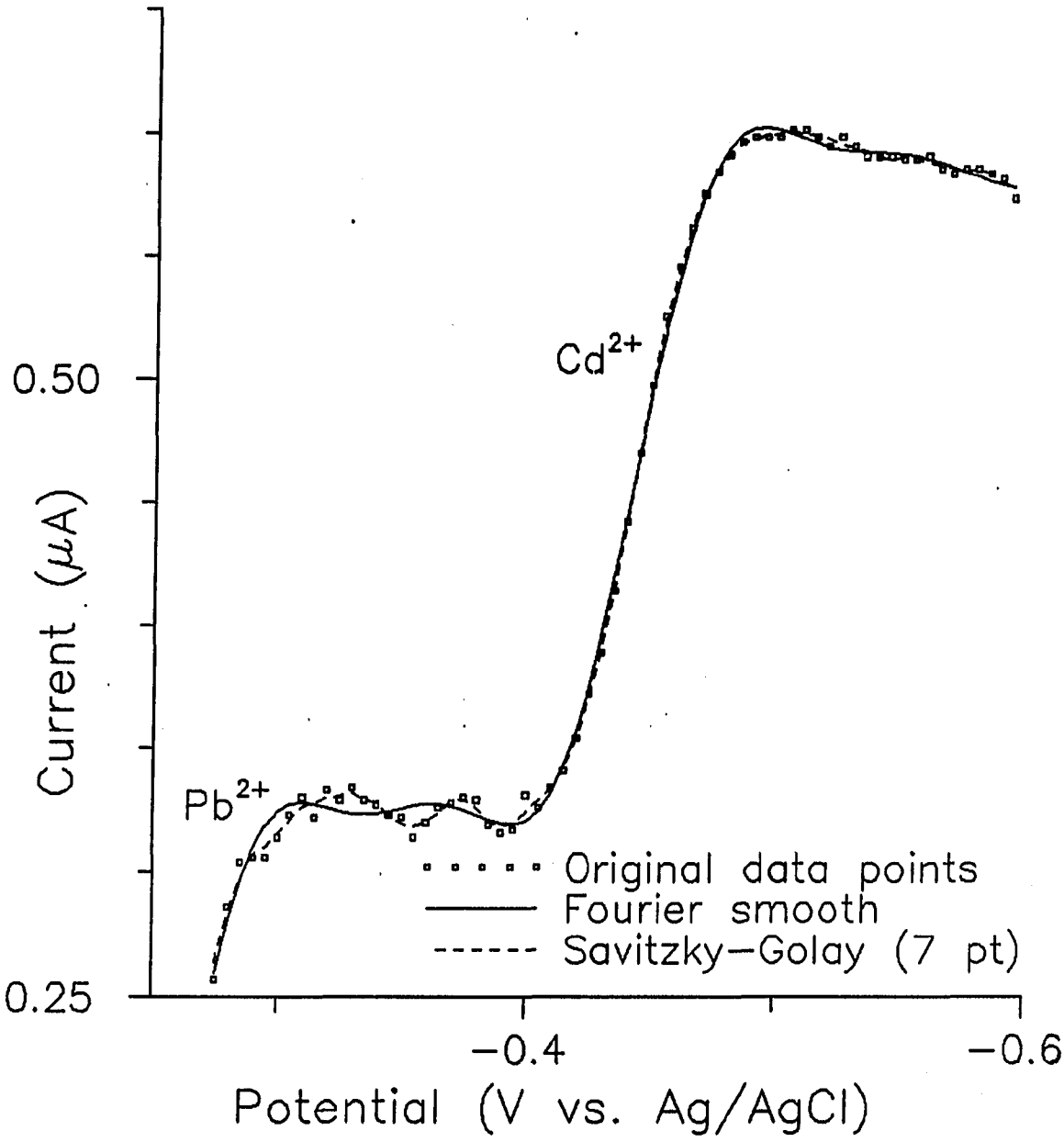

Solution contains 1 x 10^{-5} M Pb^{2+}, Cd^{2+}, 0.1 M KNO_3, and 0.001 M HNO_3

Figure 31. Comparison of data smoothing on a CPPP scan with low noise

Figure 30 shows the original data points, a seven-point boxcar smooth, and a seven-point Savitzky-Golay smooth. Note that the boxcar smooth gives a flattened response in the $E_{1/2}$ region. It shows a flat plateau response, but distorts the characteristic wave. The Savitzky-Golay curve follows the points very closely and also reduces the noise level. Though it appears to contain more noise, the more accurate smooth appears to be the Savitzky-Golay curve.

Figure 31 shows the same data points and the same Savitzky-Golay smooth as in the previous figure. In addition, the Fourier transform smooth is included in Figure 31. The first 15 points of the frequency-domain curve were kept and transformed back to the time-domain curve shown. The curve appears to follow the data points closely and also shows a more flat plateau region than does the Savitzky-Golay smooth. Neither curve shows any clear distortion of the data, and the noise in the plateau region is reduced by ca. two times for the Fourier curve.

Differentiation of the data appears to increase the noise level of the spectrum. Much of this is due to the high-frequency noise contributed by small variations in the drop size, as discussed in Chapter 6. The same data which was used in Figures 30 and 31 has been differentiated and then smoothed by the indicated method. In Figure 32 shows the original differential data and a Savitzky-Golay seven-point fit to the data. The digital nature of the measurement is clear from the original data, but the smoothed line also shows substantial noise.

In Figure 33 the same data set is shown with different smoothing comparisons. The points in this figure correspond to the Savitzky-Golay

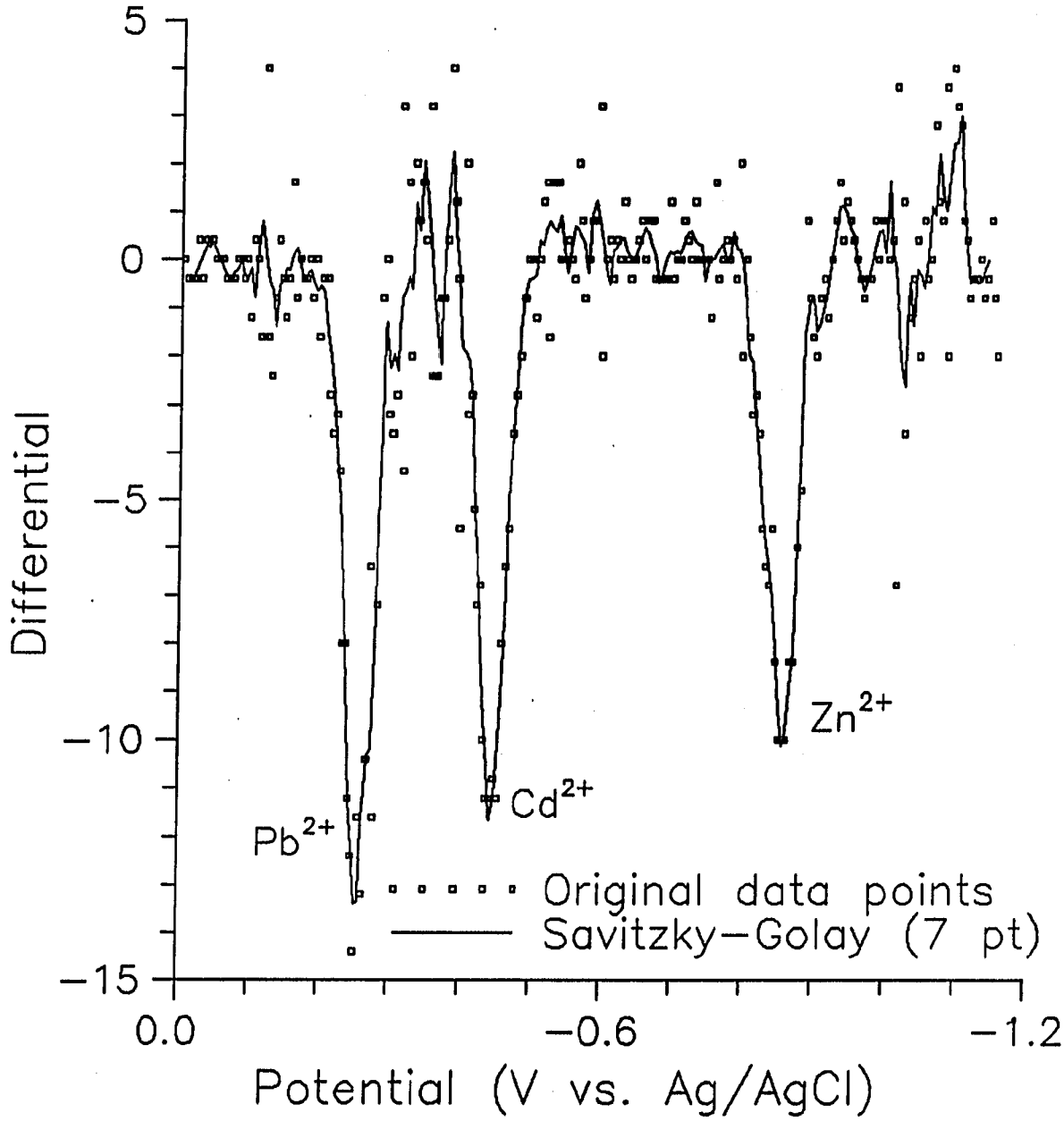

Solution contains 1 x 10^{-5} M Pb^{2+}, Cd^{2+}, and Zn^{2+} with 0.1 M KNO_3 and 0.001 HNO_3

Figure 32. Effect of data smoothing on a DCPPP scan

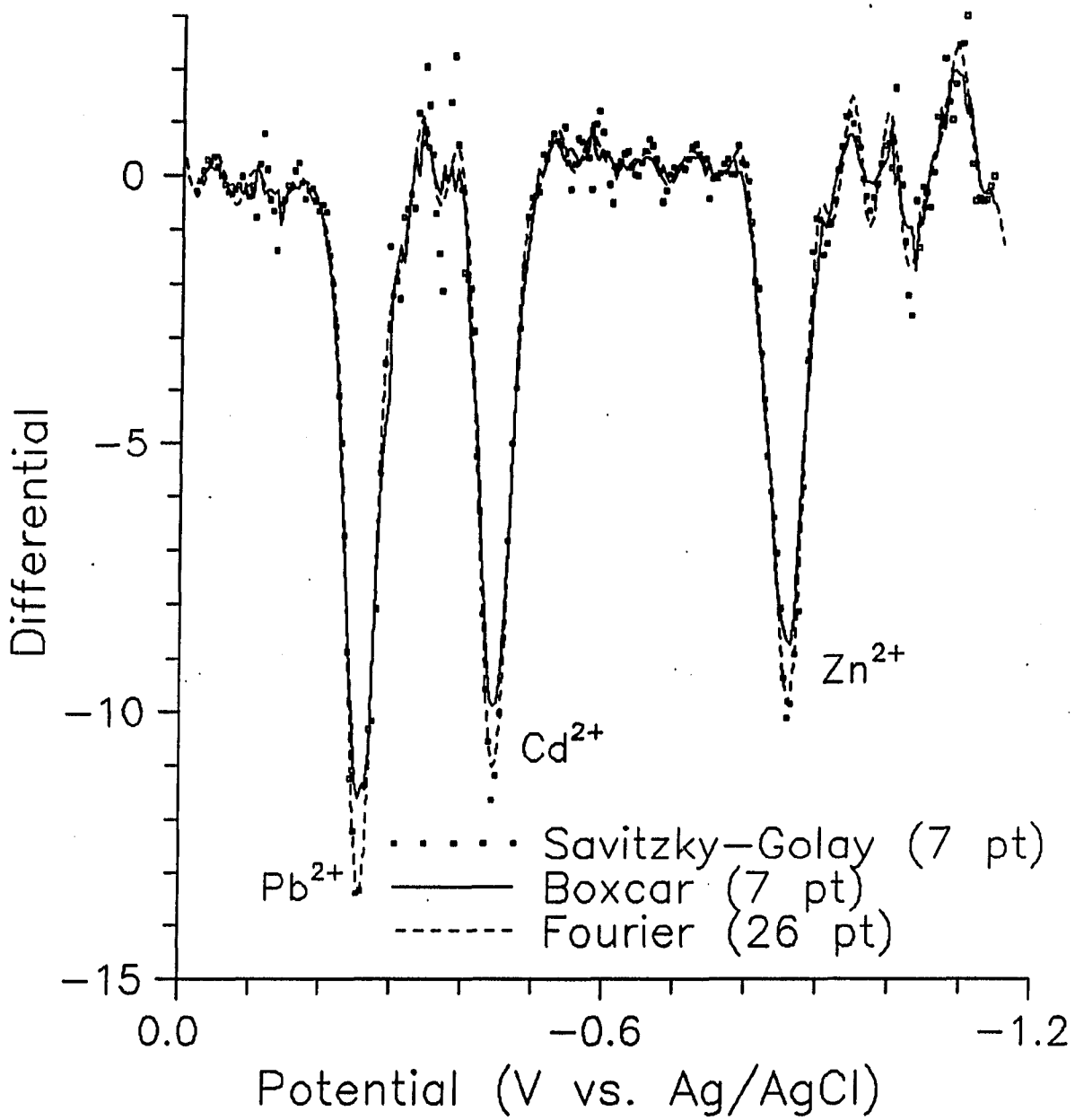

Solution contains 1 x 10^{-5} M Pb^{2+}, Cd^{2+}, and Zn^{2+} with 0.1 M KNO_3 and 0.001 HNO_3

Figure 33. Effect of data smoothing on a DCPPP scan

fit in Figure 32, along with the boxcar smooth and a Fourier fit. In this case the boxcar method cuts down considerably on noise, but it again distorts the peak height. The Fourier fit also reduces the noise, but without the distortion. The value of data smoothing is apparent from these examples.

Sets of data having higher levels of noise show the same response to smoothing with greater clarity. In Figures 34 and 35 are the differential scans of a solution containing 1 x 10^{-6} M concentrations of Pb^{2+}, Cd^{2+}, and Zn^{2+}. The unsmoothed and seven-point Savitzky-Golay fits had too much noise to be of value to the illustration, so the boxcar and Fourier smooths are compared. Note first the boxcar smooth, in Figure 34. The smoothing function was a fifteen-point boxcar filter, chosen to minimize peak distortion. Figure 35 is the Fourier fit, made by retaining the first 27 of 300 frequency points. If one were to overlay these two curves, it would appear that the same line was followed with and without noise for the boxcar and Fourier fits, respectively. This directly affects the signal-to-noise ratio.

It was found that in curves which already appear to be acceptable in terms of noise, that there was nothing to be gained by using the more sophisticated Fourier methods. On the other hand, curves with extremely high noise levels benefited greatly from the Fourier transform techniques relative to the others.

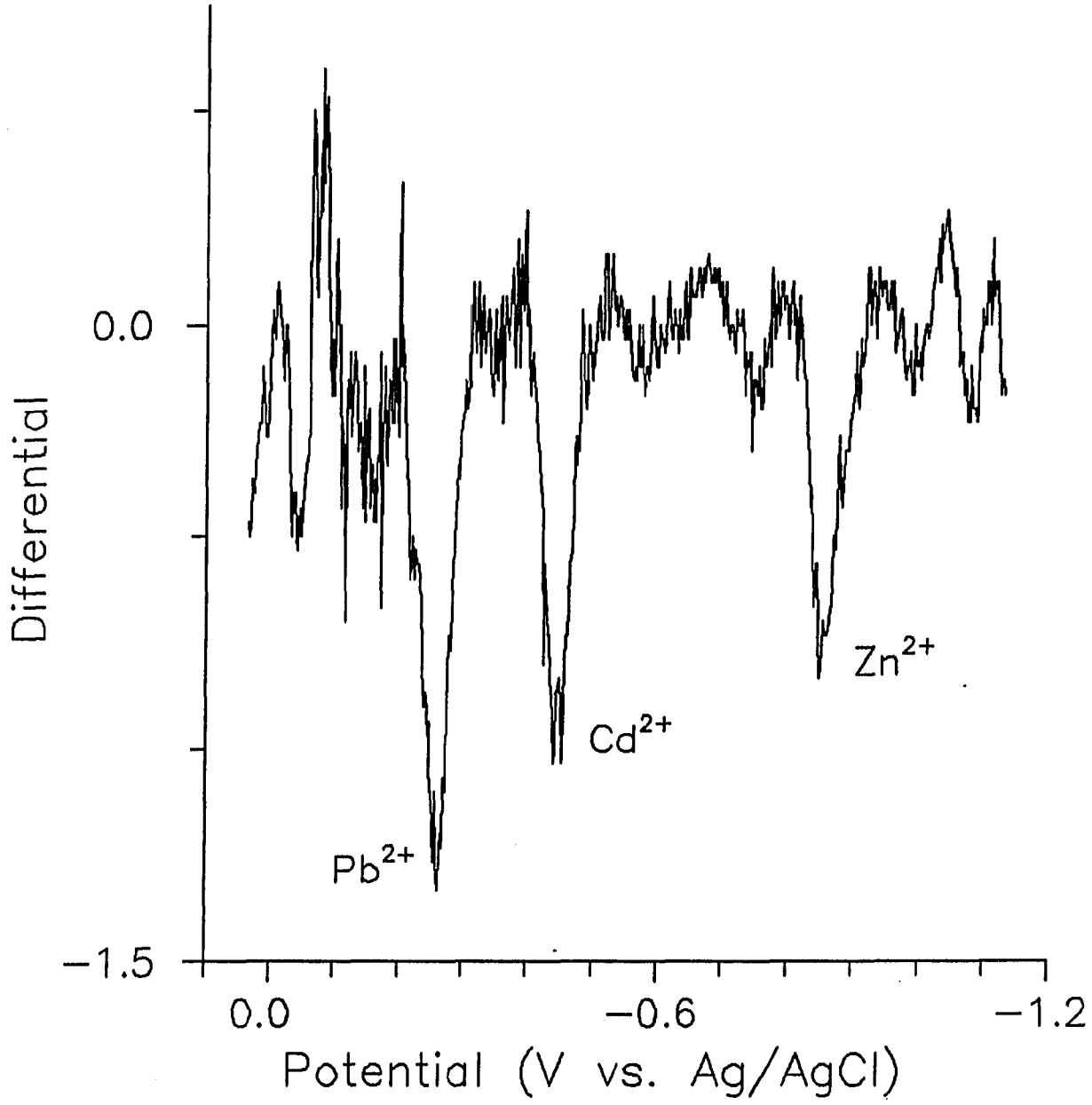

Solution contains 1 x 10^{-6} M Pb^{2+}, Cd^{2+}, and Zn^{2+} with 0.1 M KNO_3 and 0.001 HNO_3

Figure 34. Boxcar smooth of a DCPPP scan with high noise

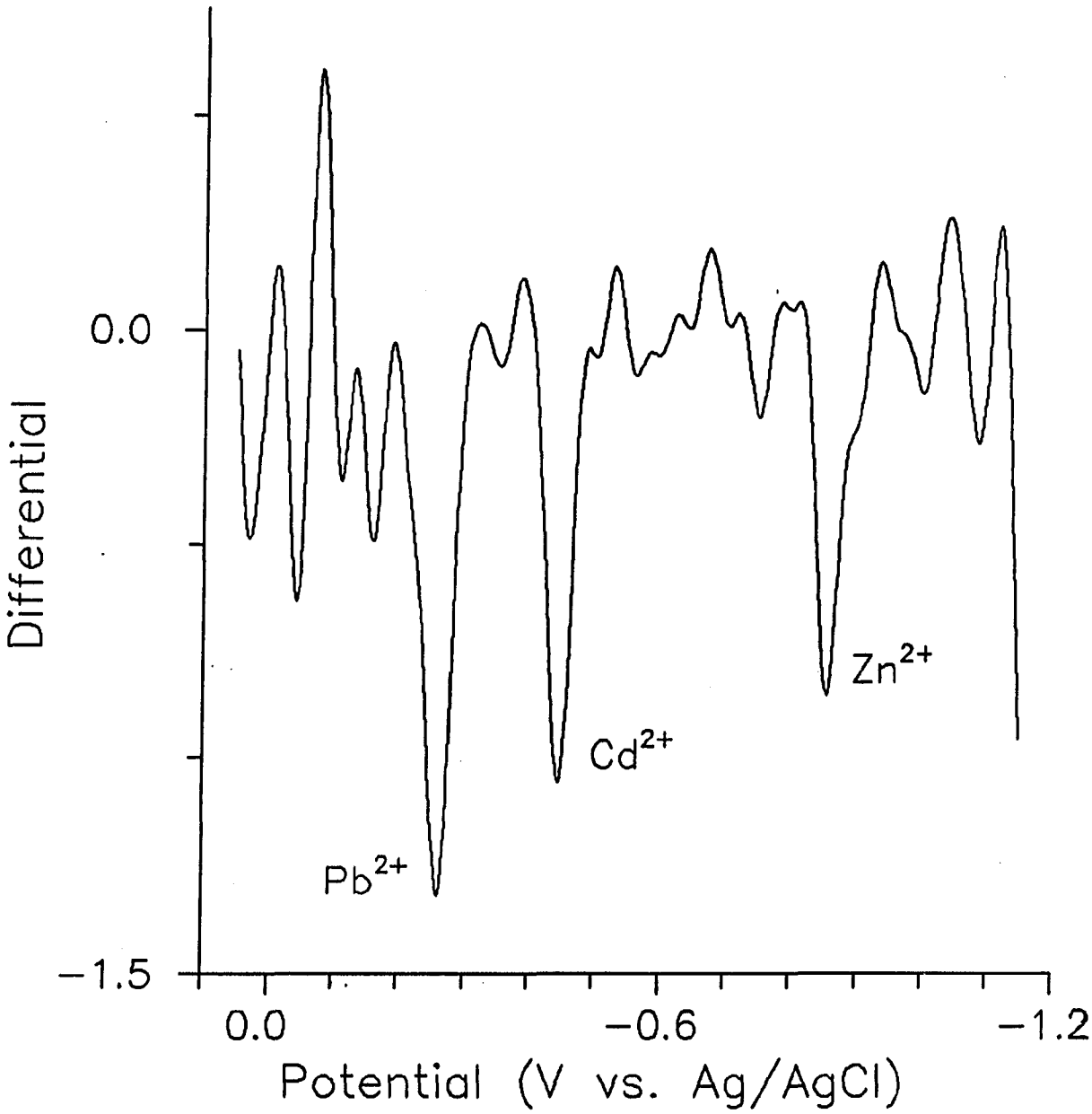

Solution contains 1 x 10^{-6} M Pb^{2+}, Cd^{2+}, and Zn^{2+} with 0.1 M KNO_3 and 0.001 HNO_3

Figure 35. Fourier transform smooth of a DCPPP scan with high noise

Limit of Detection

A study was made to find the LOD for CPPP and DCPPP and to compare that with the best polarographic method, DPP. Solutions of lead, cadmium and zinc were used for the study, and oxygen was removed only from the samples analyzed by DPP. The calibration curves are shown in Figures 36 and 37 for CPPP and DCPPP, and in Figure 38 for DPP. All samples were analyzed here in the batch mode. The LOD of flowing samples was presented in Chapter 7.

The correlation coefficients for all of the lines for CPPP and DPP were better than 0.999, while for DCPPP they were 0.9988, 0.993, and 0.9983 for lead, cadmium and zinc, respectively. The results are tabulated in Table 2 for both the batch analysis presented here and the work on flowing samples done earlier. The data for DPP represents purged solutions, while the other information came form air-saturated samples.

It was expected that the LOD for DPP would be better than for CPPP and DCPPP from the discussion in Chapter 3. That is indeed the case, though it should be noted that the difference is only one order of magnitude. Thus CPPP and NPP share about the same LOD. The limits can also be stated in terms of parts per billion (ppb). When the values for analysis of zinc are used, these limits are for DPP, 2 ppb; for CPPP, 10 ppb; and for DCPPP, 30 ppb.

Effect of data smoothing on limit of detection

The result of smoothing affects the detection limit directly. Since the LOD is defined as two or three times the noise level, a decrease in

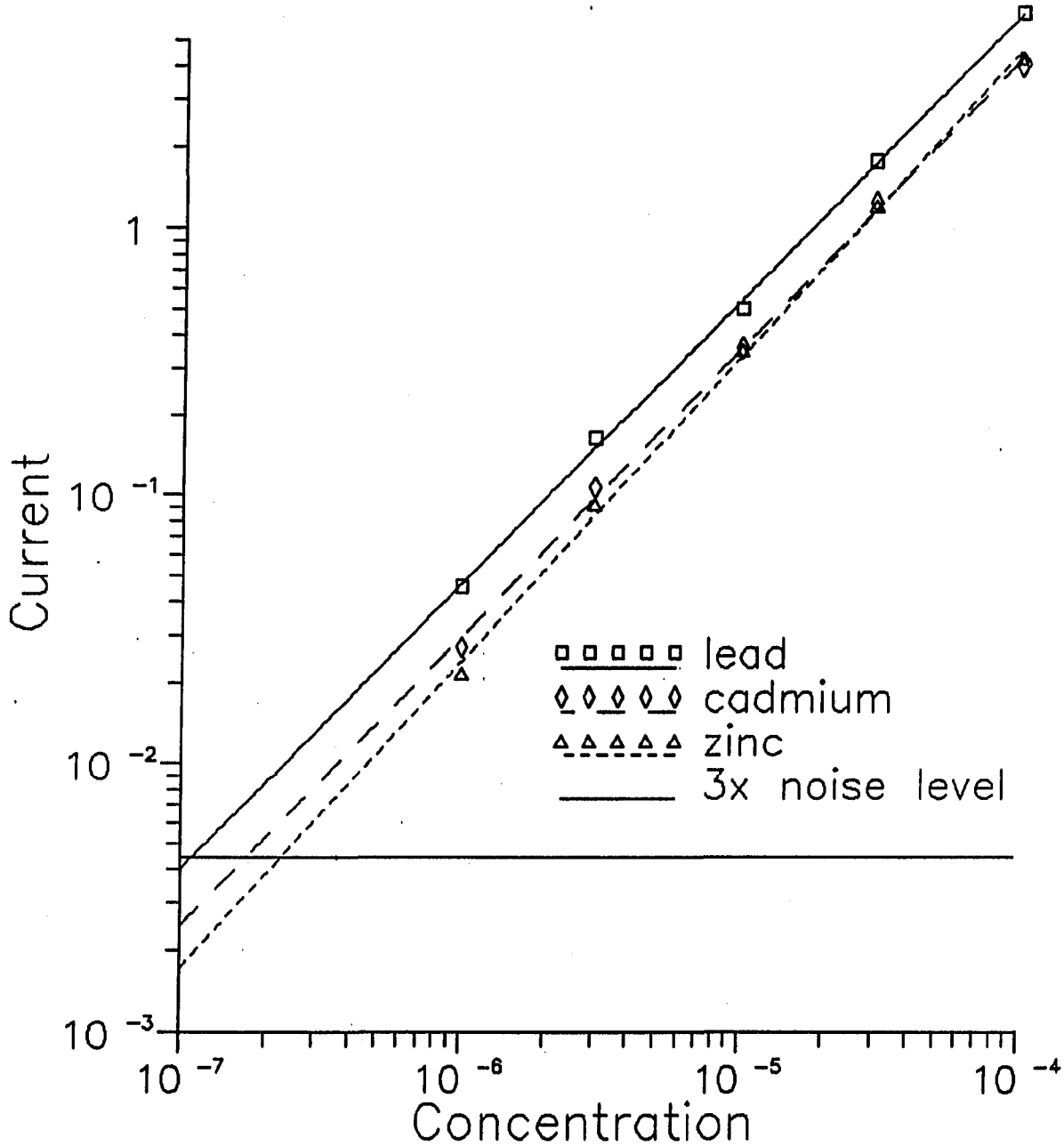

Various concentrations of metals were prepared by dilution of their nitrate salts into 0.1 M KNO_3 and 0.001 M HNO_3

Figure 36. Limit of detection for CPPP in unpurged batch solution

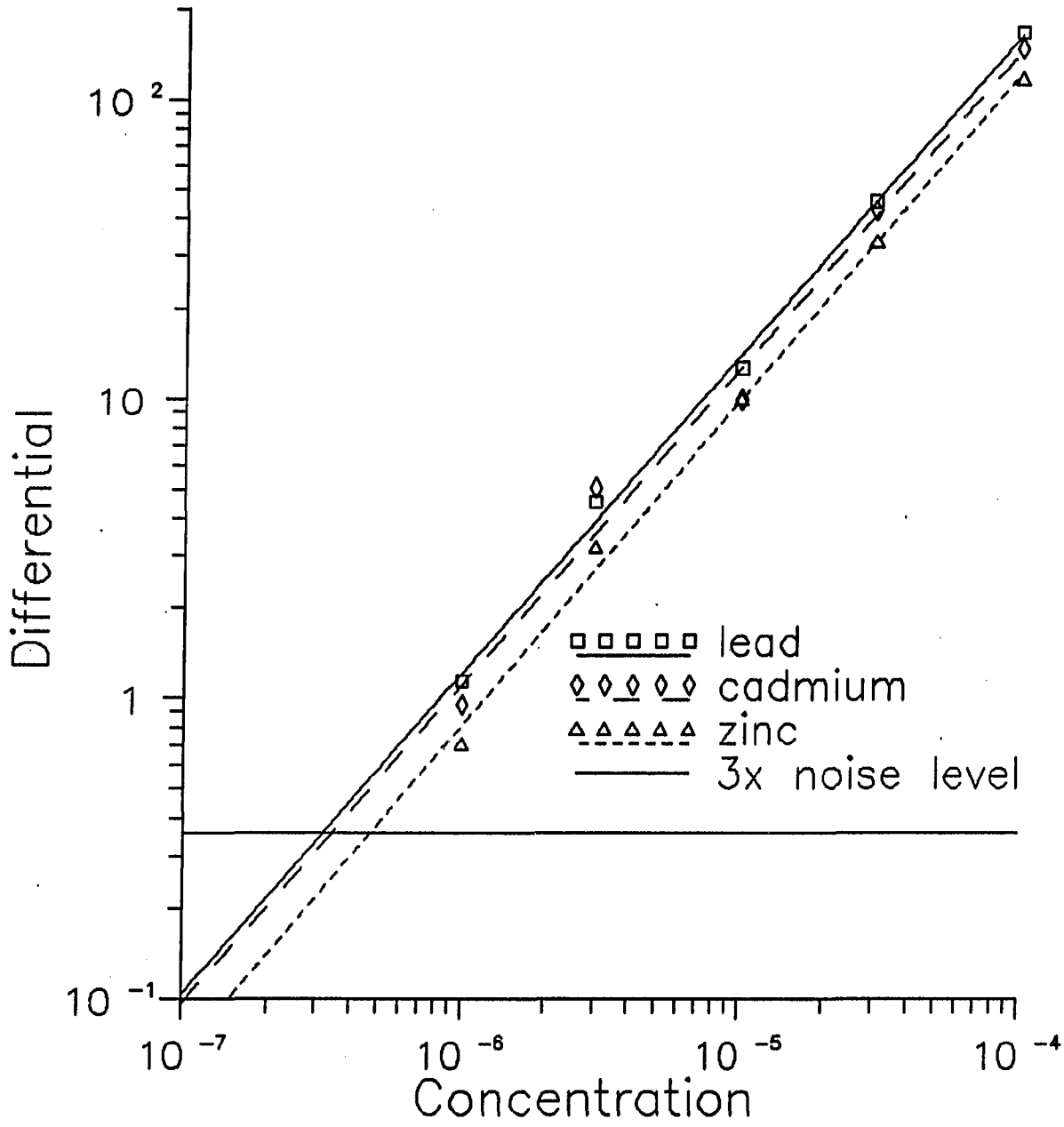

Various concentrations of metals were prepared by dilution of their nitrate salts into 0.1 M KNO_3 and 0.001 M HNO_3

Figure 37. Limit of detection for DCPPP in unpurged batch solution

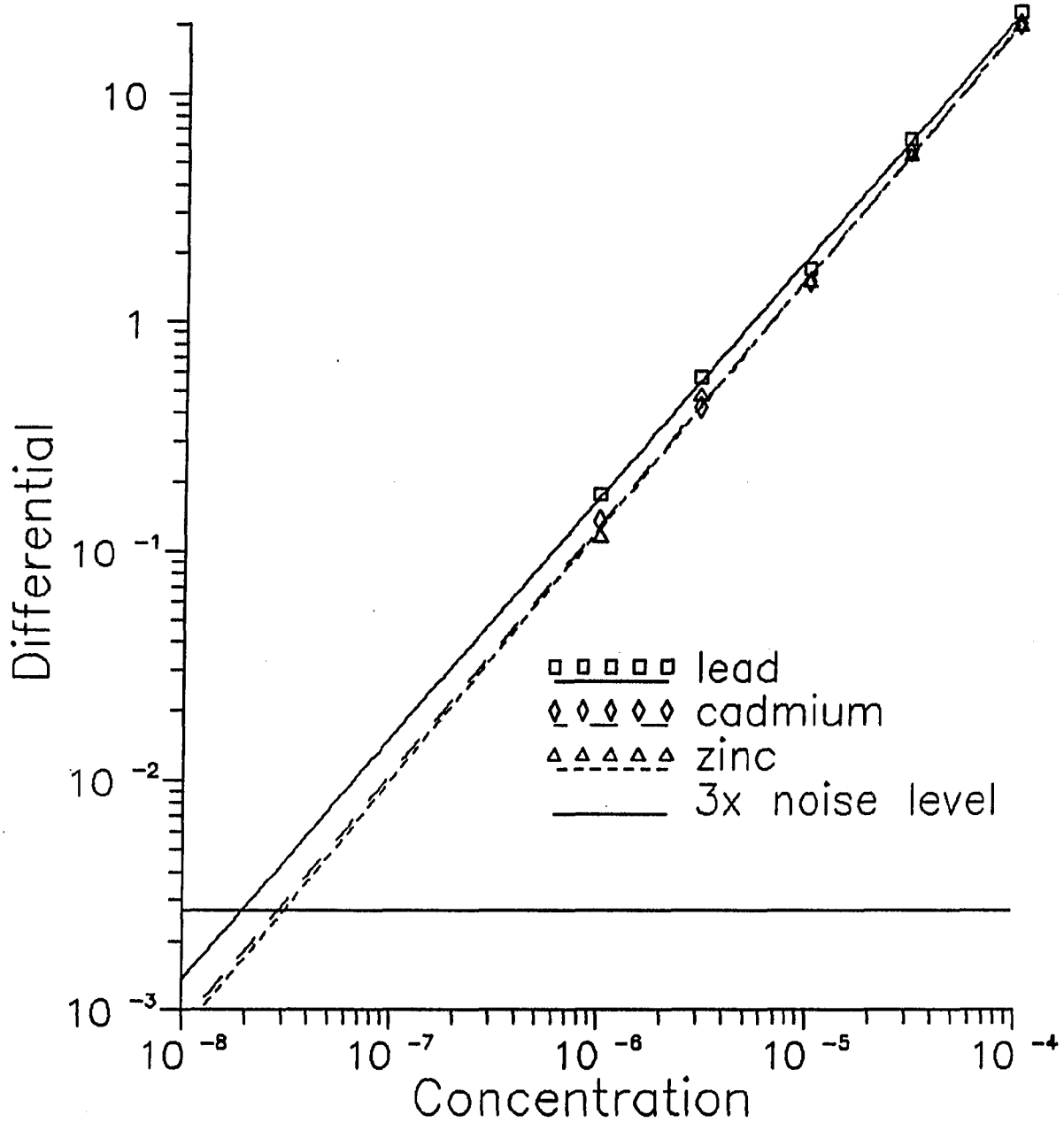

Various concentrations of metals were prepared by dilution of their nitrate salts into 0.1 M KNO_3 and 0.001 M HNO_3

Figure 38. Limit of detection for DPP in purged batch solution

that noise level means a reduced LOD. The results from the various smoothing methods have been compared, and there are differences in the resulting noise levels. The differences between smoothing methods are small, however, when compared to the difference between the unsmoothed curve and any of the filtered data sets. Comparing scans from Figures 32 and 33, the noise levels for the unsmoothed and Fourier smoothed scans are approximately 0.75 and 0.30, respectively, yielding S/N ratios of 15 and 37 for the middle peak for the original and Fourier curves. The net effect of this is a lowering of the LOD by a factor of 2.5.

One could ask why the improvement is not greater. It is expected for boxcar averaging that the improvement in S/N is proportional to $N^{1/2}$, where N is the number of points in the filter function. In this case seven points were used, so the improvement should be a factor of 2.6, approximately the improvement obtained for the Fourier method. If one were to sample points at smaller potential intervals, one could include more points in the filtering function and reduce the noise level even further. However, to accomplish the same feat by averaging points over a wider potential region serves only to reduce the information content of the data.

Table 2. Detection limits for batch and flowing samples by CPPP, DCPPP and DPP

Sample	Method	LOD (2X S/N for Batch, 3X S/N for Flowing) Lead	Cadmium	Zinc
Batch	DPP	2×10^{-8} M	3×10^{-8} M	3×10^{-8} M
	CPPP	1×10^{-7} M	2×10^{-7} M	2×10^{-7} M
	DCPPP	3×10^{-7} M	3×10^{-7} M	5×10^{-7} M
Flowing	NPP, Pot. Scan	3×10^{-5} M	2×10^{-5} M	
	CPPP, Pot. Scan	8×10^{-7} M	1×10^{-6} M	
	DCPPP, Pot. Scan	5×10^{-6} M	5×10^{-6} M	
	CPPP, Single Potential	5×10^{-7} M	6×10^{-7} M	

CHAPTER 9. SUMMARY

This work can best be summarized by looking back at previous efforts. Prior polarographic analyses in flowing solutions required removal of dissolved oxygen, which was accomplished by various methods (9-12), none of which was found to be universally acceptable (43). With the recognition that CPPP allowed detection of metals without interference from dissolved oxygen, detection in flowing streams became feasible, but was only shown for concentrations of 10^{-4} M or greater (13, 17). The elimination of the purging step alone can cut down on sample throughput time by a factor of about four, from 12 - 20 minutes to 2 - 5 minutes per analysis, depending on scan rate.

In this work an instrument has been modified to perform the CPPP technique. This simple modification, i.e., the addition of a jumper wire and a switch, can be easily made to the Princeton Applied Research Model 174A Potentiostat to allow detection with CPPP by other workers using standard existing equipment.

In this research the detection limit for CPPP has been extended for flowing stream analysis to below 10^{-6} M and to slightly lower levels for batch solution analysis. This is an improvement in the detection limit for flowing samples of more than two orders of magnitude.

A differential technique offering increased selectivity has also been introduced, DCPPP. The advantage over CPPP of increased resolution is shown, with resolution for DCPPP shown to be on the same order as for DPP. Detection limits for DCPPP are in the low 10^{-6} M range, in batch

and flowing samples. The calibration curves for both CPPP and DCPPP are shown to be linear over a range of more than two decades of concentration, from 1 x 10^{-6} M to more than 10^{-4} M.

A degree of freedom from the interference of hydrogen ion in acidic solution has been shown for CPPP and DCPPP in addition to the freedom from interference of dissolved oxygen. This allows analysis of metals such as zinc and nickel in very acidic solutions where hydrogen ion would interfere with analysis by other polarographic methods.

Finally, the effective use of smoothing has been shown on polarographic data for both CPPP and DCPPP. The viability of the method and the improvement in LOD have been shown.

It has been suggested by at least one author that the use of mercury electrodes, specifically the DME, will not "last as a competitive analytical device (for any purpose) beyond the turn of the century" (52). Bond has responded to this with several cases where the use of mercury electrodes presents the only viable solution to specific analytical problems, stating that mercury has unique and useful characteristics which make it the preferred electrode material in a number of instances. He summarizes his review by acknowledging that solid electrodes are likely to replace mercury electrodes in some situations, but that "it is highly probable that the mercury electrode will continue to survive and indeed thrive well into the next century." He goes on to say, "the analytical chemist should ensure that ... a wide range of electrode materials is available for use in flow-through electrochemical cells" (53).

Comparing polarography with other analytical methods, the first

factor in favor of polarographic methods is its low cost. A complete, computerized polarography work station can be assembled for under $15,000. When compared with costs for inductively coupled plasma (ICP) or even atomic absorption spectroscopy (AAS), polarography shows a sizable advantage. Considering the major competition of polarography to be AAS, it has been said that pulse polarography offers "a sensitivity at least as good as its main rivals at a much lower cost" (54).

Future Work

One advance which could be used to further decrease the detection limit would be the development of a single-drop technique for DCPPP. In Chapter 6 it was stated that a single-drop technique was not feasible for DCPPP, the main reason being that it would not yield a signal accurately representing the differential. Although the use of two measurement pulses per drop may not give directly meaningful faradaic signal due to the depletion of preconcentrated sample in the measurement step, it could be useful in subtracting out any charging current in the measurement and to eliminate the increased noise due to variability in drop size.

APPENDIX I.

This appendix presents the modifications made to the Head Start Electrochemistry Software from EG&G Princeton Applied Research. The program is available from EG&G PARC in its original form. The modifications described here were made to version 1.2 of the commercial program, which was the latest version available during the period of this research.

Alterations made to the program fit into two categories; those made to allow communication between computer and potentiostat, and those made for handling data within the computer. The latter changes allow storage of data within the computer in an (x,y,z) format, where x is the potential in V, y is the current in uA, and z is the point number in the scan sequence. These modifications are numbered with program lines between 27000 and 28000.

The changes affecting communication with the analytical instrument are incorporated into an open area of the program. This section in the main program is labeled "Subroutine 10" and was provided by the original author of the software for possible user modifications. These steps have line numbers of 60000 or greater and are found at the very end of the commercial program. Several comment lines appear in the program, preceded with single quote marks.

The entire program, including these modifications, was written in BASIC and was compiled and linked using QuickBASIC version 3.0. The executable form which resulted was used to collect the data presented in

this thesis.

The first set of program lines, i.e., those lines numbered between 27000 and 28000, allow storage of data in columns as potential, current, and point number. The first three lines represent existing lines in the original commercial program which were altered to allow the additional choice of the data storage option desired for this work. The remainder of the lines make substantial use of existing routines within the original software package to created the desire output.

```
27345 M$(4)="F4       Show/Store/Print Data"
27630 GOSUB 14400:PRINT "Screen/Disk/Printer (S/D/P) ";:VALID$="SsDdPp":
      VALIDEX$="":GOSUB 9400:GOSUB 9500
27636 IF A$="D"THEN 27950

27950 '
27951 'Save data to disk
27952 '
27953 GOSUB 14400:PRINT "Enter file name: ";
27954 GOSUB 9600:DATAFILE$=CSTR$
27955 F2$=DATADRIVE$+DATADIRF$+DATAFILE$+".DAT"
27956 OPEN F2$ FOR OUTPUT AS #1
27957 I=FP
27958 GOSUB 12600:LOCATE TOP+2,LEFT
27959 WHILE I<=LP
27960 TCUR=XCUR:TVAL=VAL(PV$(1,1)):TVALF=VAL(PV$(2,1)):GOSUB 34300
27962 GOSUB 34700
27963 PRINT #1,TA,
27964 TCUR=YCUR:TVAL=VAL(PV$(3,1)):TVALF=VAL(PV$(4,1)):GOSUB 34300
27965 GOSUB 34700
27966 PRINT #1,TA,
27967 PRINT #1,I
27969 I=I+1
27970 WEND
27971 CLOSE #1
27972 GOTO 27000
```

The second set of lines, i.e., beginning with line number 60000, provides the subroutine allowing operation with the Model 174A potentiostat. This subroutine makes extensive use of other routines in the larger program, especially routines for communicating command codes to the instrument and for taking readings at the instrument. Several queries are made of the user to gain information about the various settings on the front panel of the Model 174A potentiostat.

```
60000 '&L60000
60005 '*******  DEFINED SUBROUTINE 10
60010 'Largest possible line number 65529
60015 '
60050  '************************************************
60055  '*    SUBROUTINE FOR TAKING MEASUREMENTS FROM    *
60060  '*           THE PAR-174A POTENTIOSTAT           *
60065  '*                                               *
60070  '*                                               *
60075  '*           SUBROUTINE BY BRYAN ISAAC           *
60080  '************************************************
60100  GOSUB 13300
60110  GOSUB 14400
60120  PRINT "INITIAL POTENTIAL (mV): ";
60130  GOSUB 9600: INIPOT = VAL(CSTR$)
60140  GOSUB 14400
60150  PRINT "POTENTIAL SCAN RATE (mV/Sec): ";
60160  GOSUB 9600: SCANRATE = VAL(CSTR$)
60161  GOSUB 14400
60162  PRINT "DROP TIME (Sec): ";
60163  GOSUB 9600: SCANTIME = VAL(CSTR$)
60170  GOSUB 14400
60180  PRINT "FINAL POT. (mV): ";
60190  GOSUB 9600: FINPOT = VAL(CSTR$)
60194  GOSUB 14400
60195  PRINT "CURRENT RANGE (microAmps Full Scale): ";
60196  GOSUB 9600: CURRANGE = VAL(CSTR$)
60197  GOSUB 14400
60200  TOTPTS% = INT(ABS((FINPOT-INIPOT)/SCANRATE/SCANTIME))
60210  C$ = "LP " + STR$(TOTPTS%) : GOSUB 4200
60220  GOSUB 14400
60230  PRINT "FILE FOR DATA (********.DAT): ";
60240  GOSUB 9600: DATAFILE$ = CSTR$
```

```
60250  F2$ = DATADRIVE$+DATADIRF$+DATAFILE$+".DAT"
60260  GOSUB 14400
60270  OPEN F2$ FOR OUTPUT AS #1
60280  GOSUB 14400
60290  PRINT "HIT RETURN TO START: ";
60300  GOSUB 9600
60310  START = TIMER
60320  FOR I = 1 TO (TOTPTS%+1)
60340  IF (TIMER - START) < (I*SCANTIME-SCANTIME) GOTO 60340
60350  C$ = "READAUX" : GOSUB 4200
60355  CURRENT = (VAL(STR$(A%(1)))*CURRANGE/10000.)
60360  PRINT #1, ((SCANRATE*(I-1)*SCANTIME+INIPOT)/1000), CURRENT, I
60370  NEXT I
60380  CLOSE #1
65505  RETURN
```

Other commands were required in addition to the above changes in the main program. Head Start also utilizes coded commands which are relayed directly through the interface to the potentiostat. Several codes were used to prepare the potentiostat before the above subroutine was employed. The codes are give below at the left, along with a brief interpretation of their intended function.

```
DCL        Initializes the potentiostat.
PAM 0      Disables the point averaging mode -- no averaging takes place.
TMB 1667   Sets the time base to 16.67 ms per measurement.
g 10       Sends the computer to the subroutine.
DCL        Initializes the potentiostat after operation is complete.
```

APPENDIX II.

This appendix contains a computer program which allows several methods of data manipulation, including smoothing and differentiation. The program allows data smoothing by boxcar and Savitzky-Golay filters. Calculations of current differentials can be made by traditional mathematical means as well as by a first-derivative Savitzky-Golay approximation. The coefficients for both of the Savitzky-Golay smoothing schemes are taken from the original work by Savitzky and Golay (48).

This program can best be explained by breaking it into sections. The first section, i.e., program line numbers 10 - 1070, provide information and allow the user to enter a data file. Lines 1490 - 1600 contain the main menu of program capabilities, and serve as a focal point to which the program returns after completion of each operation.

Smoothing operations are contained in lines 1700 - 4570. The numbers less than 2000 are a sub-menu, giving the user choices of three smoothing routines. The first, boxcar averaging, is carried out by steps labeled 2000 through 2230. The user is allowed to choose the number of points to be included in the moving boxcar average. The second choice is technically also boxcar averaging, though the choice is given as a potential range over which to smooth, instead of a number of points. This method spans lines 3000 - 3240. Both of these options give equal weighting to all points averaged in each set. The third smoothing option is the Savitzky-Golay smooth, in lines 4000 - 4570. Two versions of this least squares smooth are offered; a five- and a seven-point smooth.

The next section, lines 5000 - 5150, makes possible the viewing of a range of seven points. This is intended to aid in determining smoothing characteristics and in any editing which may be necessary. Lines 6000 through 6330 allow multiplication or division of all x or y data points by a user-specified factor, making corrections possible in case of mistakes in providing information to the Head Start program.

The following section, lines 8000 to 8960, are used to calculate the differential. Two methods are possible, the first of which is the traditional scheme. Simply, the difference in successive current values, i.e., y, is divided by the difference in the corresponding potentials, i.e., x. This scheme is found in lines 8500 to 8560, after the choices of methods of differentiation are given.

The other differential method is an approximation of the derivative using a Savitzky-Golay approach. This method provides a degree of smoothing and calculates the derivative with coefficients provided in the reference cited above (48). Both the 5- and 7- point smoothes are included, in lines 8700 - 8960.

The remainder of the program is used to handle responses and in saving the finished file. An option is provided for the user to continue working on the same file just saved without re-entering data.

The program is equipped to handle up to 2000 points with information for x, y, and z, where x and y are the potential and current values, and z is a counter. The language used was BASIC, and the program was compiled and linked into the executable form by QuickBASIC, version 3.0.

Program SMOOTH

```
10      'THIS IS A DATA MANIPULATION PROGRAM WITH
20      'ROUTINES FOR SMOOTHING AND MANIPULATION OF DATA
30      '
40      'Written by BRYAN ISAAC
50      '
600     DIM X(2000),Y(2000),APOINT(2000)
700     PRINT "This program provides the opportunity to multiply or"
710     PRINT "divide all data points by a factor.  It includes several"
720     PRINT "smoothing routines; boxcar averaging, averaging of a"
730     PRINT "specified potential range, and 5- or 7-point Savitzky-"
740     PRINT "Golay smoothing.  It also offers the capability of taking"
750     PRINT "differentials to approximate the first derivative"
760     PRINT "response."
770     PRINT
780     PRINT
1000    INPUT "Enter full data file name: ",FILENAME$
1010    OPEN FILENAME$ FOR INPUT AS #1
1040    FOR I = 1 TO 2000
1050    INPUT#1,X(I),Y(I),APOINT(I)
1055    ON ERROR GOTO 1065
1060    NEXT I
1065    TOTAL = I-1
1070    CLOSE #1
1490    PRINT:PRINT "Respond to each request with the appropriate code."
1500    PRINT:PRINT "Mathematically edit data set (1):"
1510    PRINT "View points                    (2):"
1520    PRINT "Apply a smoothing routine      (3):"
1530    PRINT "CPPP functions-Differentials   (4):"
1540    PRINT "Save File                      (5):"
1550    INPUT "Quit without saving            (6):",TEST:PRINT
1560    IF TEST > 0 OR TEST < 7 GOTO 1590
1570    INPUT "Invalid response -- re-enter code: ",TEST:PRINT
1580    GOTO 1560
1590    ON TEST GOTO 6000, 5000, 1700, 8000, 10000, 10100
1600    GOTO 1500
1700    PRINT "   Boxcar averaging              (1):"
1710    PRINT "   Average set potential range   (2):"
1715    INPUT "   Savitzky-Golay Smooth         (3): ",TEST:PRINT
1720    ON TEST GOTO 2000, 3000, 4000
1730    GOTO 1500
2000    '
2010    'Routine for boxcar averaging
2020    '
2030    INPUT "Enter the number of points over which to smooth: ",N
2040    IF N >= TOTAL GOTO 2030
2050    TOTAL = TOTAL - N + 1
2060    FOR I = 1 TO TOTAL
2070    SX=0:SY=0
```

```
2080    FOR J = I TO (I+N-1)
2100    SX = SX + X(J)
2120    SY = SY + Y(J)
2140    NEXT J
2160    X(I) = SX/N
2180    Y(I) = SY/N
2200    NEXT I
2210    PRINT:PRINT "SMOOTH COMPLETE."
2230    GOTO 1500
3000    '
3010    'Average over a specified potential range
3020    '
3030    PRINT:INPUT "Enter potential range to average over (mV) (+/-
         x/2): ",MV
3035    MV = MV / 1000
3040    I = 1
3050    SX = 0:SY = 0
3060    J = I
3070    SX = SX + X(J)
3090    SY = SY + Y(J)
3110    J = J + 1
3120    IF ABS(X(J) - X(I)) > MV GOTO 3150
3130    IF J > TOTAL GOTO 3150
3140    GOTO 3070
3150    X(I) = SX / (J-I)
3170    Y(I) = SY / (J-I)
3190    I = I + 1
3200    IF J <= TOTAL GOTO 3050
3210    TOTAL = TOTAL - (J-I+1)
3220    PRINT:PRINT "Smooth complete."
3240    GOTO 1500
4000    '
4010    'Savitzky-Golay Smoothing
4020    '
4030    PRINT:INPUT "5-point or 7-point smooth? ",RANGE
4040    IF RANGE = 7 GOTO 4500
4050    IF RANGE <> 5 GOTO 1500
4100    PRINT:PRINT "5-Point Savitzky-Golay Smooth in Progress"
4110    TOTAL = TOTAL - 4
4120    FOR I = 1 TO TOTAL
4130    Y(I) = (-3*Y(I) +12*Y(I+1) +17*Y(I+2) +12*Y(I+3) -3*Y(I+4))/35
4140    X(I) = X(I+2)
4150    NEXT I
4160    PRINT "SMOOTH COMPLETE."
4170    GOTO 1500
4500    PRINT "7-Point Savitzky-Golay Smooth in Progress."
4510    TOTAL = TOTAL - 6
4520    FOR I = 1 TO TOTAL
4530    X(I) = X(I+3)
```

```
4540    Y(I) = (-2*Y(I) +3*Y(I+1) +6*Y(I+2) +7*Y(I+3) +6*Y(I+4)
         +3*Y(I+5) -2*Y(I+6)) / 21
4550    NEXT I
4560    PRINT "SMOOTH COMPLETE"
4570    GOTO 1500
5000    '
5010    'View a specified point range
5020    '
5100    INPUT "Enter point number: ",J
5110    FOR I = -3 TO 3
5120    IF (J + I) < 1 OR (J + I) > TOTAL GOTO 5140
5130    PRINT (J+I),(X(J+I)),(Y(J+I))
5140    NEXT I
5150    GOTO 5000
6000    '
6010    'Mathematical functions on data set
6020    '
6030    PRINT "All actions affect full (X or Y) data sets."
6040    INPUT "Curve X (1) or Y (2): ",CURVE:PRINT
6050    IF CURVE < 1 OR CURVE > 2 GOTO 6040
6060    PRINT "   Multiply                (1):"
6070    INPUT "   Divide                  (2): ",TEST:PRINT
6080    ON TEST GOTO 6250, 6250
6090    GOTO 1500
6250    CURVE = CURVE * 3 + TEST - 3
6260    INPUT "Enter factor: ",VALUE:PRINT
6270    FOR I = 1 TO TOTAL
6280    IF (CURVE = 2) THEN X(I) = X(I) * VALUE
6290    IF (CURVE = 5) THEN Y(I) = Y(I) * VALUE
6300    IF (CURVE = 3) THEN X(I) = X(I) / VALUE
6310    IF (CURVE = 6) THEN Y(I) = Y(I) / VALUE
6320    NEXT I
6330    GOTO 1500
8000    '
8010    'Take differential
8020    '
8030    PRINT "   Arrange for alternate drop differential          (1):"
8040    INPUT "   Find least-squares differential (Savitzky-Golay)  (2):
         ",TEST
8045    PRINT
8050    ON TEST GOTO 8500, 8700
8060    GOTO 1500
8500    FOR I = 1 TO (TOTAL - 1)
8510    X(I) = (X(I) + X(I+1))/2
8520    Y(I) = (Y(I+1) - Y(I))/(X(I+1)-X(I))
8530    NEXT I
8540    TOTAL = TOTAL - 1
8550    PRINT "Alternate drop differential CPPP curve calculated.":PRINT
8560    GOTO 1500
8700    INPUT "5-Point or 7-Point Convolution? ",RANGE
```

```
8710    IF RANGE = 7 GOTO 8900
8720    IF RANGE <> 5 GOTO 8700
8725    PRINT "COMPUTING 5-POINT FIRST DERIVATIVE"
8730    TOTAL = TOTAL - 4
8735    FOR I = 1 TO TOTAL
8740    X(I) = X(I+2)
8750    Y(I) = (Y(I) - 8*Y(I+1) + 8*Y(I+3) - Y(I+4))/12
8760    NEXT I
8770    PRINT "DIFFERENTIAL CALCULATED"
8780    GOTO 1500
8900    PRINT "COMPUTING 7-POINT FIRST DERIVATIVE"
8910    TOTAL = TOTAL - 6
8915    FOR I = 1 TO TOTAL
8920    X(I) = X(I+3)
8930    Y(I) = (22*Y(I) -67*Y(I+1) -58*Y(I+2) +58*Y(I+4) +67*Y(I+5)
         -22*Y(I+6)) / 252
8940    NEXT I
8950    PRINT DIFFERENTIAL CALCULATED"
8960    GOTO 1500
9000    '
9010    'Subroutines
9020    '
9100    TEST = 0
9110    IF DATA$ = "Y" THEN TEST = 1
9120    IF DATA$ = "y" THEN TEST = 1
9130    PRINT
9140    RETURN
10000   '
10010   'Save and Exit
10020   '
10030   INPUT "Enter filename for output (use *.dat): ",FILEOUT$
10040   OPEN FILEOUT$ FOR OUTPUT AS #1
10050   FOR I = 1 TO TOTAL
10060   PRINT#1,X(I),Y(I),(I)
10070   NEXT I
10080   CLOSE #1
10100   PRINT:INPUT "Do you wish to work with another file? (Y/N) ",DATA$
10110   GOSUB 9100
10120   ON TEST GOTO 10150
10130   GOTO 11000
10150   INPUT "Do you wish to work with the file just created? (Y/N)
         ",DATA$
10160   GOSUB 9100
10170   ON (TEST+1) GOTO 1000,1500
10180   GOTO 10150
11000   END
```

APPENDIX III.

This appendix describes the smoothing program which was designed to perform the Fourier transform fit on polarographic data, and which is also equipped to handle any two-dimensional curve. The program is based on equations found in a paper by Aubanel et al. (50). Although the work by Aubanel et al. contained algorithms which were more advanced and which were claimed to decrease the number of calculations required, this author was unable to successfully incorporate these algorithms into an operational program. The program used in this research is based instead on equations (16) through (20) in the same paper. This program is discussed in more detail in the earlier chapter on noise considerations.

The equations from the reference cited (50) are reproduced in order below. The terms R and I, along with their subscripts, represent the real and imaginary portions of the calculated frequency spectrum. The terms x_0 to x_j are the members of the reconstructed time-domain scan, where the higher frequencies have been eliminated according to choices made by the user, and defined by the variable f_k in the program. The explanations of other variables are found in the original paper and the interested reader is encouraged to read the discussion there.

The program can be divided into small sections based on the equation each section relates to. Equation (16) corresponds to program lines 600 through 640.

$$R_0 = \frac{1}{N} \sum_{j=1}^{N-2} (x_j - x_0 - jb) \qquad (16)$$

Equations (17) and (18) are calculated by program lines 1080 through 1220.

$$R_k = \frac{1}{N} \sum_{j=1}^{N-2} (x_j - x_0 - jb) \cos\left(\frac{2\pi jk}{N}\right) \qquad k=1,2,\ldots,n-1 \qquad (17)$$

$$I_k = \frac{-1}{N} \sum_{j=1}^{N-2} (x_j - x_0 - jb) \sin\left(\frac{2\pi jk}{N}\right) \qquad k=1,2,\ldots,n-1 \qquad (18)$$

Equation (19) is shown in lines 2000 through 2070.

$$\tilde{x}_0 = x_0 + R_0 + 2 \sum_{k=1}^{n-1} R_k \qquad (19)$$

Equation (20) is calculated by lines 2100 through 2200.

$$\tilde{x}_j = x_0 + jb + R_0 + 2 \sum_{k=1}^{n-1} R_k \cos\left(\frac{2\pi kj}{N}\right) - I_k \sin\left(\frac{2\pi kj}{N}\right) \qquad j=1,2,\ldots,N-1 \qquad (20)$$

Other lines in the program are used to read in the data file to be analyzed, to inform or ask questions of the user, or to print the resulting smoothed curve into a software data file in a form appropriate for use with a graphing software package or for printout as x and y data points, along with point numbers. Most of the variables in the equations are also used in the computer program in recognizable form.

The program was written in BASIC language and was compiled and linked into an executable file by QuickBASIC, version 3.0.

Program: FOURIER.exe

```
10      DIM A(2000),X(2000),R(1001),I(1000)
100     INPUT "Enter data file name: ", FILENAME$
110     OPEN FILENAME$ FOR INPUT AS #1
120     FOR I = 0 TO 2000
130       INPUT#1, A(I),X(I),PT
140       ON ERROR GOTO 160
150     NEXT I
160     N=I
170     CLOSE #1
500     NZERO = 1
510     B = (X(N-1)-X(0))/(N-1)
600     SUM = 0
610     FOR J = 1 TO (N-1)
620       SUM = X(J)-X(0)-(B*J)+SUM
630     NEXT J
640     R(0) = SUM/N
1000    PRINT:PRINT "N/2 = ",N/2
1010    INPUT "Enter n   (1<n<(N/2)) : ", SMALLN
1020    IF SMALLN <= INT((N+1)/2) GOTO 1050
1030    PRINT "n too large"
1040    GOTO 1000
1050    IF SMALLN <= NZERO GOTO 2000
1080    ARG = 2*(3.141593)/N
1100    FOR K = NZERO TO (SMALLN-1)
1110      SUMR = 0
1120      SUMI = 0
1130      ARGK = ARG*K
1140      FOR J = 1 TO (N-1)
1150        ARG1 = X(J)-X(0)-(J*B)
1160        ARG2 = ARGK*J
1170        SUMR = SUMR + (ARG1*COS(ARG2))
1180        SUMI = SUMI + (ARG1*SIN(ARG2))
1190      NEXT J
1200      R(K) = SUMR/N
1210      I(K) = -(SUMI)/N
1220    NEXT K
1900    IF NZERO < SMALLN THEN NZERO = SMALLN
2000    SUM = 0
2010    FOR K = 1 TO (SMALLN-1)
2020      SUM = SUM + R(K)
2030    NEXT K
```

```
2040    PRINT "[BELL]" :INPUT "Enter filename for smoothed curve:
          ",FILNAM2$
2050    OPEN FILNAM2$ FOR OUTPUT AS #1
2060    NEWX = X(0)+R(0)+(2*SUM)
2070    WRITE #1, A(0),NEWX,0
2100    FOR J = 1 TO (N-1)
2110      SUM = 0
2120      ARGJ = ARG*J
2130      FOR K = 1 TO (SMALLN-1)
2140        ARG3 = ARGJ*K
2160        SUM = SUM+((R(K)*COS(ARG3))-(I(K)*SIN(ARG3)))
2170      NEXT K
2180      NEWX = X(0)+(J*B)+R(0)+(2*SUM)
2190      WRITE #1, A(J),NEWX,J
2200    NEXT J
2210    CLOSE #1
3000    PRINT "[BELL]" :INPUT "Quit (1) or smooth differently (2) ? ",
          QUERY
3010    IF QUERY = 2 GOTO 1000
3020    END
```

LITERATURE CITED

1. Stulik, K.; Pacakova, V. "Electroanalytical Measurements in Flowing Liquids"; Ellis Horwood Limited: Chichester, England, 1987, p. 9.

2. Kolthoff, I. M.; Lingane, J. J. "Polarography", 2nd ed.; Interscience Publishers, Inc.: New York, NY, 1952. Vols. 1 and 2.

3. Meites, L. "Polarographic Techniques", 2nd ed.; Interscience Publishers: New York, NY, 1965.

4. Bond, A. M. "Modern Polarographic Methods in Analytical Chemistry"; Marcel Dekker, Inc.: New York, NY, 1980.

5. Riley, T.; Watson, A. "Polarography and Other Voltammetric Methods"; John Wiley & Sons: Chichester, England, 1987.

6. Heyrovsky, J. Chem. Listy 1922, 16, 256.

7. Riley, T.; Watson, A. "Polarography and Other Voltammetric Methods"; John Wiley & Sons: Chichester, England, 1987, p. 3.

8. Manning, W. M. Ecology, 1940, 21, 509.

9. Bratin, K.; Kissinger, P. T. J. Liq. Chromatogr. 1981, 4, Suppl. 2, 321.

10. Brown, J. N.; Nervins, M.; Van der Linden, J. H. M.; Lynch, R. J. J. Chromatogr. 1981, 204, 115.

11. MacCrehan, W. A.; Durst, R. A. Anal. Chem. 1978, 50, 2108.

12. Bond, A. M.; Hudson, H. A.; van den Bosch, P. A. Anal. Chim. Acta 1981, 127, 121.

13. Neuburger, G. G.; Johnson, D. C. Anal. Chim. Acta 1986, 179, 381.

14. Hara, M.; Nomura, N. Bunseki Kagaku 1983, 32, E185.

15. Hara, M.; Nomura, N. Talanta 1984, 31, 105.

16. Hara, M. Talanta 1985, 32, 41.

17. Hara, M.; Nomura, N. Chem. Lett. 1986, 219.

18. Hara, M.; Nomura, N. Talanta 1986, 33, 857.

19. Parry, E. P.; Osteryoung, R. A. Anal. Chem. 1965, 37, 1634.

20. Bond, A. M. "Modern Polarographic Methods in Analytical Chemistry"; Marcel Dekker, Inc.: New York, NY, 1980, p. 139.

21. Kronenberger, K.; Strehlow, H.; Elbel, A. W. Leybold Polarograph. Ber. 1957, 5, 62.

22. Barker, G. C.; Gardner, A. W. Z. Anal. Chem. 1960, 173, 79.

23. Sturrock, P. E.; Carter, R. J. Crit. Rev. Anal. Chem. 1975, 5, 201.

24. Muller, O. H. "The Polarographic Method of Analysis"; Mack Printing Co.: Easton, PA, 1941.

25. Muller, O. H. "The Polarographic Method of Analysis"; Mack Printing Co.: Easton, PA, 1941, p. 87.

26. Kolthoff, I. M.; Lingane, J. J. "Polarography", 2nd ed.; Interscience Publishers, Inc.: New York, NY, 1952. Vol. 1, p. 395.

27. Stulik, K.; Pacakova, V. "Electroanalytical Measurements in Flowing Liquids"; Ellis Horwood Limited: Chichester, England, 1987, p. 97.

28. Riley, T.; Watson, A. "Polarography and Other Voltammetric Methods"; John Wiley & Sons: Chichester, England, 1987, p. 25.

29. Riley, T.; Watson, A. "Polarography and Other Voltammetric Methods"; John Wiley & Sons: Chichester, England, 1987, p. 165.

30. Oldham, K. B.; Parry, E. P. Anal. Chem. 1970, 42, 229.

31. Maitoza, P.; Johnson, D. C. Anal. Chim. Acta 1980, 118, 233.

32. Hsi, T.; Johnson, D. C. Anal. Chim. Acta 1985, 175, 23.

33. Osteryoung, J.; Kirowa-Eisner, E. Anal. Chem. 1980, 52, 62.

34. Christie, J. H.; Jackson, L. L.; Osteryoung, R. A. Anal. Chem. 1976, 48, 561.

35. Model 303 Static Drop Mercury Electrode: Operating and service manual; EG&G PARC, Trenton, NJ, 1978.

36. Meites, L. "Polarographic Techniques", 2nd ed.; Interscience Publishers: New York, NY, 1965, p. 383.

37. Riley, T.; Watson, A. "Polarography and Other Voltammetric Methods"; John Wiley & Sons: Chichester, England, 1987, p. 180.

38. Burge, D. E. J. Chem. Ed. 1970, 47, A81.

39. Muller, O. H. J. Chem. Ed. 1941, 18, 320.

40. Fisher, D. J.; Belew, W. L.; Kelley, M. T. In "Polarography 1964", Hills, G. J., Ed.; Interscience Publishers: New York, NY, 1966. Vol. 1, p. 89.

41. Heyrovsky, J.; Ilkovic, D. Collect Czech. Chem. Commun. 1935, 7, 198.

42. Christie, J. H.; Osteryoung, R. A. J. Electroanal. Chem. 1974, 49, 301.

43. Toth, K.; Nagy, G.; Feher, Z.; Horvai, G.; Pungor, E. Anal. Chim. Acta 1980, 114, 45.

44. Trojanek, A.; Opekar, F.; Holub, K. J. Electroanal. Chem. 1988, 251, 41.

45. Dessy, R. "Lab Automation: A Rational Approach"; American Chemical Society: Washington, DC, 1978.

46. Bialkowski, S. E. Anal. Chem. 1988, 60, 355A.

47. Bialkowski, S. E. Anal. Chem. 1988, 60, 403A.

48. Savitzky, A.; Golay, M. J. E. Anal. Chem. 1964, 36, 1627.

49. Cameron, D. G.; Moffatt, D. J. J. Test. Eval. 1984, 12, 78.

50. Aubanel, E. E.; Myland, J. C.; Oldham, K. B.; Zoski, C. G. J. Electroanal. Chem. 1985, 184, 239.

51. Lam, R. B.; Isenhour, T. L. Anal. Chem. 1981, 53, 1179.

52. Kissinger, P. T. In "Laboratory Techniques in Electroanalytical Chemistry", Kissinger, P. T.; Heineman, W. R., Eds.; Marcel Dekker, Inc.: New York, NY, 1964. Ch. 22, p. 611-635.

53. Johnson, D. C.; Weber, S. G.; Bond, A. M.; Wightman, R. M.; Shoup, R. E.; Krull, I. S. Anal. Chim. Acta 1986, 180, 187.

54. Riley, T.; Watson, A. "Polarography and Other Voltammetric Methods"; John Wiley & Sons: Chichester, England, 1987, p. 160.

SECTION II.

VERSATILE LASER-BASED ANALYTICAL INSTRUMENT FOR DETECTION OF JET-COOLED MOLECULAR SPECIES

CHAPTER 1. INTRODUCTION

One of the most important problems facing analytical chemistry is the development of methods which are selective, sensitive, quantitative, and which can be applied to a wide variety of samples. The detection of specific compounds present at low levels in complex mixtures represents a challenge which generally requires elaborate procedures for separation and detection. The majority of existing techniques exhibit strong capabilities in one or two areas, e.g., they may be sensitive and quantitative, but they lack selectivity or may only be useful for a limited range of compounds. The powerful capabilities of these techniques and the lack of certain necessary features has led to a proliferation of analytical systems which use these methods in combination, known as hyphenated techniques.

Methods such as gas chromatography (GC) and high performance liquid chromatography (HPLC) are standard separation techniques which are known for their excellent selectivity. Detection techniques including mass spectrometry (MS) and laser-induced fluorescence (LIF) provide good sensitivity in an analysis. The combination of GC-MS still lacks, however, the capability to selectively differentiate between certain geometric isomers. Though this is indeed a difficult task, it is a requirement which is especially important in view of the considerable recent interest in carcinogenic materials, since the degree of carcinogenicity depends to a large extent on isomeric substitution (1).

The high power, spectral purity, directionality, and coherence of

the laser make it an excellent tool for a detection scheme, as it affords the additional dimension of selectivity in addition to the sensitivity of fluorescence or ionization detection. The use of low analysis temperatures allows one to use this spectral selectivity to an advantage. Thus low temperature fluorescence provides a sensitive method with the selectivity to distinguish between these isomeric compounds (2).

This thesis focuses on the application of jet spectroscopy to analytical chemistry and on extension of the range of molecules amenable to analysis in the jet. Because of the low temperatures achieved in the expansion, laser spectroscopy in the cooled jet stream offers spectral selectivity powerful enough to differentiate geometric isomers and even various isotopes (3). Since jet spectroscopy usually utilizes a detection scheme based on laser induced fluorescence and/or multiple photon ionization (MPI), it offers good sensitivity to great numbers of compounds. The technique has been employed to a large extent by molecular spectroscopists to probe the fundamental optical spectroscopy of polyatomic species, but until recently has stirred little interest among analytical chemists (4).

This thesis will review the development and the theory of jet-cooled spectroscopy as it relates to analytical chemistry and will discuss additions to the technique that spread its applicability to more varied samples, specifically to those of low volatility.

An instrument has been developed which will allow the application of jet spectroscopy to a wide variety of samples and which will afford both fluorescence and ionization analysis. This instrument will be covered in

detail. Results from this instrument will be used to make a comparison of the two laser-based detection schemes for jet spectroscopy, i.e., fluorescence and ionization, and will be used to recommend a method of analysis for jet-cooled molecules.

CHAPTER 2. LITERATURE REVIEW

The supersonic jet was introduced in 1951 by Kantrowitz and Grey as an improvement over the effusive oven beam, the chief benefit being the increase in intensity in the molecular beams (5). Though these workers were aware of the cooling of molecules in the expansion, they did not exploit this feature of the new technique. In 1974, Smalley et al. noted the cooling of the internal modes of NO_2 in a jet and put this property to use, greatly simplifying the fluorescence excitation spectrum of the molecule (6).

Jets have since been used to a great extent in molecular spectroscopy, though their application to analytical aspects of spectroscopy was not made for nearly another decade. Early reviews of the method reflect this (2, 7), with the acknowledgment in 1983 that analytical applications had only just begun to appear (2). Though the major use of jets and the spectral cooling they exhibit continues to be in the study of molecular spectroscopy, this chapter will focus on the analytically relevant advances in the field.

Analytical Use of Supersonic Jets

Supersonic jets have been used for the study of molecular spectroscopy since 1974 when Smalley's paper was published, but the first recognition of the analytical utility of supersonic jet spectroscopy was delayed until the work of Hayes, Small, and co-workers in 1981, when they

published their concept of quantitative analysis using sample introduction by gas chromatography (GC) and analysis of the jet expansion by laser-induced fluorescence (LIF) (8). In a subsequent paper they showed the ability to detect low-level quantities of 2-methylnaphthalene in a naphthalene sample, demonstrating the selectivity of the technique for analytical purposes (9). Detection was shown at 250 parts per million (ppm) of the doped impurity. Although detection limits were not investigated in this work, an expected detection limit of 50 parts per trillion was calculated.

In another paper from the same research group, detection of each component in a mixed sample of naphthalene, 1-methylnaphthalene, and 2-methylnaphthalene was demonstrated, using scanned fluorescence photoexcitation of the expanding jet (10). Unambiguous identification of components was made by use of the dispersed fluorescence spectra.

Work by Lubman and Kronick followed with detection of jet-cooled species by resonance-enhanced multiphoton ionization, monitored by time-of-flight mass spectrometry (TOFMS) (11). They noted the spectral selectivity of excitation as well as the mass selection of TOFMS for a variety of aromatic molecules. Fragmentation was shown to increase with laser power, while the production of only parent ions was noted at low laser energy.

Quantitative detection

Quantitative analysis was first demonstrated in the jet in 1982 by Hayes and Small, using sample introduction via a packed GC column (12).

The concept of this work was discussed in their earlier proposal (8) and is described here. The chromatographic column was used in this work simply as a means of quantitatively introducing the sample, and was not designed to provide selectivity. Instead, selectivity was achieved spectrally by fluorescence excitation of each species. Non-selective excitation was also used to monitor all eluting aromatics. Detection limits of 14 - 60 ng were attained for naphthalene and two methylnaphthalenes, and the linear range of response was found to be ca. 3 orders of magnitude. These compounds were also detected in direct injections of a crude oil sample.

A second paper published later in the same year by Amirav et al. demonstrated quantitative detection in the jet using a differing approach (13). A pulsed planar slit nozzle was developed, with which they were able to attain increased sample density by a factor of ca. 10^2 in the jet expansion relative to the standard pulsed concentric nozzle. Using this system they were able to measure a fluorene impurity at approximately 1 ppm in a sample of biphenyl. In the same paper they were able to selectively discriminate among species of 9,10-dichloroanthracene according to ^{35}Cl and ^{37}Cl isotopes.

The basic theory of supersonic jet expansions as introduced by Kantrowitz and Grey has been incorporated into many varied applications. Some of these techniques include thermospray (14), electrospray (15), and the introduction of gas chromatographic (16), supercritical fluid chromatographic (17), and inductively coupled plasma (ICP) (18) samples into mass spectrometers. This chapter will not cover these applications, but

will concern itself only with cooled jets and their application to analytical spectroscopy.

From the initial quantitative studies by Hayes and Small, and by Amirav et al., the use of supersonic expansions for analytical spectroscopy has grown considerably in the last seven years, as is illustrated in several reviews (4, 19, 20). Because of the extensive coverage of these reviews, the study here will be limited to only a survey of the advances in the field. The areas of progress covered here are nozzle sources, excitation and detection variations, and sample introduction interfaces.

Jet nozzle variations

Several variations of the nozzle source have been used. The continuous expansion used by Hayes and Small in the first quantitative study has been almost completely replaced by pulsed expansions, which initially were introduced by Hagena (21) as an attempt at reducing the pumping capacity required to attain supersonic expansion without the cost of elaborate pumping systems. The decreased duty cycle results in less of a load on the pumps. When used with pulsed laser excitation, which decreases the duty cycle even more, no additional loss of analysis time is realized due to the pulse expansion.

Amirav et al. further modified the pulsed valve by developing a planar slit nozzle (22-24). They were able to obtain an increase in sample density in the expansion relative to the standard pulsed concentric nozzle, as well as to increase the path length of the sample and

probe interaction.

Another modification was the application of sheath flow hydrodynamic focusing (25). The sheath flow nozzle was used to focus the expanding gases, increasing the analyte density ca. 30 times relative to an unfocused expansion. A detection limit of 50 pg of naphthalene has been demonstrated with this nozzle interfaced to a capillary GC column (25).

Excitation and detection schemes

Many variations in detection have been seen, but laser-induced fluorescence (LIF) and multiphoton ionization (MPI) with detection by TOFMS appear to be the most common. The use of LIF requires that the analyte be fluorescent. MPI, on the other hand, requires higher laser power. When these criteria are met, both of these methods are very sensitive, as has been shown above for LIF.

Another mode of detection which is less commonly used has been absorption, often used in combination with the longer path length and higher number densities of the planar nozzle (13). Absorption is less sensitive as a method than LIF and MPI, and in principle can be applied only to measurement of absorbances of 10^{-4} or greater (13).

Additional studies on absorption have been carried out inside the cavity of a laser. Goldstein et al. have used intracavity laser techniques to demonstrate quantitative absorption studies of NO_2 (26). Though they did not state detection limits, they did show Beer-Lambert behavior for 1-10% NO_2 in the jet.

The laser has been the most widely used excitation source for

analysis, though lamp excitation has also been used. Imasaka et al. were the first to introduce this concept, using a 150 W Xenon lamp for fluorescence excitation (27, 28). They dispersed the source radiation in a monochromator and then focused it onto the jet. Though analytical utility was shown, the sensitivity was found to be ca. 7 orders of magnitude poorer than that of a similar laser-based instrument (4).

A later paper on lamp-excited fluorescence used the selectivity of dispersed fluorescence to discriminate among compounds (29, 30). A 300 W Xenon arc lamp was focused onto the jet and although the resulting fluorescence appeared to have rather broad features, 3 of 4 compounds in a mixture were identified.

Other methods which have been used to take advantage of the molecular cooling offered by jet expansions are infrared (IR) emission (31) and absorption (32) spectroscopies, Fourier transform IR (FTIR) (33, 34), conventional Raman spectroscopy (35), coherent anti-Stokes Raman spectroscopy (CARS) (36), and microwave spectroscopy (37). These methods have been used to gain information about species in the jet, but the major quantitative efforts have been with fluorescence and ionization methods.

Interfaces with other techniques

Several analytical instruments have been interfaced to supersonic jets. Many of these techniques contribute additional selectivity to the method, while some are useful means of introducing samples other than gases into the expanding gas stream, thereby expanding the range of molecules amenable to analysis using jet spectroscopy.

First among these techniques are some of the chromatographic methods, including gas chromatography (GC), as used in the study by Hayes and Small (12). Capillary column GC (CC-GC) was first interfaced to the jet by Pepich et al. (38) and was developed into a quantitative technique by Imasaka et al. (39). Stiller and Johnston used the method to achieve a detection limit of 50 pg for naphthalene (25).

Supercritical fluid chromatography (SFC) has also been interfaced to the jet. This advance was made by two separate groups who reported their work within a month of each other. Fukuoka et al. characterized the use of five various supercritical fluids (40), and Sin et al. used supercritical CO_2 in their work (41). The latter group also adapted the interface for use with pulse nozzles (42). None of these studies was quantitative.

Imasaka et al. extended their supercritical fluid/jet interface to the development of a jet interface with high performance liquid chromatography (HPLC) (43). They used a normal phase chromatographic separation with methanol near supercritical conditions as the eluent and obtained a detection limit of 40 ng for anthracene.

One method which has been used for the task of seeding non-volatile species into the jet expansion is a combination of thermospray and thermal desorption. Rizzo et al. were able to study the amino acid tryptophan, a thermally labile, non-volatile solid, by this method (44, 45).

Another method which is appropriate for use with non-volatile species is laser desorption (LD). This was introduced by Schlag and coworkers in 1985 (46). They were able to desorb tryptophan and retinal,

two unstable, non-volatile compounds, into the jet by pulsing with an infrared (IR) laser, followed by MPI analysis with ultraviolet (UV) laser excitation. Tembreull and Lubman followed with LD of cytosine and adenine (47). LD/jet analysis has since been applied to native chlorophylls (MW 892) (48), small (49) and large (50) peptides, nucleosides (51), amino acids (52), polymers (53), bovine insulin (MW 5927) (54) and other clinically important biomolecules (55). The capability of the technique for sequencing of peptides has also been demonstrated (50). A sub-femtomole detection limit was achieved for protoporphyrin IX dimethyl ester by Hahn et al. using the combination of LD and MPI (56).

From the many applications cited, it is clear that a wide range of compounds and samples can be studied with the use of jet-cooled expansions. There remain many opportunities for progress in the development and application of analytical jet spectroscopy.

CHAPTER 3. INSTRUMENTATION

The supersonic jet system used in this research was designed with two major goals in mind. The first goal was to integrate fluorescence and ion detection with jet spectroscopy, allowing work to be done with fluorescing molecules and with analytes ionizable by MPI. The second goal was the ability to work both with high vapor pressure samples and with samples of low vapor pressure, which normally cannot be seeded into the jet flow in detectable quantities.

Complete vacuum chambers incorporating jet nozzles were not available commercially at the time this research was initiated. Although commercial nozzles were available separately, they did not allow any means of sample introduction other than by establishing a vapor pressure of sample in the small reservoir behind the nozzle orifice. In addition, no other existing jet apparatus on the premises proved adequate. One was a continuous flow jet system (a pulsed jet flow was desired for this work), and the other was limited to vapor pressure equilibrium sample introduction.

Given these considerations, a substantially modified jet system was constructed. It was designed to allow introduction of gas or liquid samples, which would include anything which could be dissolved. It was designed to have the capability of taking information by monitoring fluorescence as well as ions produced by MPI.

The use of samples in various phases requires a variety of sample introduction schemes. Introduction of analyte via more than one method

also requires that the physical structure of the instrument be amenable to each scheme. Given the vast differences of gaseous, liquid, and solid samples, no single structure was deemed suitable for use with all samples. The specific features necessary for each sample type were addressed by the use of two interchangeable modules; one which was suitable to gas chromatography effluents and another which allowed laser desorption of frozen liquid samples.

The use of ion detection required pressure in the detection region of the chamber be less than 10^{-4} torr. The throughput of the pulsed valve, however, resulted in pressures in the range of 10^{-4} torr, even with full use of the available pumping capacity. Though fluorescence analysis can be performed under these conditions, a significant reduction in pressure must be achieved to allow the handling and detection of ions. This was accomplished by skimming the initial expansion, and accepting only a small fraction of the jet flow into the analysis region. Because the region above the skimmer was evacuated by a diffusion pump and the analysis chamber was also pumped out, the pressure in the analysis region was reduced to even lower levels through differential pumping.

The design of this analytical supersonic jet spectroscopy instrument was modular in nature. The valve, interchangeable sample units, and MPI detector and ion extraction apparatus could each be separated from the rest of the vacuum system. In view of this, each unit is discussed in detail individually.

Valve

The valve served the purpose of establishing the jet carrier gas flow for the expansion. Because of the vacuum pump requirements necessary to achieve acceptable low pressures in the chamber and because a pulsed laser excitation source was used, a pulsed gas source could be employed. The valve was therefore designed to provide short gas pulses which permit fully established supersonic flow while allowing the diffusion pumps to maintain good vacuum conditions.

Valve actuator module

The valve itself consisted of a small plunger, or actuator, driven by a double solenoid. As the current signals were sent to the solenoid, the plunger was lifted off its O-ring seat and is then forced back down, allowing a pulse of carrier gas to flow through the nozzle orifice and out into the vacuum chamber. Between pulses the valve was closed to flow.

In some other jet expansion systems a single solenoid was used to lift the actuator and initiate the gas pulse (21, 57-59). When the solenoid current was discontinued, the valve was closed by the force of the vacuum, the closing often assisted by a small spring. The instrument constructed for this work employed a second solenoid to speed and ensure closure of the valve. The additional solenoid also offered control of pressure in the chamber allowing the user to customize the pulse duration through variation of the timing difference between opening and closing current pulses to the solenoids.

Construction of the valve module was similar in style to that of other double solenoid driven valves (60-62). A diagram of the valve is given at the top of Figure 1. A small cylindrical actuator, made from ferromagnetic steel to give good response to the solenoid coil, was positioned centrally within the coils of the solenoids. One end of the actuator, the body of which was machined down in mass in order to increase speed of response, rested on an O-ring seat over the channel leading to the sample introduction module. An aluminum disc was mounted onto the actuator and positioned between the solenoid coils to limit plunger travel.

The two 100-turn solenoid coils were positioned one above the other, with the upper coil used to draw the actuator off the O-ring, opening the valve, and the lower coil quickly closing the valve, sealing it at the O-ring. The solenoids were controlled and supplied with current by a valve driver and timing unit which was also constructed for this work. At the repetition rate used for these experiments, i.e., 10 Hz, no cooling of the solenoids was required.

The valve module was mounted onto the sample introduction unit, with carrier gas added just above the O-ring seat. To provide desired backing pressures, which could vary considerably from atmospheric pressure, and to ensure high carrier gas purity, the valve unit was enclosed by a stainless steel cover with electrical feedthroughs to allow electrical contact between solenoids and control unit.

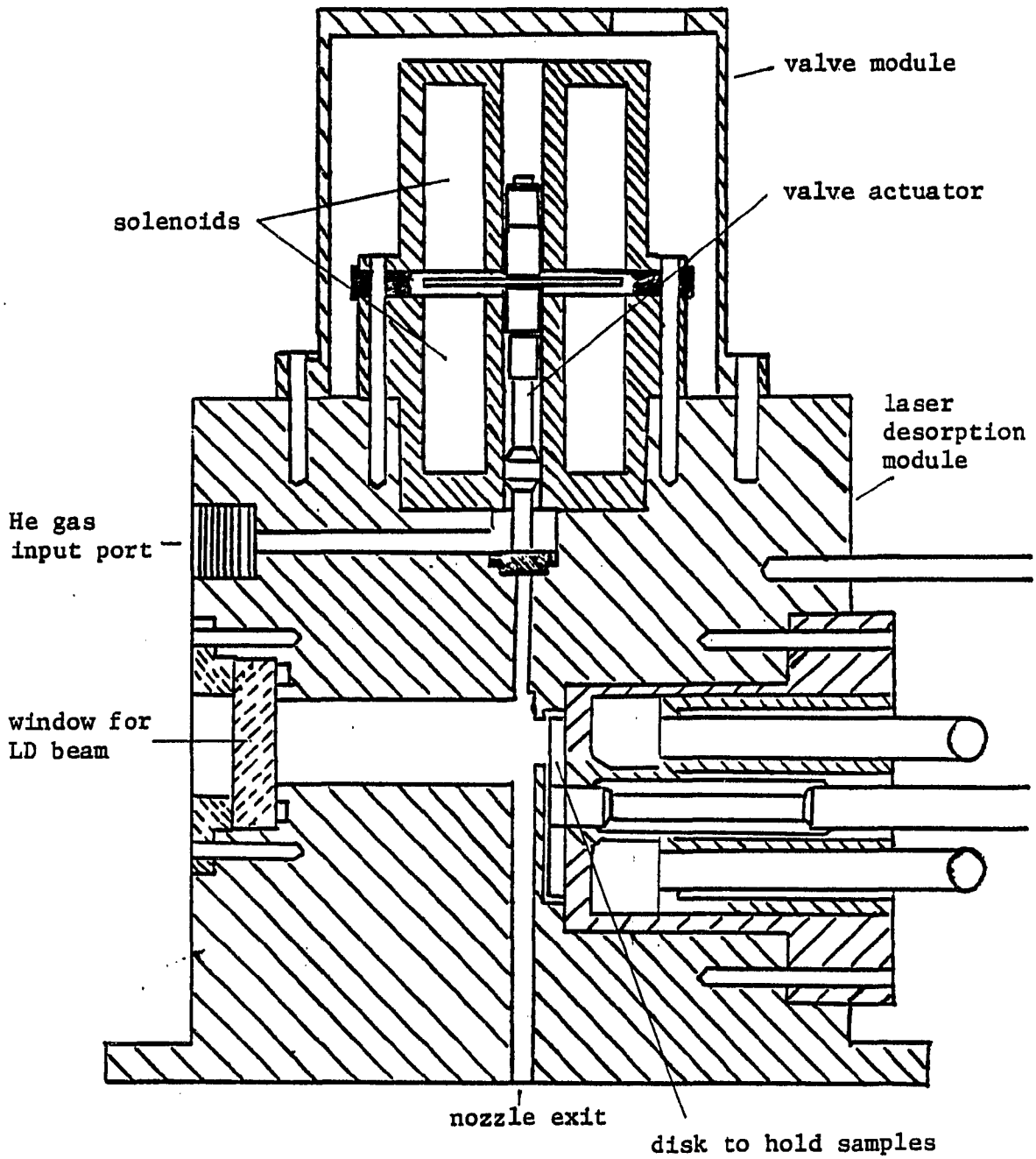

Figure 1. Assembled laser desorption sample introduction module with valve module above

Valve driver and timing unit

An electronic pulsed valve driver and timing unit similar to that used by Hopkins et al. (62) was constructed for the pulsed valve. It afforded control of both solenoids, allowing variation of pulse duration and of the timing relative to the laser pulse.

A trigger from the laser ca. 3 ms prior to the light pulse initiated a variable delay of 0 to 5 ms between the trigger and the activation of the valve opening pulse, controlling the upper solenoid. The delay between the laser trigger and the opening of the valve allowed control of the temporal overlap between the jet expansion pulse and the probe laser radiation. The leading edge of the 400 μs valve-opening pulse triggered a timing delay between the opening and closing pulses which was adjustable from 0 to 1 ms. The lower solenoid was magnetized by this second pulse, applied for 600 μs. The variable delay between upper and lower solenoid pulses regulated the duration of the expansion gas flow. A small spring was added later to speed the closing of the valve.

Sample Introduction Modules

Two interchangeable sample introduction modules were constructed for this instrument, one to work with gas chromatography effluents and another to accommodate frozen liquid samples for introduction by laser desorption. Despite their differing functions, certain similarities are noted here. Both were machined from stainless steel and were designed in a cylindrical shape, with a channel through the central vertical axis

providing the path for carrier gas flow. Each was machined to hold the valve assembly which was bolted to the top of the module, and included an O-ring seat against which the valve actuator rested. Both modules included a port to accept carrier gas and direct it to a point immediately above the actuator seal. Finally, the bottom side of each sample module fit into an adjustable mount on the vacuum chamber where another O-ring provided a seal. Figure 1 shows the laser desorption module with the valve module in place above it.

The exit of the central channel into the vacuum chamber formed the nozzle for the supersonic expansion. The channel was in the center of both sample modules, with the nozzle orifice at the bottom. The orifice size was 2 mm in diameter and the region behind the nozzle was a simple cylindrical channel. The surface on the underside of the nozzle exit was smooth and could be used to bolt a small plate with a smaller orifice size into place, though for all work done in this thesis the original orifice was used. After escaping the sample module through this nozzle orifice, the gas pulse expanded into the vacuum chamber.

For the characterization of much of the instrument and for some simple experiments, sample was introduced by allowing it to attain a vapor pressure in the carrier gas stream. This allowed a constant supply of sample for a long period of time. When working with samples in this manner, either of the two interfaces can be used, as the sample was allowed to reach equilibrium vapor pressure in a small temperature-controlled chamber positioned along the carrier gas intake line. The control of temperature allowed variation of the concentration of sample

in the carrier gas, since vapor pressure is dependent on temperature. The sample was thus mixed into the expansion stream behind the carrier gas port and the valve, after which either sample interface allowed passage through the central channel to the nozzle.

Gas chromatography sample module

The gas chromatography sample module was designed to accept the effluent from a GC column. The effluent would be already in the gas phase, with the sample entrained in its flow. Thus only mixing with the jet carrier gas would be needed with expansion to bring about cooling.

In view of this, a channel to accept the end of a GC column or transfer line was drilled perpendicular to the central jet carrier gas channel. This port was 1/4 in. diameter, allowing for the use of packed columns or capillary columns, and was designed for placement of the column end just beside the central channel. Space was allowed for auxiliary heating elements to maintain appropriate column temperature and to keep analytes in the vapor phase. This module is shown in Figure 2.

The hole in which the column was to be placed was drilled completely through the unit as a precaution in the event that flow rate through a packed column would be great enough to effect a higher chamber pressure than desired. In this case a small pump could be placed across the jet channel from the end of the column in order to provide additional pumping capabilities near the GC column. It should be clear from the low duty cycle of the laser and the valve that not all of the GC effluent would be sampled or entrained in the expansion pulses. In the case of capillary

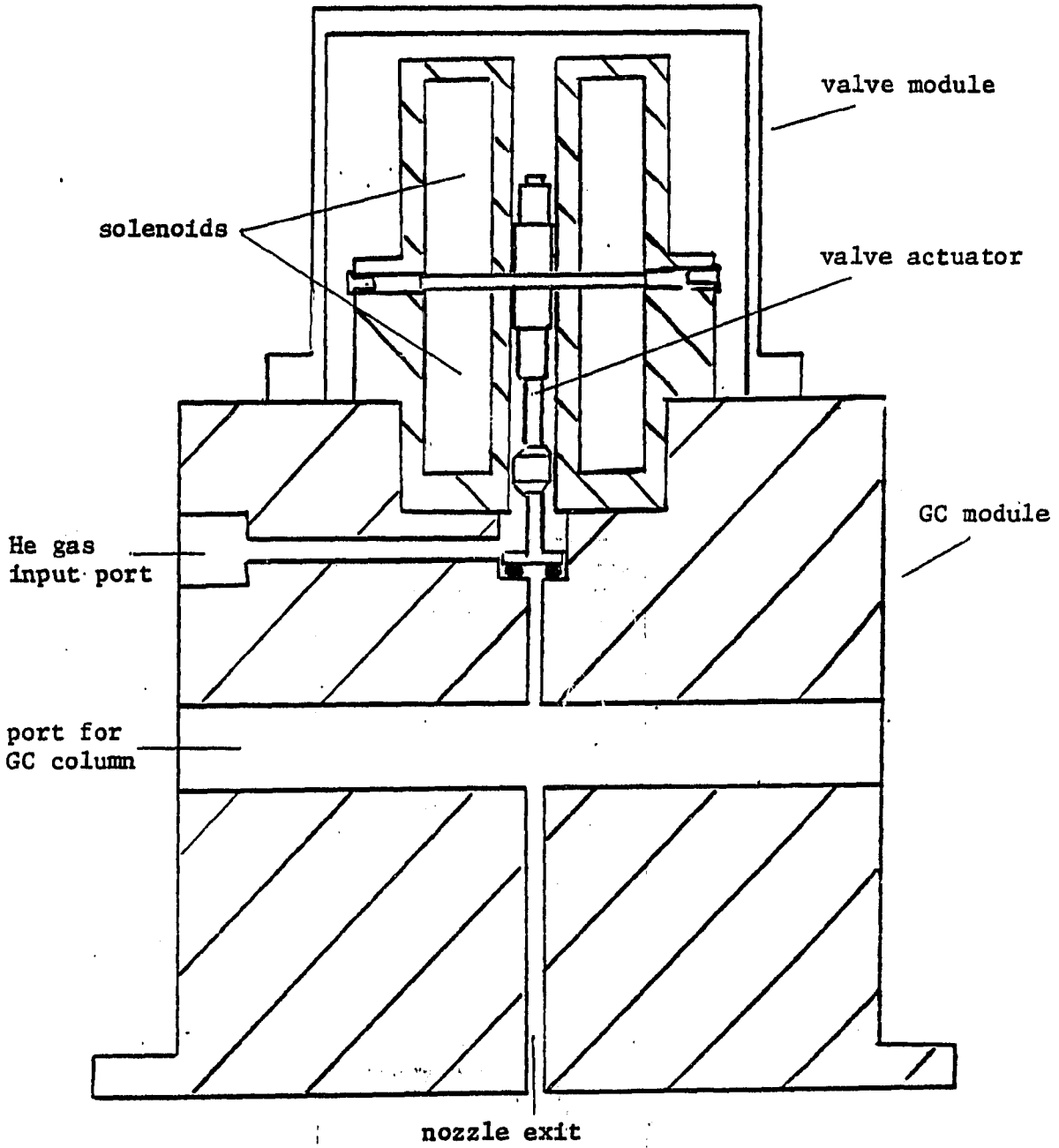

Figure 2. Gas chromatography sample introduction module

columns the lower flow rate would make auxiliary pumping unnecessary.

Laser desorption sample module

A second sample introduction module was designed for use with solid samples to be vaporized by laser desorption. This provided the desired capability of incorporating samples with very low vapor pressure into the jet expansion. Samples included in this category are many liquids as well as solids. In keeping with the spirit of the physical design of the module it was actually preferable that solid samples be dissolved to liquid form since the structure of this module was specifically geared to the analysis of liquids which could be frozen to the end of the sample rod, or "cold finger." Because the samples are of low vapor pressure even at room temperature, they could be put into the vacuum system while frozen onto the sample mount and held in position until the laser pulse desorbed and vaporized them into the passing pulsed gas stream.

The desorption module is shown in Figure 3 and was structurally more complicated than its chromatography counterpart, as it contained a built-in cold finger for maintaining samples in the frozen state. The sample was held on a disc capable of accommodating six samples which could be rotated successively into position for analysis. The sample-supporting disc was positioned such that the single sample under observation was beside the carrier gas channel. The stainless steel disc was mounted at the end of a stainless steel rod surrounded by a liquid nitrogen (LN_2) jacket. Cooling to 77 K was desired in order to affix liquid samples to the disc surface by quick freezing as well as to limit loss of sample by

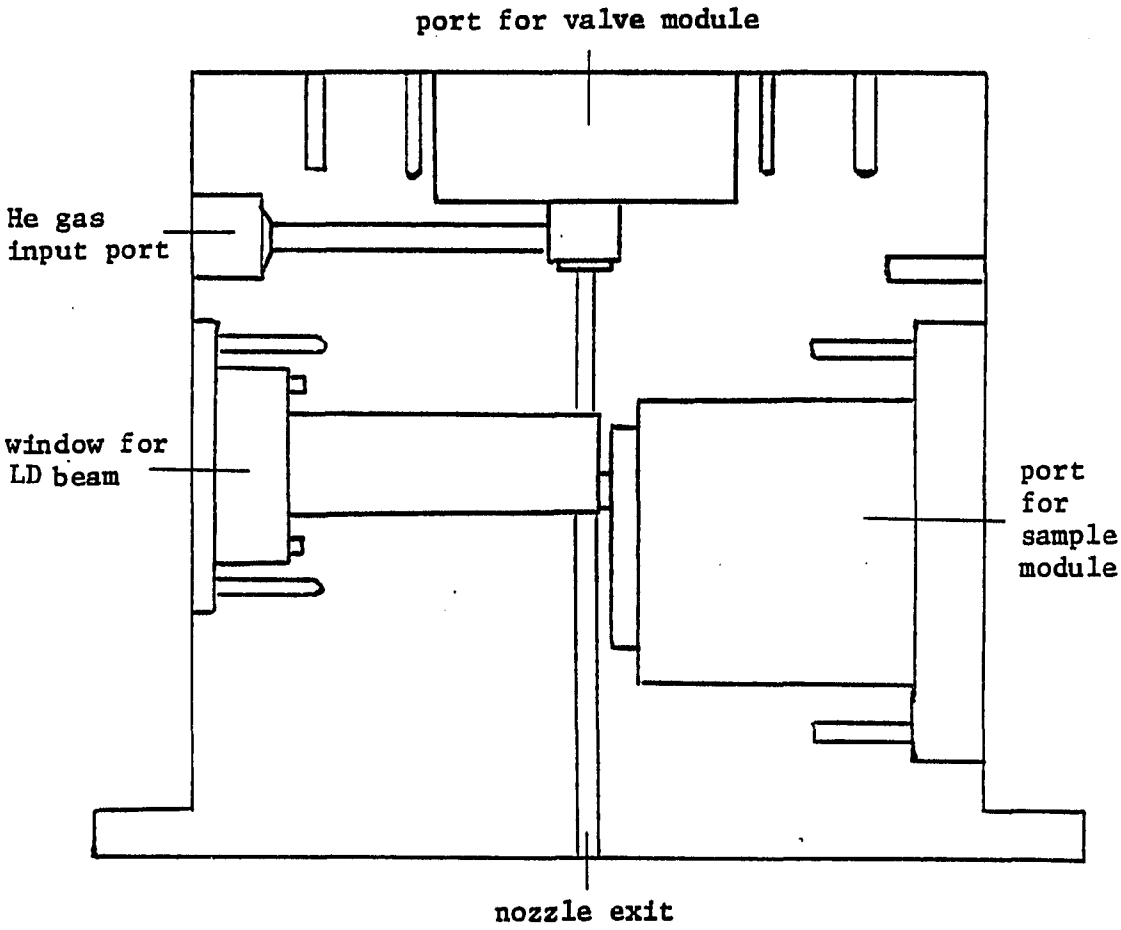

Figure 3. Laser desorption sample introduction module, unassembled

sublimation or vaporization.

The LN_2 jacket was constructed as a shell fitting over the sample disc and cold finger rod from which it could be separated when required. An O-ring on the rod and an O-ring between the LN_2 jacket and the module body prevented any vacuum leaks. The jacket and sample holder could be removed from the module to allow for preparation of sample, though in a further modification an access channel was drilled so that direct injection of liquid sample onto the cold disc could be made. The small access channel was equipped with a septum at its exit which allowed insertion of a syringe needle, while still maintaining the necessary vacuum.

Opposite the channel from the sample disc was another channel drilled for the desorption laser beam. It had a quartz window sealed in place with an O-ring and a metal bracket which could be tightened to hold vacuum. The desorption laser beam was directed through the window and focused by a lens outside of the system onto the portion of the sample disc aligned into position. Vaporization of sample by the desorption pulse sent analyte into the carrier gas stream and then into the interrogation region of the instrument.

The desorption laser pulse was timed to vaporize sample into the carrier gas pulse, allowing it to be carried away with the jet expansion pulse. Unlike the GC module, no auxiliary pumping of excess sample was necessary, as sample was released only when the low-duty desorption laser was pulsed. To increase the concentration of sample in the expansion, the repetition rate of the desorption laser was increased to vaporize more sample into each gas pulse, building up sample concentration.

Detection Systems

The spectroscopic instrument was designed to offer analysis by fluorescence excitation or by multiphoton ionization. As was discussed in the introductory chapter, these methods have similar yet differing characteristics and applications. This instrument was further designed to be used with either detection scheme, whether separately or using simultaneous detection. Although the instrumental system was designed to afford detection by both means, certain sacrifices in the capability of fluorescence measurement have been made in order to make feasible the detection of ions.

Fluorescence detection

Detection of fluorescence was accomplished conventionally with the use of collection optics, monochromator, and photomultiplier tube. Only the initial collimating lens was inside the vacuum chamber, while all other components were outside the instrument and attached to the supporting framework. The collimating lens was held in a mount which allowed the lens to be moved in any direction. The lens was placed at approximately the distance of the focal length, 5 cm from the jet and laser excitation crossing point. A large three in. diameter quartz window near the excitation region allowed maximum fluorescence collection and holds vacuum. All other components were standard equipment used in the usual manner and are described later.

Ion detection

The multiple photon ionization analysis module consisted of ion extraction and collection components and an ion multiplier. At the point of excitation and subsequent ionization an ion was extracted by the application of a potential gradient set up by two charged grids. The ion was then propelled and directed by several additional grids and plates through a flight tube region to an ion multiplier. Some accessories which were incorporated into the module to enhance analysis were a small flight tube cooled by a liquid nitrogen (LN_2) jacket and a turbomolecular pump. The LN_2 jacket and turbopump served the common purpose of reducing the pressure in the ion analysis arm of the chamber.

The ionization region is shown in Figure 4. It contained several ion optics and was surrounded by a LN_2 cooled copper canister with holes drilled to accommodate the jet expansion, incoming and outgoing laser radiation, and photon and ion collection. A stainless steel 90% transmission grid was positioned across the jet from the flight tube at ca. 1.25 cm from the point of laser interaction. The grid was maintained at a highly positive potential in order to repel the positive ions. A second high transmission grid placed symmetrically opposite the expansion from the first was held at a slightly less positive potential and with the first grid established a potential gradient which propelled the positive ions toward the flight tube.

A third grid 2.5 cm farther along the ion flight tube accelerated the ions in the direction of the ion multiplier, and deflection plates mounted vertically in the flight tube were used to account for any

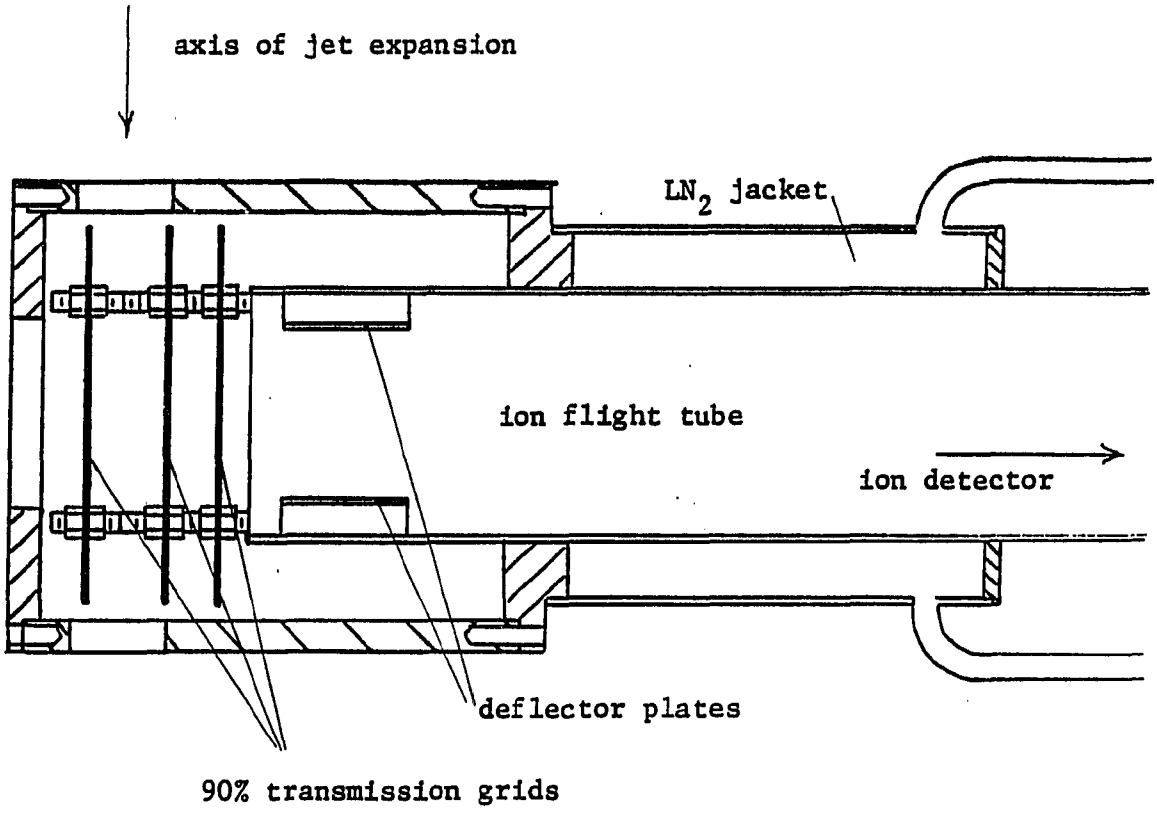

Figure 4. Ionization region module

momentum remaining from the directed expansion flow. Each of the three transmission grids were mounted onto threaded teflon rods within the copper canister shield and their distance from the ionization region was adjustable along the axis of the flight path. The deflection plates were set into fixed teflon brackets at the top and bottom sides of the horizontal flight tube.

A high voltage divider was constructed to give an adjustable potential for each of the grids and for the deflection plates. A high voltage supply provided the input to the device and was used for the potential at the first grid. The voltage divider gave an adjustable output for the second grid which was usually set at about 80% of the input potential. The deflection plates were then supplied with a potential which was variable from 0 to 250 volts. The acceleration grid and flight tube were maintained at electrical ground.

The flight tube was incorporated into the instrument to allow for the application of time-of-flight mass spectrometry (TOFMS), though at the time none of the sophisticated electronics and monitoring equipment necessary for TOFMS were present. The flight tube provided for a distance from ionization region to ion multiplier of ca. 50 cm and had mounting flanges to afford extension of the flight tube to any desired length. The flight tube was cooled by a LN_2 jacket extending over 40% of its length. This jacket was the same that provided cooling for the copper canister shielding the ionization region. The commercial ion multiplier tube was mounted on a teflon stud at the end of the flight tube.

Vacuum Chamber

The stainless steel vacuum chamber was designed as one piece, but can be thought of in two sections, separated by a nickel beam skimmer with an orifice of ca. 1 mm. Only a small fraction of the jet pulse expanding from the nozzle orifice was passed through the skimmer orifice, creating the cooled, collimated molecular beam for analysis. Most of the expansion was skimmed and pumped away by a 4 in. oil diffusion pump in the upper chamber. A smaller amount of gas reached the second chamber which was pumped by a 6 in. oil diffusion pump equipped with a LN_2 cooled cryobaffle. This differential pumping allowed pressures of roughly 10^{-7} torr to be attained in the second chamber.

The upper section of the vacuum chamber was a shallow cylinder along the axis of the jet expansion with an arm to one side leading to the diffusion pump. The sole purpose of this section was to provide the pumping capacity to remove the majority of the jet carrier gas which was skimmed from the expansion.

The lower chamber was also positioned cylindrically along the jet axis, with the diffusion pump located directly below the analysis region. This chamber had two small arms in which light baffles were mounted and a third extension for the ion detector, flight tube, and turbopump. Both sections also had ports for vacuum gauges.

Between the two sections was the beam skimmer, the mount for which was constructed to be adjustable in distance from the orifice, along the axis of the molecular beam. A screw outside of the system provided a mechanical adjustment for the skimmer height, which could be monitored

visually through a small window in the wall of the upper vacuum chamber. The mount accepted a variety of skimmer sizes and the distance from the nozzle to skimmer could be varied from ca. 0.5 cm to 2 cm.

CHAPTER 4. EXPERIMENTAL CONDITIONS

The general experimental arrangement used in this work was similar to that employed in other jet cooled laser induced fluorescence systems, employing a tunable dye laser, the vacuum chamber and pumps, and a monochromator with a photomultiplier for detection. A diagram of the instrumental layout can be seen in Figure 5.

It should be noted that the laser was physically separated from the chamber and was situated in an adjoining room. Laser excitation was directed to the analysis instrument through an opening in the wall between the two rooms. This arrangement was used to accommodate other experimental systems in addition to that described here utilizing the same laser.

The excitation laser used in these experiments was a Nd:YAG pumped dye laser equipped with KDP frequency doubling crystals. The Quanta-Ray DCR-1 Nd:YAG laser was upgraded to DCR-1A status with the addition of a Nd:YAG amplifier rod. The pulsed 1.064μm fundamental laser wavelength was frequency-doubled by a KDP crystal to the 532 nm output which was used to pump the dye laser. This 532 nm emission was separated from other frequencies by a Quanta-Ray PHS-1 prism harmonic separator mounted between the Nd:YAG laser and the Quanta Ray PDL-1 dye laser.

The pulsed visible fundamental from the dye laser was then directed to an InRad KDP second harmonic generator and was frequency-doubled into the ultraviolet (UV) region of the spectrum. The InRad frequency doubler was equipped with beam sensing photodiodes and an "AutoTracker" servo

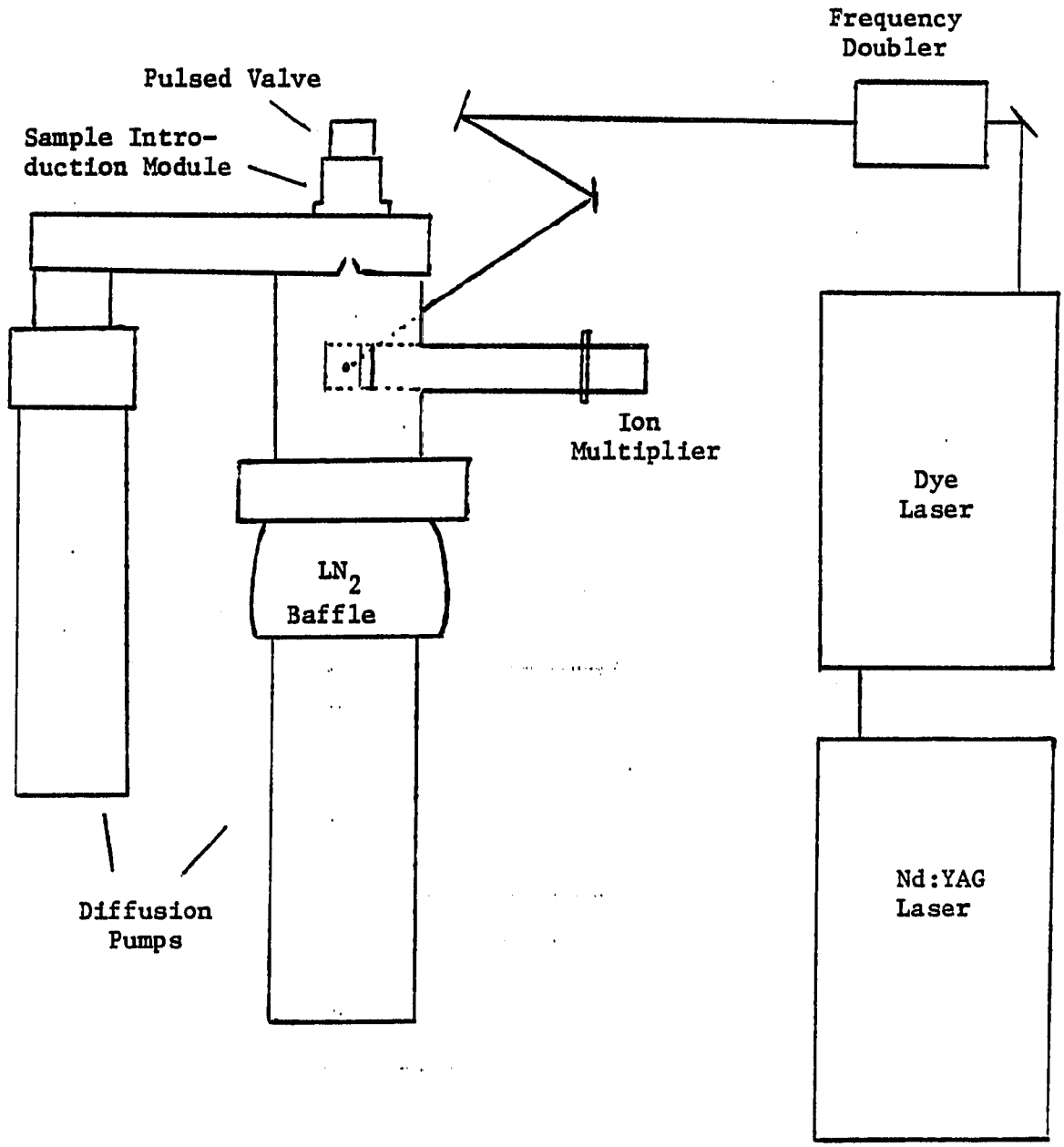

Figure 5. Schematic of instrumental apparatus

tracking mechanism which automatically tuned the angle of the KDP crystal for optimized frequency doubling as the dye laser frequency was scanned.

The resulting pulsed UV laser beam was directed by mirrors to the vacuum system where it entered through a Brewster's angle quartz window and was defined by homemade light skimmer baffles to a beam diameter of ca. 2 mm. The light skimmer cones were designed to reduce scattered laser light in the analysis region (63). Beyond the Brewster's angle window and the laser beam skimmers, the beam reached the interaction region where it intercepted the molecular beam skimmed from the jet expansion. After passing out of the analysis chamber through another Brewster's angle window, the excitation beam was directed to a reference cell containing a dilute solution of Rhodamine B laser dye. The resulting Rhodamine B fluorescence was monitored by a reference photomultiplier tube through an optical cut-off filter used to reduce scatter of the UV laser radiation from the reference cell.

The pulsed valve has been described in detail in the previous chapter. It was used with backing pressures of helium carrier gas ranging from 1 to 2 atmospheres. For most of the instrument characterization and testing, a sample was introduced in the carrier gas stream after it was allowed to attain an equilibrium vapor pressure in a small temperature-controlled chamber along the gas intake line. The GC sample module, also described earlier, was used for evaluation of instrument characteristics.

The upper section of the vacuum chamber was evacuated by a 290 L/s Stokes 150-series 4 in. oil diffusion pump. During operation of the valve, pressure in this chamber was maintained at 5 - 200 mtorr,

depending on pulse characteristics of the valve, which was controlled by the valve driver and timing unit described in the previous chapter. The average pressure was kept at ca. 50 - 80 mtorr during normal operation.

A portion of the expansion was skimmed by a 1.02 mm orifice Beam Dynamics nickel beam skimmer and expanded into the analysis region of the vacuum chamber. This lower section was pumped by an 805 L/s CVC PAS-65D 6 in. oil diffusion pump, backed by a 50 L/s mechanical pump. A small Leybold-Heraeus Turbovac 50 turbomolecular pump with a pumping speed of 55 L/s provided additional pumping capacity for the ion detector and flight tube arm of this lower chamber. The turbopump was in turn backed by a small Welch pump. Pressure during operation of the valve was 2 to 5 x 10^{-6} torr in the lower chamber.

Fluorescence from the excitation laser and jet interaction region was collected using a f/1.0 lens mounted inside the chamber, then focused onto the slit of a f/3.5 Instruments SA 0.10 meter monochromator and detected by a water-cooled photomultiplier tube at a wavelength slightly longer than that of the laser excitation. Since fluorescence excitation was monitored, the monochromator acted chiefly to discriminate against scattered laser radiation and was not used for wavelength resolution.

The outputs from the signal and reference photomultipliers were sent to a Quanta-Ray DGA-1 dual gated charge amplifier which gave the ratio of signal to reference as the output. This normalized the scanned fluorescence excitation with respect to the laser, accounting for the shot-to-shot fluctuations in the laser beam intensity. The amplifier gate time for the fluorescence measurements was preset on the DGA-1 to 4.5 μs.

Ions produced by multiphoton ionization at the point of jet interrogation by the laser were sent toward the detector by three biased grids and two biased deflectors. Two 90% transmission stainless steel grids (Buckbee Mears) on either side of the ionization area were held at ca. 3100 and 2600 volts, providing a potential gradient of approximately 200 V/cm, propelling the positive ions toward the flight tube and detector. A third grid at the flight tube entrance was used to accelerate the ions and was held along with the flight tube assembly at electrical ground. The small deflector plates were usually held at about 120 V to offset the vertical motion of the ions.

Ions were detected with a Model MM1 ion multiplier mounted on a teflon stud at the end of the flight tube. The potential applied to the detector ranged from -3000 to -4200 V, depending on the application. The DGA-1 gated analyzer was used in the same manner as for fluorescence detection with the gate time adjusted to 18μs. The longer gate time required was due to the travel time of the ions through the flight tube. This time was measured at ca. 9μs with an oscilloscope.

All chemicals were reagent grade and were used as purchased with no further purification.

CHAPTER 5. RESULTS AND DISCUSSION

Results in this thesis range from the characterization of the newly developed analytical instrument to showing the analytical information which can be gained through the use of the instrument. Because this is the first work covering details of the apparatus, considerable information as to instrument function and capabilities is presented.

Characterization of Analysis Instrument

The apparatus used in this work was substantially made in-house by the author and by the machine shops on campus. As for any new instrument, it required testing of the various functions, ranging from the degree of vacuum which could be maintained to the analytical utility of the instrument.

Vacuum characteristics

A large number of joints are found in the vacuum chamber, so leak testing occupied some time. The various stages of the instrument required differing levels of operating pressures, and characterization was done to those levels and below. The vacuum chamber consists of two sections, with the upper section used for differential pumping to maintain the best possible vacuum conditions in the lower chamber. These chambers were usually separated by a small beam skimmer with an orifice of 1 mm. When the skimmer was not in place, the opening between

chambers was ca. 3 cm, and the analysis instrument became essentially one chamber. With the skimmer removed, the pressure was tested to below 1×10^{-6} torr, using both diffusion pumps.

When the skimmer was put into position, the lower section, which was the vacuum chamber intended for the laser and molecular beam interaction region, was separated from the upper chamber. This lower section held the ion detector and was the section demanding the lowest operating pressures. With the skimmer in place the pressure was tested down to as low as 3×10^{-7} torr. Lower levels, e.g., pressures below 1×10^{-7} torr, which was the limit of the ion gauge used for pressure measurement, were achieved after a period of pumping out the helium expansion gas. The upper section, designed to handle a much higher gas throughput, was only tested to 1×10^{-4} torr. The vacuum line connected to the mechanical pump used to pump away the output from the diffusion pumps was tested down to less than 1 mtorr.

Valve function

A second stage of testing of the instrument was the verification of the nozzle valve function. This involved testing of the valve actuator and of the valve driver and timing controller. The method used to verify the valve function was simply monitoring pressure in the evacuated chamber. Early tests indicated that the valve was either open or closed, i.e., there appeared to be no pulsing of gas flow.

Adjustments in the vertical position of the valve indicated that the valve actually did move in the channel, but that it did not repetitively

open and then seal the orifice as intended. In the action of the solenoid-driven valve, some effects were observed of what appeared to be long-term magnetism, e.g., several minutes, induced in the solenoids, the actuator, or even the solenoid housing. It was discovered that the addition of a thin non-magnetic spacer to the solenoid housing both above and below the disk on the valve actuator circumvented the effects of this apparent magnetism and allowed the opening and closing of the valve as designed.

Even so, very slight changes in vertical position of the valve were found to result in large variations of gas throughput. The position of the valve seat was engineered to be adjustable in distance relative to the large disk on the actuator. The motion of the disk is limited vertically by the housing between the two solenoid coils. However, it was soon found that only a small range of distance settings was acceptable, and that manual adjustment over this small range was rather difficult and tedious. Adjustments in the timing control of the opening and closing pulses to the valve were used to fine-tune the adjustment of the valve seat seal. With practice the adjustment of the valve became a feasible task. It should be noted that because of this interaction between valve-opening distance and pulse timing there was a small range in each of these quantities which would result in the desired operational vacuum chamber pressures.

After these adjustments were made, a small spring was added above the actuator to ensure its closure. It was found by manipulating the timing of the expansion pulse relative to the timing of the interrogation

laser pulse, that insertion of the spring sharpened the tailing end of the molecular beam pulse. Timing adjustments with the valve driver were still possible with the spring in place, so it appeared that the spring aided in faster closure of the valve when the closing solenoid current pulse was applied. As far as the author was able to determine, the only effect of the spring was to shorten the duration of the expansion pulse. This was advantageous in that a slight benefit was realized in pumping requirements. The duration of the molecular beam pulse was ca. 200 μs, determined by adjusting the delay time between the valve pulse and the laser excitation pulse.

Fluorescence

After the valve adjustments were made and some degree of control over the variables of the system was achieved, observation of fluorescence from jet-cooled samples could be attempted. The molecule used in the initial testing was aniline, and later molecules used were 2-methylnaphthalene and indole. Aniline was chosen because it has a very high fluorescence quantum yield, the fluorescence excitation spectrum of aniline has been well characterized by others, and because it is quite volatile, yielding a high number density of molecules in the jet.

After alignment of the laser beam optics, the nozzle and skimmer, and the fluorescence collection optics, the laser was set to a frequency near the origin band of the $S_1 \leftarrow S_0$ transition. Aniline was incorporated into the expansion gas by putting a drop of sample onto a small piece of glass wool placed in the helium background gas input line,

allowing aniline to mix with the helium at its room temperature vapor pressure. This mixing took place above the valve so that the expansion gas was mixed before expansion occurs. When the nozzle was activated, the laser was scanned over the region where the aniline origin band was expected to be. This procedure would be similar for any new molecule to be observed, as the frequency of the origin band can be estimated from the room temperature UV spectrum.

There are many adjustable parameters which can be manipulated to optimize the fluorescence response. One is the choice of monochromator wavelength. The use of a frequency having a high intensity for dispersed fluorescence will increase the signal. To find such a frequency, either a dispersed fluorescence scan can be taken or the monochromator can be manually slued over wavelengths just lower in energy than the excitation laser. Care must be taken to avoid measurement of scattered incident laser radiation. The monitored wavelength was 310 nm in the case of aniline while the excitation beam was scanned from 295 to 285 nm.

Another variable is the extent to which the excitation laser beam is focused. The use of a lens before the chamber would provide higher laser power densities and may excite more fluorescence. For aniline in this instrument it was found that the best conditions were with no lens present. This appears to be due to an increase in the production of ions resulting from the increased laser intensity.

One other parameter that was investigated was the use of the beam skimmer. It was found that when the skimmer was removed the chamber pressure was still adequate for the diffusion pumps, in the high 10^{-4} to

10^{-5} torr range. The quality of the signal without the skimmer was more noisy than with the skimmed expansion. The increased noise may be due to a higher number of light scatterers in the chamber.

Cooling in the jet expansion

The chief benefit of the supersonic jet expansion to molecular spectroscopists and to analytical chemists is the cooling of the analyte that can be obtained. This results in sharp, well defined transitions which aid spectroscopists in establishing characteristics of the molecule and which yield greater selectivity to analytical chemists. The degree of cooling achieved in the jet is dependent chiefly on the backing pressure and on the nozzle diameter, though factors such as the choice of carrier gas can affect cooling. For an examination of these factors, the reader is referred to several reviews (4, 64-66) and the references contained therein.

The experimental characteristics which could be adjusted were optimized in the instrument to gain the best possible cooling for aniline, the test molecule. The sample backing pressure was adjusted, i.e., the pressure applied with the helium carrier gas, the pulse duration of the valve was adjusted, the distance from the nozzle orifice to the skimmer was varied, and the relative timing between laser and beam was varied. When all of these variables were optimized, a sample vibration temperature of 35 Kelvin was measured, as will be shown.

The measurement of actual vibrational temperature can be done mathematically by comparing the ground state population with that of an

excited state. In the measurement just given, the lowest excited vibrational level of aniline was used, the frequency of its transition being 291 cm^{-1}. This is the inversion mode, and the lowest transition resulting from an excited level. The intensity values, assumed to be proportional to population, and the energy level relative to the ground state are inserted into the equation,

$$e^{-\omega/kT} = \frac{I_{(excited)}}{I_{(ground)}}$$

The value used for ω is 40.8 cm^{-1}, the energy level of the aniline inversion mode above the ground state, k is Boltzmann's constant, and T is the temperature in Kelvin.

The cooling characteristics of the expansion are not always precisely reproducible, due to the many variables involved. While values for this inversion mode of 35 - 40 K were obtained several times, vibrational temperatures of 45 - 75 K for aniline were more typical. This variation may be an indication that fully developed flow through the nozzle was not always established. It may also be that this variation was due to differences in timing reproducibility between the laser and jet expansion pulse.

Cooling of other molecular modes than the vibrational mode is accomplished to a much greater extent in the jet. The cooling proceeds in the order of translational modes, rotational, and then vibrational modes. The mechanism of cooling in the expansion has been discussed thoroughly by others (4, 64-66) and is characterized briefly as follows.

As molecules move through the nozzle orifice, they travel out of a region where each has its own random thermal motion, given by the Boltzmann distribution. Each molecule has a velocity vector in its own direction. In passing through the orifice, molecules begin to collide with each other. In these collisions energy is exchanged, so that molecules begin to move in the same direction. As the translational motion becomes uniform, rotational modes are also cooled by collision, through the exchange of energy between translation and rotational modes. The vibrational cooling occurs in this manner as well, though to a lesser extent. The resulting beam of molecules has a high velocity, but a low spread in the velocity range. It is this narrow distribution that is the reason for the apparent cooling.

Though the degree of cooling has been surpassed in other systems, that achieved here is sufficient for use in analytical spectroscopy in the application proposed. Illustrated in Figure 6 is the spectrum of aniline at a vibrational temperature of 35 K, overlaid with the room temperature aniline spectrum for the same frequency region. Note that the sharpness of the bands in the jet-cooled spectrum allows for a great increase in selectivity among species absorbing photons in the same energy region.

Multiphoton ionization

Aniline was also used as the test molecule for observation of signal from two photon ionization. The characteristics which make aniline a good test molecule for fluorescence, combined with an ionization

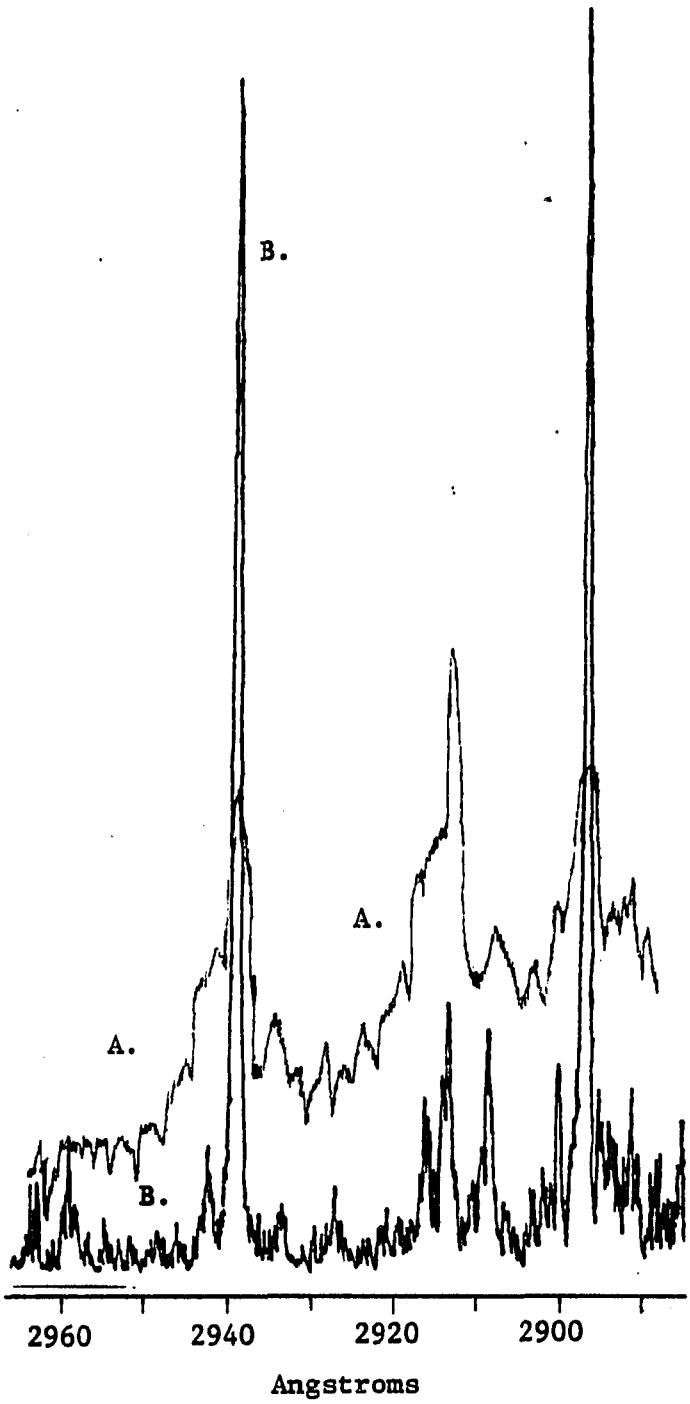

Figure 6. Fluorescence excitation spectrum of aniline at room temperature (A.) and cooled to 35 Kelvin (B.)

potential of less than twice the energy of the first excited state, also make it an excellent candidate for MPI study.

Determination of species by detection of ions produced by MPI required several adjustments in experimental operation. The proper function of the detector, an ion multiplier, is limited to pressures below ca. 1×10^{-4} torr. Because of this, it was required that the beam skimmer be in place and that differential pumping be used. A turbomolecular pump was also used to aid in evacuation of the chamber. The operating pressures for typical analyses were ca. 2 to 4×10^{-6} torr.

The search for a signal resulting from MPI followed the same format as for fluorescence. Usually the laser frequency was scanned over the low energy range of the first absorption region in the room temperature spectrum. If a jet-cooled fluorescence excitation spectrum exists, the MPI scan should be very similar, with ion production at the same wavelengths as the transitions observed by fluorescence. One helpful piece of information to know is whether the ionization potential is less than twice the energy of the first excited state relative to the ground state. The efficiency of MPI is reduced considerably for molecules with ionization potentials at higher energies than this level, because a three photon process is required instead of absorption of only two photons.

The theory of MPI has been discussed in many recent reviews and the reader is referred to those for more detailed coverage of the subject (19, 67-70). Briefly, enough energy must be added to a molecule in order to reach the ionization potential. Ionization energies for most organic species of interest are typically 7-13 eV (19), equivalent to the energy

of one vacuum UV photon. A more reasonable way of adding this energy to the molecule is by absorption of more than one photon of lower energy. Two near-UV photons are commonly enough to ionize most of these organic species.

Addition of two photons can take place when a molecule absorbs a single photon and goes to a real excited state. The excited state lifetime is typically on the order of 10^{-8} seconds, so if a second photon is absorbed by the same molecule within that interval of the first photon, then ionization results. Excitation can also take place through the use of a so-called virtual state. Because the lifetime of such a state is usually about 10^{-15} seconds, two photons must be absorbed within a very short period. The former method is called resonance two photon ionization and the latter, non-resonance ionization.

Selectivity is gained in MPI by the use of this resonance: because of the difference in lifetimes of the intermediate state in both processes, the resonant process is a factor of ca. 10^{7} more efficient than its non-resonant partner. Because resonance reflects the absorption spectrum, the selectivity that results from resonance MPI gives this spectrum. Thus the cooling of the analyte in the expansion results in sharp transitions for the MPI spectrum.

It was expected that production of ions would require a higher photon flux than fluorescence excitation. A focusing lens was inserted into the laser beam path prior to the chamber and was found to increase the ion signal. No other modifications of the system were necessary other than the optimization of the potentials applied to the transmission

grids and the deflection plates designed to direct the ions produced to the ion multiplier. The potentials applied to the grids were ca. 3100 V, 2600 V, and electrical ground, beginning with the grid farthest from the detector. The deflector plates were held at ca. 120 V. The effect of the potential applied to the deflector plate was minimal. The potential applied to the ion multiplier ranged from -3000 to -4500 V, depending on the sensitivity desired.

Comparison of fluorescence and multiphoton ionization

Comparison of fluorescence excitation and MPI as detection methods was carried out with both aniline and indole. Comparative spectra are given in Figures 7 and 8 for each of these molecules.

The most noticeable feature is the reduced noise on each of the MPI spectra. Because the detector is not sensitive to scattered laser light in this frequency range, the background signal is much lower than for fluorescence detection. The signal-to-noise ratios are improved by a factor of about 30 in the case of both molecules. When one considers that there is only a slight variation in experimental requirements, the MPI method is clearly the better detection scheme for species which undergo two-photon ionization.

It should be noted that both MPI and LIF spectra show the same features. As explained in the earlier section on MPI, this is because both spectra involve excitations to the same excited state. For MPI a second photon raises the energy beyond the ionization potential, while in LIF the molecule decays by releasing a photon.

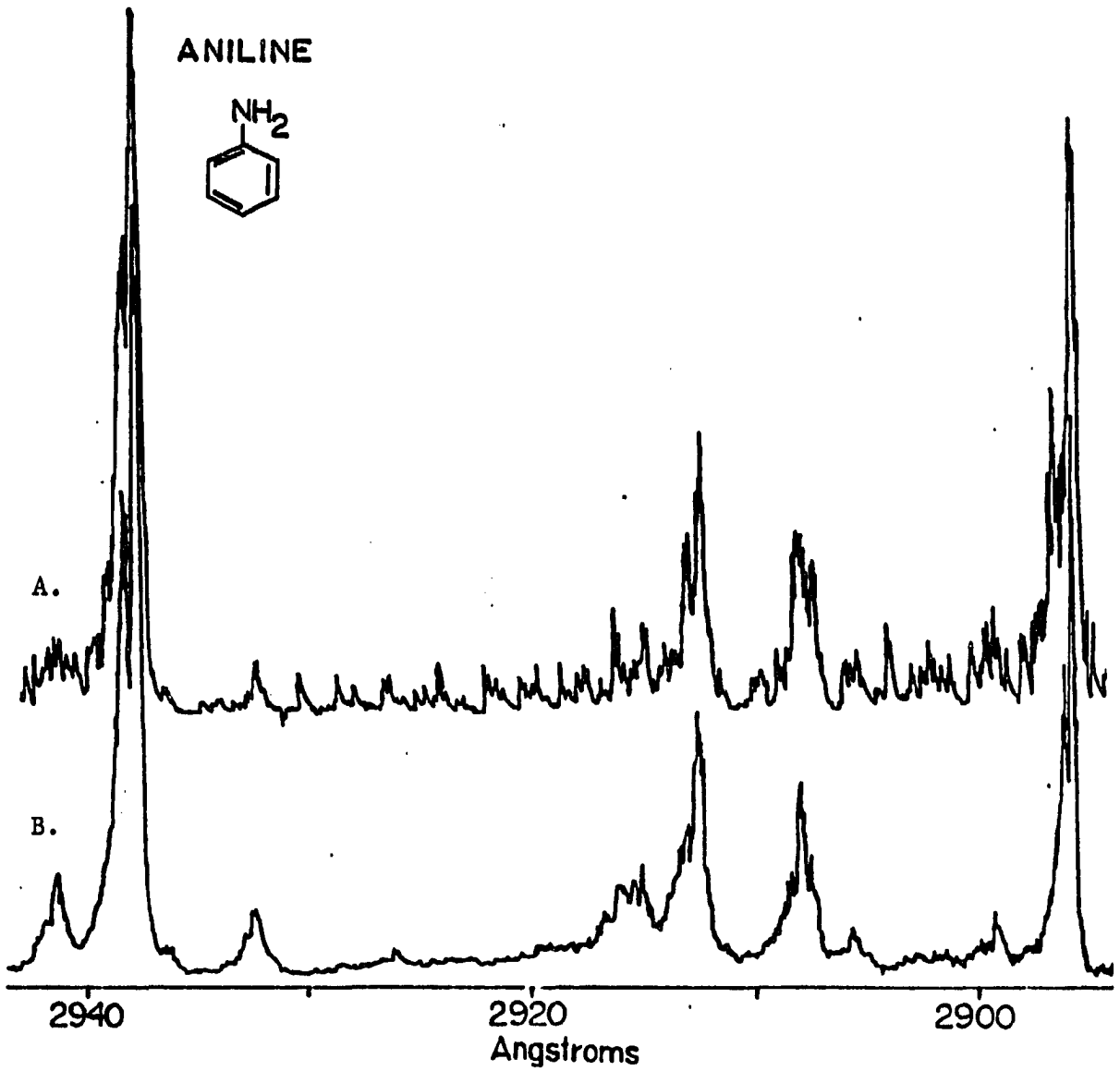

Figure 7. Comparison of fluorescence excitation (A.) and multiphoton ionization (B.) for aniline

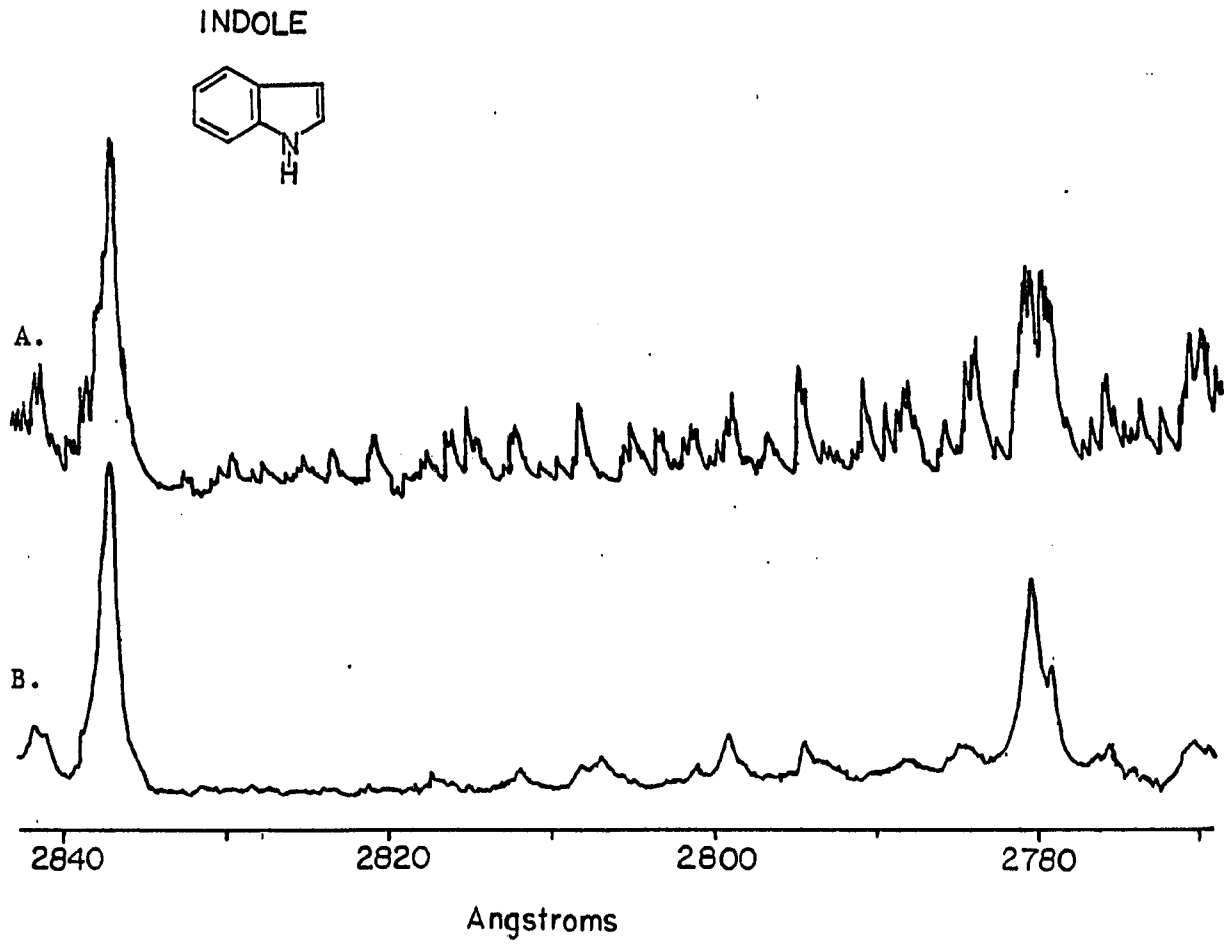

Figure 8. Comparison of fluorescence excitation (A.) and multiphoton ionization (B.) for indole

Laser desorption efforts

Efforts to observe aniline introduced by laser desorption did not yield any discernible signal by either detection scheme, fluorescence or MPI. Desorption was attempted with the 308 nm output of the XeCl excimer laser, softly focused onto the sample holder. Observation was made by fluorescence excitation and multiphoton ionization using the UV interrogation beam from the Nd:YAG-pumped dye laser.

Aniline was frozen to the sample holder by several means, the first by placing a drop of liquid aniline on the end of the sample rod and freezing it by pouring liquid nitrogen through the jacket surrounding the sample rod. In later attempts the aniline was mixed with glycerin and then put onto position on the sample disk by injecting it with a syringe through a septum and the drilled access hole while the sample rod was already cooled and the chamber pumped down. A mixture of analyte with glycerin on the laser desorption sample rod was used successfully and reported to be a sample matrix which allowed analyte to be desorbed gradually in even quantities (71).

While no signal was observed with sample introduction by laser desorption in this laboratory, at least two other laboratories (46-49, 55, 72) had reported entrainment of laser-desorbed samples into the supersonic jet prior to the conclusion of this work in 1987. In retrospect, several differences between this work and that of the two laboratories are notable and these are covered here.

In the apparatus used by Tembreull and Lubman (47), the desorption pulse came from a CO_2 laser (wavelength = 10.6μm). In their work they

found that desorption wavelengths of 249 nm and even 532 nm were optimal choices. They believed fragment ions were formed in the desorption process at the shorter wavelengths.

A second difference from the work of Tembreull and Lubman was that the desorption surface they used was downstream from the nozzle orifice, i.e., after the expansion was already forming. In the apparatus designed for our work, the desorption step took place behind the nozzle orifice, the intent being that molecules desorbed would be more quantitatively entrained in the expanding pulsed beam. Arrowsmith et al. have investigated entrainment of desorbed molecules into the jet (73) and find the arrangement used by Tembreull and Lubman to provide excellent incorporation into the expansion. Tembreull and Lubman also used a shorter beam pulse, the stated goal being to have a higher analyte density at the probe region, rather than spreading the analyte out into a longer beam pulse.

In addition, the surface from which desorption took place was of a different material, either an aluminum rod (47) or a rod of Macor machinable ceramic (49, 55). The surface used in the instrument for this work was stainless steel.

Analytical Determination of Jet-Cooled Molecules

Quantitative determination of species in the jet can be accomplished by measurement of fluorescence excitation or multiphoton ionization at a frequency absorbed by the molecule. For jet-cooled species, the number

of frequencies where absorption and subsequent fluorescence or ionization occurs is reduced in comparison with room-temperature species. This sharpening of the spectrum indicates that a higher population of absorbers is in the ground state. In fact, for molecules where the vibrational energy level spacings are large, e.g., hundreds of reciprocal centimeters, the ground state is frequently the only state which is significantly populated (64).

The choice of analytically useful lines is usually made from the set of ground state transitions, because the ground state is most heavily populated. Of this set of frequencies, the greatest sensitivity can usually be gained by working with the excitation characterized by the highest intensity, usually the 0_0^0 vibronic band of the $S_1 \leftarrow S_0$ transition. This is the band recommended for analytical use in this work.

Aniline

Since aniline was used as a test molecule for several of the previous characterizations of the analytical instrument, several LIF and MPI spectra were given, in Figures 6 and 7. Laser excitation of aniline was done with the Nd:YAG-pumped dye laser using Rhodamine B as the laser dye. Fluorescence was monitored at 310 nm through a 1/10 m monochromator.

The MPI spectrum of aniline over a broader range of frequency is illustrated in Figure 9 at a vibrational temperature of ca. 40 - 45 K. The origin band is toward the low energy end of the spectrum at 293.78 nm, and the other band nearest in intensity, at 289.62 nm. The band used to determine the vibrational temperature is at 291.27 nm, measured in

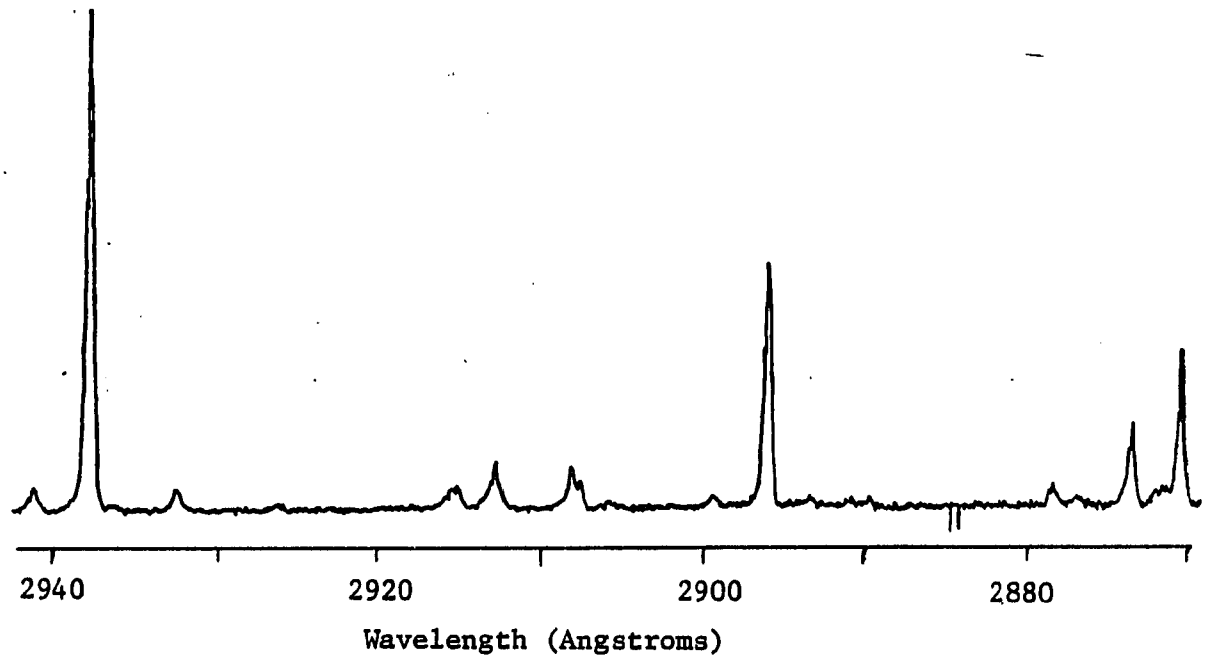

Figure 9. Large frequency range spectrum of aniline (MPI)

this spectrum at an intensity of 9% of the origin.

The excitation bands observed are listed in Table 1 with the average intensity observed. It should be noted that the relative intensities do vary from one scan to the next, an effect which may represent changes not accounted for within the duration of each scan. From the group of bands listed, the best candidates for quantitative determination of aniline are the lines at 34039.1 cm^{-1} and at 34528.0 cm^{-1}, or 293.78 nm and 289.62 nm, respectively. Other bands are either far less intense or result from states other than the ground state.

Table 1. Observed transitions for aniline having intensities greater than 5% relative to the origin band

Wavelength (Angstroms)	Frequency (cm^{-1})	Distance from Origin (cm^{-1})	Spectral Assignment (74)	Average Intensity (vs. origin)
2941.3	33998.6	-40.5	T_1^1 [a]	6 %
2937.8	34039.1	0.0	0_o^o	100
2932.6	34100.0	60.9	S_1^1 [c]	5
2915.1	34304.1	265.1	$I_1^1T_1^1$	6
2912.7	34332.4	293.3	I_1^1	14
2908.2	34385.5	346.5	I_o^1 [b]	10
2896.2	34528.0	488.9	$6a_o^1$	59
2874.0	34794.7	755.6	$1_o^1T_1^1$	24
2871.0	34831.1	792.0	1_o^1	42

[a] This represents a combination band, described in the citation (74).
[b] See Mikami, N.; Hiraya, A.; Fujiwara, I.; Ito, M.; Chem. Phys. Lett., 1980, 74, 531.
[c] Represents an unidentified non-totally symmetric mode (74).

While the limit of detection (LOD) cannot be determined from the aniline spectra, it can be estimated from the signal-to-noise ratio (S/N) at this concentration. For the case of fluorescence, S/N values were commonly ca. 50 on spectra for the room temperature vapor pressure samples. For MPI, typical ratios obtained were ca. 600, with occasional scans at S/N ratios of ca. 1000. The concentration in the jet is approximately 3 parts per thousand if an equilibrium vapor pressure was attained. The detectable concentration could be estimated to be about 180 ppm at a S/N of three for LIF and ca. 15 ppm (10 ppm in the best cases) for MPI.

The detection limit value would appear to be far better if one could account for the duty cycle of the valve and laser as well as the dilution of sample into the expansion gas. However, since these factors are necessary to some extent, the LOD remains at a level which can be bettered by many other methods. The advantage of extreme selectivity, however, remains in the corner of jet-cooled spectroscopy.

Indole

For the case of indole, the same recommendations for determination hold. The best spectral feature for determining the quantity and presence of indole is the origin band, as was shown in Figure 8. It is clear from the scan that detection of indole is not as good as in the case of aniline, with respect to S/N characteristics. Thus, the use of any other band is not of analytical value.

There are several reasons why the fluorescence of indole is not as

intense as the fluorescence from aniline. The first is the lower volatility of indole. Although the vapor pressure for indole was not available, its melting and boiling points are higher than for aniline (75). The methyl-substituted molecules can be compared, with the methyl-substituted aniline, 3-toluidine, attaining a vapor pressure of 1 torr at 41 °C, and the 3-methyl indole reaching the same vapor pressure at 95 °C (75). Aniline is more volatile than the methyl-substituted isomer, and it is expected that the same is true for indole, but from the comparison given and from the differences in melting and boiling points, it must be assumed that indole is substantially less volatile than aniline.

The quantum yields can also be compared, though again the desired information is not available for indole. Quantum yields can be compared for both aromatics in cyclohexane, 0.08 for aniline, and 0.39 for indole (76). These values may not accurately represent the quantum yield in the vapor phase, as is shown by Sonnenschein et al., who measured a quantum yield for aniline in the jet expansion of 0.28, relative to the quantum yield of the $S_1(0)$ transition of 9,10 dichloroanthracene, taken to be 1.00 (77). Even if indole does have a higher quantum yield, the lower vapor pressure reduces the number density in the jet such that the observed fluorescence intensity is much less than for aniline.

This accounts for the fact that detection limits for indole are not as favorable as for aniline. The S/N ratio for the scan shown is ca. 10 for LIF and ca. 140 for MPI. This yields an LOD of ca. 1 part per thousand for LIF and of ca. 70 ppm for MPI.

Estimate of detection limit

A study was made of the detection limit for the instrument using aniline in order to gain a feel for the quantitative characteristics of the instrument. The study was made by varying the concentration of aniline introduced into the jet. This was accomplished by the use of a small temperature-regulated sample container in the path of the carrier gas, which allowed introduction of a known, yet changeable, concentration of aniline.

The aniline sample was allowed to attain an equilibrium vapor pressure dependent on the temperature of the bath surrounding the sample chamber. The signal was determined as suggested previously, by using LIF and MPI at the origin band. The 1/10 m monochromator was set as before, at 310 nm, for the fluorescence work. Temperature points used were room temperature (26.5 °C), the melting point of ice (0.0 °C), and the melting point of an ice-and-salt bath (measured at -6.0 °C).

Knowledge of the temperature allows one to find the partial vapor pressure of the species of interest, which is related to temperature. Tables for vapor pressure of pure compounds are available (78, 79), but formulas for calculating the vapor pressure of aniline are applicable only for the temperature range of 102 - 185 °C (79). The vapor pressures at the temperatures used in this work were extrapolated from the data tables given by Stull (78), using the temperature-pressure data for temperatures ranging from 34 - 120 °C. This extrapolation gave a straight line when plotted as log P vs. 1/T, where T is in Kelvin. The pressure was calculated in torr (mm Hg). The resulting equation is given

below and was used to calculate vapor pressures at the temperatures used in this work.

$$\log_{10} P = \frac{-3.49648 \times 10^{-4}}{T} + 3.25699 \times 10^{-3}$$

The correlation coefficient for the calibration used to find this equation was 0.9992.

The resulting concentration values, as partial pressure, in units of torr, were plotted vs. signal to determine linearity of response and to estimate the detection limit. This calibration curve for aniline is given in Figure 10, and has a correlation coefficient of 0.9988.

The S/N was calculated as ca. 25 for fluorescence and ca. 400 for MPI at the lowest concentration, i.e., for equilibrium vapor pressure at -6.0 °C). Detection at three times the S/N would put a limit on vapor pressure concentration for aniline of 4.8 mtorr for fluorescence and 0.3 mtorr for MPI. The limits given here correspond to concentrations of 6×10^{-6} mole of aniline per mole of carrier gas for fluorescence and 4×10^{-7} mole/mole for MPI. In relative mass units this is 100 ppm for fluorescence and 9 ppm for MPI. These figures give a more accurate estimate for the limit of detection than the estimate from a single peak and associated S/N as was used in the discussion previous.

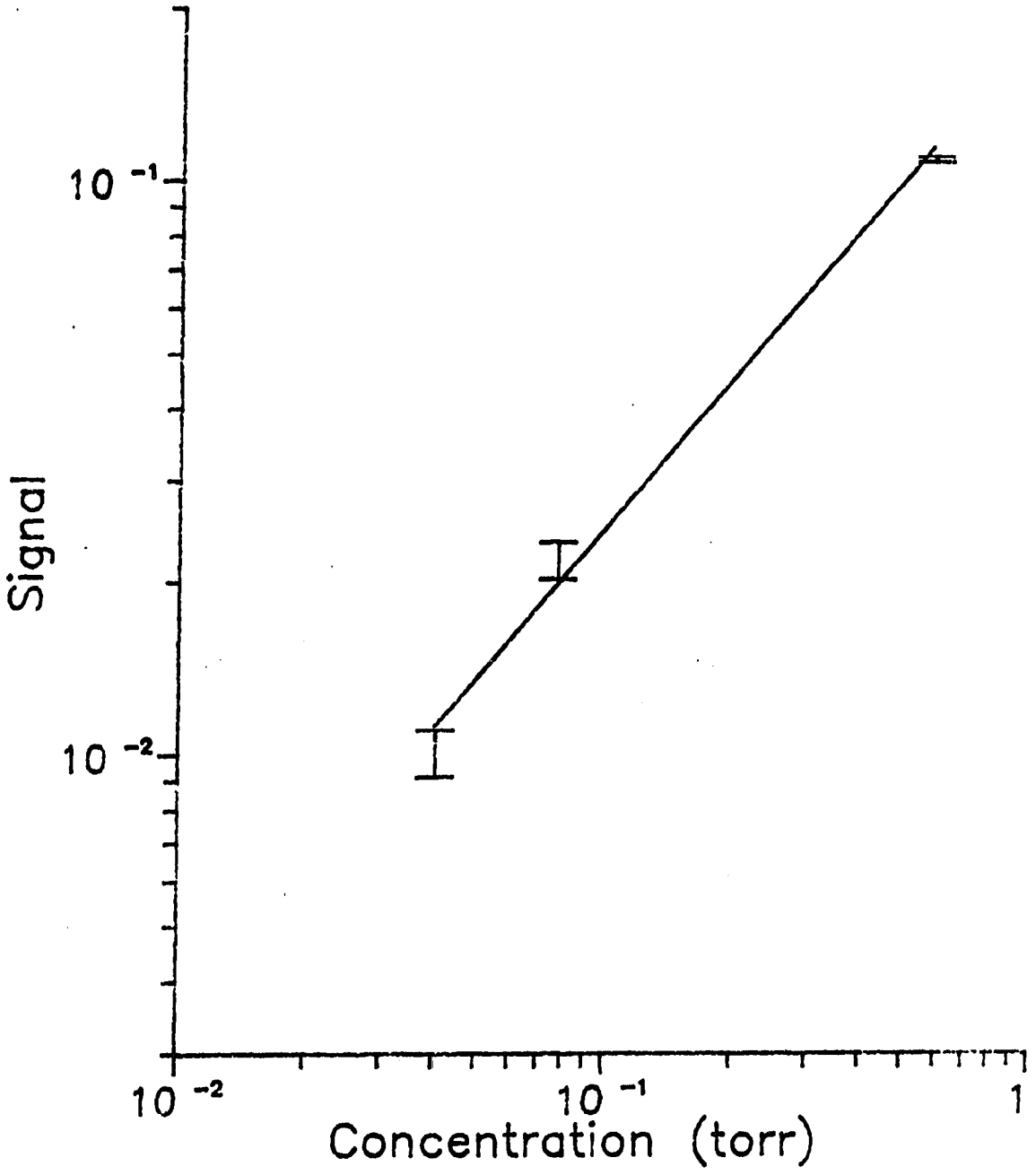

Figure 10. Linearity of response for aniline (MPI)

CHAPTER 6. FUTURE WORK

There is strong evidence in the recent work done that a good future exists for analytical supersonic jet spectroscopy. A thorough review published recently covers the advances of past years in more detail than has been done in this dissertation (4). The technique will continue to grow as new hyphenated methods are developed which offer some of their own advantages, such as more universal detection, and which also take advantage of the spectroscopic selectivity offered by cooling. This chapter covers some future possibilities for improvement of the analytical instrument constructed in our own laboratories.

Modifications to the Instrument

In view of the successful laser desorption results obtained in the laboratories of Lubman at the University of Michigan (47, 49, 51, 55, 71), several modifications to the instrument could be made to better emulate the apparatus used in their work in the hope of obtaining like results. These adaptations are in two categories, the first of which involves possible changes in the wavelength used for desorption.

The work done in our laboratories involved an excimer laser and a Nd:YAG laser, both of which are equipped with dye lasers. The wavelengths provided range from 308 nm with the XeCl excimer laser fundamental to 1.064 m with the fundamental of the Nd:YAG laser. The wavelength used by workers in Lubman's laboratories was the 10.6 μm fundamental of

CO_2 laser. Tembreull and Lubman stated that they believe higher energy photons cause ionization and fragmentation of desorbed sample within the duration of a single laser pulse (47). If ions or fragment ions are produced in our instrument, they would be deflected out of alignment by the presence of the charged ion extraction grids surrounding the analysis region. A change of laser wavelength or even a decrease in desorption laser intensity may in fact allow measurement of samples produced by desorption in the unmodified instrument.

An instrumental modification which should be considered involves the arrangement of the laser desorption sample module and the nozzle orifice. In the current system the laser desorption sample rod is positioned behind the nozzle orifice, prior to expansion, while in the instrument used by Lubman the rod was placed 4 mm downstream from the orifice, i.e., within the expansion chamber. It is possible that in our apparatus newly vaporized sample may be redeposited onto the wall of the small channel immediately after desorption. Because the module is relatively cold due to the presence of liquid nitrogen-cooled parts, sample would not come off of the wall back into the expansion as with the heated channel used in the thermospray work of Rizzo et al. (44, 45).

The orifice could also be modified in size by attaching a plate with a smaller diameter opening to the base of the sample module. This would allow the continued use of the interchangeable sample introduction modules while permitting the use of changeable orifice sizes. This change could also result in improved cooling in the expansion compared with what could be achieved with the nozzle channel originally drilled by

the machine shop.

A major change which may result in less hassle in the day-to-day operation of the instrument is a change in the design of the pulsing mechanism of the pulsed valve. Adjustment of the valve actuator is occasionally necessary and, as was stated in the section on the valve in the previous chapter, adjustment of the valve was a tedious process. If a design change were undertaken, the move should be toward a shorter pulse duration in order to reduce pump requirements and increase stability so that reproducibility in temperature characteristics of the expansion would be ensured.

A final suggestion would be dependent on the intended use of the apparatus. As a research tool, it would of course undergo further modification to take on the next task of interest. If, however, it should become a routine analysis tool, it appears wise to optimize it for what it does best; detection via MPI. It has been shown that fluorescence and MPI detection schemes are both compatible. In fact, analysis with both detection methods operating simultaneously was the routine mode of operation, and several figures with simultaneous detection by LIF and MPI have been given in this thesis. Although the optimization involved for MPI would include just the insertion of a focusing lens and occasional optimization of other variables such as extraction grid potentials, the increase in MPI detection sensitivity would be a worthy reward.

LITERATURE CITED

1. Irving, C. C. In "Structural Correlates of Carcinogenesis and Mutagenesis"; Asher, I. M.; Zervos, C., Eds.; U. S. Department of Health, Education, and Welfare: Rockwell, MD, 1977, 140.

2. Hayes, J. M.; Small, G. J. Anal. Chem. 1983, 55, 565A.

3. Amirav, A.; Even, U.; Jortner, J. Anal. Chem. 1982, 54, 1666.

4. Hayes, J. M. Chem. Rev. 1987, 87, 745.

5. Kantrowitz, A.; Grey, J. Rev. Sci. Instrum. 1951, 22, 328.

6. Smalley, R. E.; Ramakrishna, B. L.; Levy, D. H.; Wharton, L. J. Chem. Phys. 1974, 61, 4363.

7. Johnston, M. V. Trends Anal. Chem. 1984, 3, 58.

8. Brown, J. C.; Hayes, J. M.; Warren, J. A.; Small, G. J. In "Lasers in Chemical Analysis"; Hieftje, G. M.; Lytle, F. E.; Travis, J. C., Eds.; Humana Press: Clifton, NJ, 1981; Chapter 11.

9. Hayes, J. M.; Chiang, I.; McGlade, M. J.; Warren, J. A.; Small, G. J. In "Laser Spectroscopy for Sensitive Detection"; Gelbwachs, J. A., Ed.; SPIE: Bellingham, WA, 1981; Vol. 286, 117.

10. Warren, J. A.; Hayes, J. M.; Small, G. J. Anal. Chem. 1982, 54, 138.

11. Lubman, D. M.; Kronick, M. N. Anal. Chem. 1982, 54, 660.

12. Hayes, J. M.; Small, G. J. Anal. Chem. 1982, 54, 1202.

13. Amirav, A.; Even, U.; Jortner, J. Anal. Chem. 1982, 54, 1666.

14. Blakely, C. R.; Vestal, M. L. Anal. Chem. 1983, 55, 750.

15. Dole, M.; Mack, L. L.; Hines, R. L.; Mobley, R. C.; Ferguson, L. D.; Alice, M. B. J. Chem. Phys. 1968, 49, 2240.

16. Ryhage, R. Anal. Chem. 1964, 51, 359.

17. Randall, L. G.; Wahrhaftig, A. L. Rev. Sci. Instrum. 1981, 52, 1283.

18. Olivares, J. A.; Houk, R. S. Anal. Chem. 1985, 57, 2674.

19. Lubman, D. M. Anal. Chem. 1987, 59, 31A.

20. Johnston, M. V. Trends Anal. Chem. 1988, 7, 94.

21. Hagena, O. F. Z. Angew. Phys. 1963, 16, 183.

22. Amirav, A.: Even, U.; Jortner, J. Chem. Phys. Lett. 1981, 83, 1.

23. Amirav, A.: Even, U.; Jortner, J. J. Chem. Phys. 1982, 67, 1.

24. Amirav, A.: Even, U.; Jortner, J.; Ramsay, D. A. Can. J. Phys. 1983, 61, 278.

25. Stiller, S.; Johnston, M. V. Anal. Chem. 1987, 59, 567.

26. Goldstein, N.; Brack, T. L.; Atkinson, G. H. Chem. Phys. Lett. 1985, 116, 223

27. Imasaka, T.; Fukuoka, H.; Hayashi, T.; Ishibashi, N. Anal. Chim. Acta 1984, 156, 111.

28. Imasaka, T.; Hirata, K.; Ishibashi, N. Anal. Chem. 1985, 57, 59.

29. Yamada, S.; Smith, B. W.; Voigtman, E.; Winefordner, J. D. Analyst 1985, 110, 407.

30. Yamada, S.; Smith, B. W.; Voigtman, E.; Winefordner, J. D. Appl. Spectrosc. 1985, 39, 513.

31. Venkateshan, S. P.; Ryali, S. B.; Fenn, J. B. Ber. Bunsen-Ges. Phys. Chem. 1984, 88, 245.

32. Mizugai, Y.; Kuze, H.; Jones, H.; Takami, M. Appl. Phys. B. 1983, 32, 43.

33. Snavely, D. L.; Colson, S. D.; Wiberg, K. B. J. Chem. Phys. 1981, 74, 6975.

34. Dubal, H.-R.; Quack, M.; Schmitt, U. Chimia 1984, 38, 438.

35. Luijks, G.; Stolte, S.; Reuss, J. Chem. Phys. 1981, 62, 217.

36. Duncan, M. D.; Byer, R. L. IEEE J. Quantum Electron. 1979, QE-15, 63.

37. Zivi, H.; Bauder, A.; Gunthard, Hs. H. Chem. Phys. Lett. 1981, 83, 469.

38. Pepich, B. V.; Callis, J. B.; Sheldon Danielson, J. D.; Gouterman, M. Rev. Sci. Instrum. 1986, 57, 878.

39. Imasaka, T.; Okamura, T.; Ishibashi, N. Anal. Chem. 1986, 58, 2152.

40. Fukuoka, H.; Imasaka, T.; Ishibashi, N.; Anal. Chem. 1987, 59, 419.

41. Sin, C. H.; Pang, H. M.; Lubman, D. M.; Zorn, J. Anal. Chem. 1986, 58, 487.

42. Pang, H. M.; Sin, C. H.; Lubman, D. M.; Zorn, J. Anal. Chem. 1986, 58, 1581.

43. Imasaka, T.; Yamaga, N.; Ishibashi, N. Anal. Chem. 1987, 59, 419.

44. Rizzo, T. R.; Park, Y. D.; Peteanu, L.; Levy, D. H. J. Chem. Phys. 1985, 83, 4819.

45. Rizzo, T. R.; Park, Y. D.; Peteanu, L.; Levy, D. H. J. Chem. Phys. 1986, 84, 2534.

46. Weyssenhoff, H. v.; Selzle, H. L.; Schlag, E. W. Z. Naturforsch., A 1985, 40A, 674.

47. Tembreull, R.; Lubman, D. M. Anal. Chem. 1986, 58, 1299.

48. Grotemeyer, J.; Boesl, U.; Walter, K.; Schlag, E. W. J. Am. Chem. Soc. 1986, 108, 4233.

49. Tembreull, R.; Lubman, D. M. Anal. Chem. 1987, 59, 1003.

50. Grotemeyer, J.; Schlag, E. W. Org. Mass Spectrom. 1988, 23, 388.

51. Li, L.; Lubman, D. M. Int. J. Mass Spectrom. Ion Proc. 1989, 88, 197.

52. Grotemeyer, J.; Walter, K.; Boesl, U.; Schlag, E. W. Int. J. Mass Spectrom. 1987, 78, 69.

53. Imasaka, T.; Tashiro, K.; Ishibashi, N. Anal. Chem. 1989, 61, 1530.

54. Grotemeyer, J.; Schlag, E. W. Org. Mass Spectrom. 1987, 22, 758.

55. Tembreull, R.; Lubman, D. M. Anal. Chem. 1987, 59, 1082.

56. Hahn, J. H.; Zenobi, R.; Zare, R. N. J. Am. Chem. Soc. 1987, 109, 2842.

57. Behlen, F. M.; Mikami, N.; Rice, S. A. Chem. Phys. Lett. 1977, 60, 364.

58. Otis, C. E.; Johnson, P. M. Rev. Sci. Instrum. 1980, 51, 1128.

59. Behlen, F. M.; Rice, S. A. J. Chem. Phys. 1981, 75, 5672.

60. Adams, T. E.; Rockney, B. H.; Morrison, R. J. S.; Grant, E. R. Rev. Sci. Instrum. 1981, 52, 1469.

61. Adriaens, M. R.; Allison, W.; Feuerbach, B. J. Phys. E 1981, 14, 1375.

62. Hopkins, J. B.; Langridge-Smith, P. R. R.; Morse, M. D.; Smalley, R. E. J. Chem. Phys. 1983, 78, 1627.

63. Butler, J. E. Appl. Optics 1982, 21, 3617.

64. Levy, D. H. Science 1981 (4518), 214, 263.

65. Smalley, R. E.; Wharton, L.; Levy, D. H. Acc. Chem. Res. 1977, 10, 139.

66. Levy, D. H.; Wharton, L.; Smalley, R. E. In "Chemical and Biochemical Applications of Lasers", Moore, C. B., Ed.; Academic Press: New York, NY, 1977; Vol. 2, p. 1.

67. Smalley, R. E. J. Chem. Ed. 1982, 59, 934.

68. Vestal, M. L. Mass Spectrom. Rev. 1983, 2, 447.

69. Gobelli, D. A.; Yang, J. J.; El-Sayed, M. A. Chem. Rev. 1985, 85, 529.

70. Becker, C. H.; Gillen, K. T. J. Opt. Soc. Am. B 1985, 2, 1438.

71. Li, L.; Lubman, D. M. Rev. Sci. Instrum. 1988, 59, 557.

72. Grotemeyer, J.; Boesl, U.; Walter, K.; Schlag, E. W. Org. Mass Spectrosc. 1986, 21, 645.

73. Arrowsmith, P.; de Vries, M. S.; Hunziker, H. E.; Wendt, H. R. Appl. Phys. B 1988, 46, 165.

74. Chernoff, D. A.; Rice, S. A.; J. Chem. Phys. 79, 70, 2511.

75. "CRC Handbook of Chemistry and Physics", 60th Ed., Weast, R. C., Ed.; CRC Press: Boca Raton, FL, 1979.

76. Berlman, I. B. In "Handbook of Fluorescence Spectra of Aromatic Molecules, Second Ed."; Academic Press: New York, NY, 1971.

77. Sonnenschein, M.; Amirav, A.; Jortner, J. J. Phys. Chem. 1984, 88, 4214.

78. Stull, D. R. Ind. Eng. Chem. 1947, 39, 517.

79. Boublik, T.; Fried, V.; Hala, E. "The Vapour Pressure of Pure Substances"; Elsevier: Amsterdam, the Netherlands, 1984.

SUMMARY AND DISCUSSION

Two new instruments have been presented which offer new capabilities for analytical chemistry. The addition of an instrument for CPPP and DCPPP analyses allows one to look at solutions by polarography without the requirement of removing oxygen from the sample. The sensitivity is shown to be approximately equal to NPP, and the selectivity of DCPPP is shown to be about that of DPP. This allows the sensitive, selective detection of trace metals in batch and flowing samples in a timely fashion. In addition to application to flowing samples, the method is shown to give a degree of freedom from interference from reduction of hydrogen ion in acidic solution.

An instrument has been developed for jet spectroscopy which was designed to extend the range of application for the method. While full utilization of the instrument was not accomplished, a method was shown for analysis of volatile species by either LIF or MPI. This method offers sensitivity on a scale matched by few techniques, and detection at ppm levels was shown.

As one who desires to be an educator in chemistry, it is a rare opportunity to investigate projects in two separate areas of analytical chemistry. It is my desire that this will result in additional breadth which can now be put to advantage in the discipline of education.

ACKNOWLEDGMENTS

The work presented here would not have been possible without the support and guidance of many people. Although it seems a small "thank you," these acknowledgments are made with deep gratitude.

Dr. Gerald J. Small has been very helpful with the spectroscopy project as well with guidance and suggestions when it became apparent that the primary goals of the project were not being met. Dr. John M. Hayes provided counsel in the same areas and was of valuable assistance with technical direction for the design of the instrument and in problems encountered with equipment.

Dr. Dennis C. Johnson provided the opportunity to continue the pursuit of this degree with the polarography project. He has given valuable assistance in the lab and has been an admirable model.

Thank you to Dr. Small and Dr. Johnson for direction in research as well as for making available the funding necessary to carry out this work. Thank you for research support and for the opportunity to teach for several semesters, allowing me to prepare myself for education in college chemistry.

My time at Iowa State has allowed me to work with numerous others in various offices and labs. I pray that God will watch over you and I wish you well in your graduate work and your lives ahead. Special thanks go to Mike Kenney, Warren Jackson, Dr. Barbara Reitsma, Dr. Kevin Gillie, Dr. Bill LaCourse, and many others that have shared the times spent here.

My life did not begin at Iowa State. I have been provided with

love, friendship, and wise direction from many sources. I have appreciated this beyond words. Mom and Dad, thank you for your love, your prayers, and your constant encouragement and support. You know the gratitude I feel.

One other deserves far more thanks than can be expressed here. Sue, you have provided me with love I could not have imagined. Your support through the good and the bad times has not wavered. You have made our home a sanctuary at the end of the day where I am fully accepted and loved. Only you can know the love and thanks I have for you. Thank you.

My relationship with Jesus Christ must be acknowledged, for beneath everything, He has made me who I am. To God be the honor and the glory forever.